Nutrient Availability Alters Metabolism and Methods Use in the Malaria Parasite

Audrey Caroline Brown
Bowling Green, KY

Bachelor of Science, Western Kentucky University 2016

A Dissertation presented to the Graduate Faculty of the University of Virginia in Candidacy for the Degree of Doctor of Philosophy

Department of Biology
April 2022

Jennifer Guler (advisor)
Alan Bergland
Girija Ramakrishnan
Cristian Danna
Michael Timko

Signature Page

Dr. Jennifer Guler

Dr. Alan Bergland

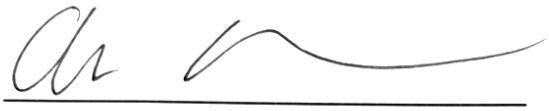

Dr. Girija Ramakrishnan

Dr. Cristian Danna

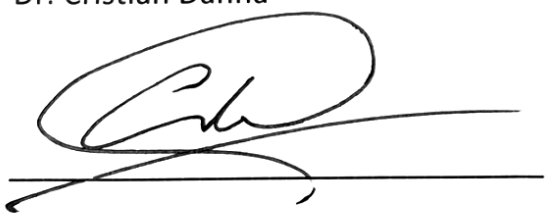

Dr. Michael Timko

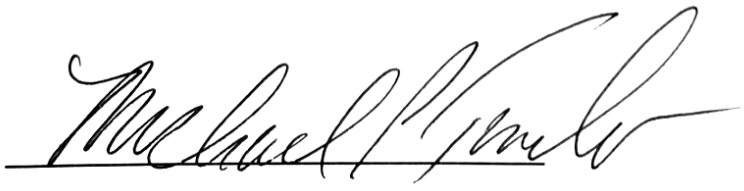

Dedication Page

To my advisor, Jenny Guler for your consistent and purposeful mentorship in all aspects of science. Whenever I am asked what you are like as an advisor, I tell people that I always feel more optimistic about my work and confident as a scientist leaving your office than I do going in, and that speaks volumes!

To my thesis committee members, Alan Bergland, Girija Ramakrishnan, Cristian Danna, and Michael Timko for your time and feedback that has helped my project grow over the years.

To my fellow lab members Michelle Warthan, Jen McDaniels, Maureen Carey-Medlock, Adam Huckaby, Shiwei Liu, Anush Aryal, and Noah Brown. None of this research or my development as a scientist would have been possible without all of you.

To the Petri lab group for the thoughtful insight and discussion that always helped me think about my research in new and creative ways.

To my Biology of Parasitism 2020+1 cohort: you taught me how to dare more and to sleep less.

To my friends Phil Tubergen, Kim Arena, Luke Dillard, and Chris Robinson for your camaraderie and support over the years.

To every unnecessary coffee break I've ever taken. Looking back, they might have been necessary after all.

To my family who still don't completely understand what I've been doing the past five and a half years but are happy to support me anyway.

To Jenny Rosner: maybe you aren't family... but you are.

To my horse: You never knew when the rejection letters came or the experiments failed or *there was a global pandemic*, but you were always there, a steady presence in an unsteady world.

Table of Contents

List of Figures

List of Tables & Boxes

List of Supplemental Materials

Chapter 1:
Introduction to the Malaria Parasite

Summary

This dissertation is focused on how metabolism of the malaria-causing parasite, *Plasmodium falciparum,* changes in response to stressful conditions and how these metabolic adjustments cause increased parasite tolerance to antimalarial drug treatment.

There is intricate interplay between parasites and their environment as pathogens respond to nutrient availability, physical forces, and immune pressure. Mounting evidence indicates non-genetic, metabolic changes in response to these environmental factors can modulate pathogen sensitivity to drug treatment. **Chapter 2** reviews, in detail, what is known about changes in growth, survival, and virulence as a consequence of parasite environment. Yet, there are still open questions about the extent of environmental impact on drug uptake, activation, and other effects relevant to parasite drug sensitivity. One technical barrier to answering these research questions is access to high quality *in vitro* ring stage parasites and non-traditional parasite forms (quiescent rings and *ex vivo* clinical rings). Ring stage parasites have become a focus of interest in the malaria community because, relative to other more metabolically active stages of the malaria replication cycle, rings demonstrate decreased susceptibility to the World Health Organization frontline antimalarial drug, artemisinin. Further, a small proportion of rings enter a growth arrested quiescent state upon drug administration allowing survival of artemisinin treatment. The exact mechanisms by which rings stage *P. falciparum* survive drug treatment, such as how parasites enter and exit from quiescence, is poorly understood; however, current evidence heavily suggests survival can be mediated through non-genetic, metabolic changes.

In **Chapter 3**, I present the "SLOPE" method for enrichment of *in vitro*, *ex vivo*, and quiescent ring stage parasites. Prior to the publication of Chapter 3, there was no effective method for the enrichment of these populations leading to considerable host-contributed noise in samples, which limited success of sensitive downstream analyses, particularly of non-genetic, metabolic changes through methods such as proteomics and metabolomics. The development of this effective enrichment method will dramatically improve our ability to study ring stage parasites, as well as ring-derived forms.

While developing the SLOPE enrichment method, which relies on a cholesterol dependent lytic agent, we incidentally noted a reduction of cholesterol on *in vitro* parasite infected erythrocyte membranes that was not present *ex vivo*. It was discovered this discrepancy is due to the considerably lower level of cholesterol provided by *in vitro* media formulations compared to levels in human host plasma. This, paired with other examples of impacts from the non-physiological nutritional environment *in vitro* detailed in Chapter 2, led us to explore the effect of physiologically relevant nutrient limitation on parasite drug sensitivity.

In **Chapter 4**, parasites were subjected to metabolic nutrient stress by either 1) decreasing a single metabolite type that has been previously proposed as drug target (i.e., purines or thiamine) or 2) using a media formulation with reductions in many metabolites that simulates the physiological human plasma environment. The adaptive benefits of these mild nutrient stress conditions overshadowed any adverse effects leading increased ring stage parasite survival of artemisinin treatment. While these nutrient stress levels were developed to mimic conditions parasites may encounter in the context of a clinical infection, the extent to which drug survival is truly impacted *in vivo* merits further investigation. The potential for nutrient stress to be inducing quiescent ring stage parasites as a mechanism to facilitate increased artemisinin survival in this context also remains unknown. We presume that metabolic stress occurs more frequently *in vivo* compared to the stable, nutrient-rich *in vitro* environment; therefore, the observation that more a physiological environment increases artemisinin tolerance has ramifications for how *in vitro* antimalarial drug treatment results translate to *in vivo* studies.

The availability of effective antimalarial drugs is critical to prevent malaria mortality numbers from rising and work toward malaria eradication. Yet, clinical malaria resistance has now been reported to both the recommended frontline antimalarial treatment and all available partner drugs. My goal to understand how *Plasmodium falciparum* modulate metabolism to cope with stress will lead to a more accurate understanding of how malaria parasites will respond to drug treatment in a human infection. Understanding this stress responsive ability of parasites to cope with antimalarial pressures will provide foundations for the development of powerful targeted adjuvants to combat the emergence and spread of future malaria drug resistance.

Plasmodium Species & Global Distribution

Malaria is caused by infection with parasitic protozoa in the *Plasmodium* genus. There are over 100 *Plasmodium* species, which infect a diversity of animals including reptiles, birds, and mammals. Cases of malaria in humans are caused by five species of *Plasmodium*:

Plasmodium vivax, *Plasmodium malariae, Plasmodium ovale*, *Plasmodium knowlesi, and Plasmodium falciparum* [26].

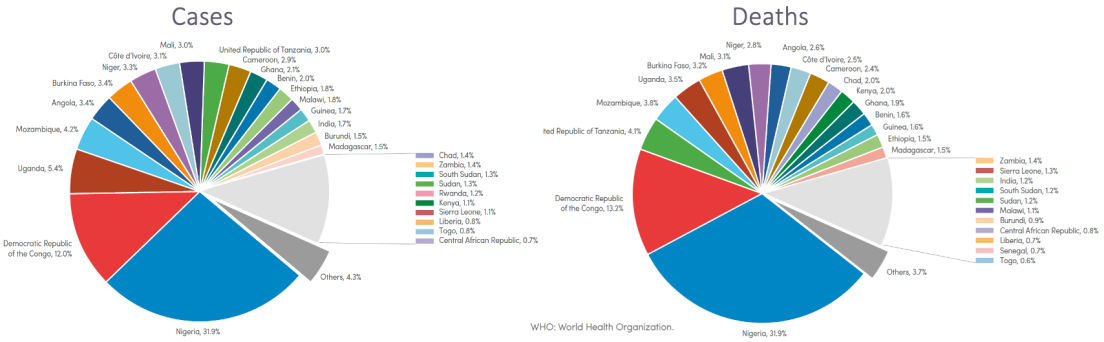

Figure 1.1. Global distribution of malaria cases and deaths from all *Plasmodium* species. Figure modified from WHO World Malaria Report 2021.

In 2020, there were an estimated 241 million malaria cases resulting in 627,000 deaths. Malaria is endemic to 85 countries across five continents; however, approximately 95% of cases and deaths occur in Africa (**Figure 1.1**; WHO WMR ref). *P. falciparum* infection accounts for the vast majority of malaria morbidity and mortality with the next most prevalent species being *P. vivax* at only 2% of global cases. *P. falciparum* predominates in Sub-Saharan Africa with a lower burden also present on other continents, while *P. vivax* is primarily restricted to Latin America and Southern Asia (**Figure 1.2**; [28]). *P. malariae* has a similar global distribution to that of *P. falciparum* but is considerably less frequent [26]. *P. ovale* and *P. knowlesi*, are found in low numbers in Africa and Southern Asia, respectively [26, 31]. Given the predominance of *P. falciparum* across the globe and the tractability of this species for *in vitro* propagation, it is unsurprising that *P. falciparum* is the prominent species of focus for malaria research. Consistent with this trend, experiments detailed in the following chapters chiefly revolve around the study of *P. falciparum*.

Transmission & Life Cycle

P. falciparum has a complex life cycle with stages in both the mosquito vector and the human host (**Figure 1.3**). Obligatory sexual reproduction occurs within the mosquito midgut. After sexual developmental stages, infectious sporozoites are transmitted to humans via bite from an infected female *Anopheles* mosquito. Once in the human host, sporozoites migrate to the liver to invade hepatocytes. Here parasites undergo an astounding expansion over the course of one week, producing 10,000-30,000 merozoites per successful sporozoite invasion of hepatocyte [32]. Merozoites then egress from hepatocytes to invade erythrocytes in the blood stream. Parasites undergo 48h cycles of erythrocyte invasion, asexual replication, egress, and reinvasion. Each cycle, rather than

continued asexual proliferation, a small fraction of parasites commits to sexual development producing male and female gametocytes. Gametocytes are transmissible to mosquitos via blood meal where they again undergo sexual reproduction in the midgut to complete the parasite lifecycle. However, it is asexual blood stage parasite replication that causes all signs and symptoms of malaria disease.

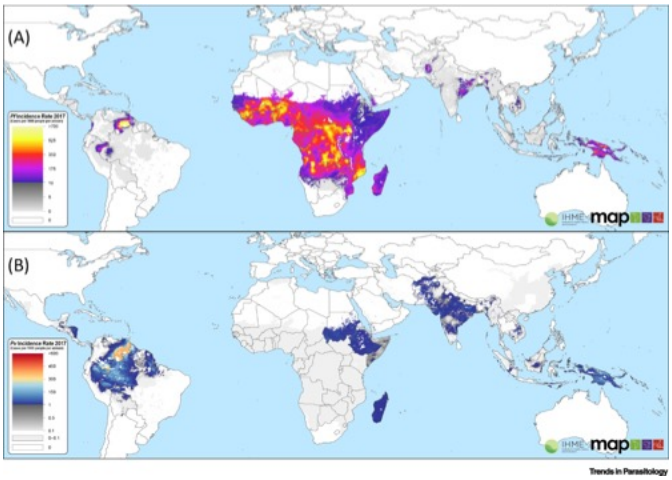

Figure 1.2. Geographic distribution of the two most prevalent malaria causing species, A) *P. falciparum* and B) *P. vivax*. Figure from Price, *et al*.

Malaria Symptoms & Treatment

Common symptoms of malaria include, headache, nausea, malaise, and a cyclical fever coinciding with the 48h asexual blood replication cycle [26]. With diagnosis and proper treatment, malaria is typically curable. However, severe cases of malaria may lead to death. Severe manifestations of the disease may include anemia, hypoglycemia, hypotension, kidney injury, metabolic acidosis, respiratory distress, and cerebral malaria [26]. Complications from these symptoms can result in multiple organ failure, coma, and death [26, 33, 34].

Naturally acquired immunity to malaria is built relatively slowly over multiple infections [35]. This leaves young children in endemic areas most vulnerable to malaria as antibodies against the disease build with exposure and age. Immunity elicited through vaccines has been a goal of the malaria research community for decades, yet limited success has been achieved for reasons summarized by Gonzales, *et al*.: “i) sequence variation in vaccine targets that resulted in parasite strain-specific responses, ii) inability of the vaccine to elicit sufficiently high antibody titers necessary for protection, and iii) quick waning of elicited immune responses” [36].

Lack of sterilizing immunity from natural infection or vaccination means malaria control is heavily dependent on exposure prevention and management of diagnosed cases with drug treatment [26]. The most widely used exposure prevention strategies include i) intermittent prophylactic drug treatment of pregnant women and infants and ii) vector control through use of insecticide-treated bed nets and indoor residual spraying of long-

lasting insecticide. Even with these prevention measures, nearly 250 million cases of malaria occur annually. These cases can be treated with antimalarial drugs.

The current World Health Organization recommendation for the treatment of malaria is artemisinin (**ART**) combination therapy [37]. The rapid acting, potent antimalarial, ART, is delivered along with a longer acting partner drug, such as mefloquine or piperaquine. The administration of multiple drugs with different molecular mechanisms of action is used to reduce the opportunity for development of drug resistance. However, clinical resistance has now been reported to both ART and all available partner drugs [32, 38, 39].

Artemisinin Resistance

ART treatment is known to cause broad metabolic disruption in *P. falciparum* through alkylation and damage of numerous parasite proteins [40, 41]. Interestingly, ART induces a reduced metabolic state in a small percentage of exposed parasites (<<1%). This state, termed quiescence, allows some parasites to survive until drug pressure is removed [42]. Quiescence can be induced on parasite genetic backgrounds with or without ART resistance conferring mutations [43, 44]. Drug treatment can be survived by parasites

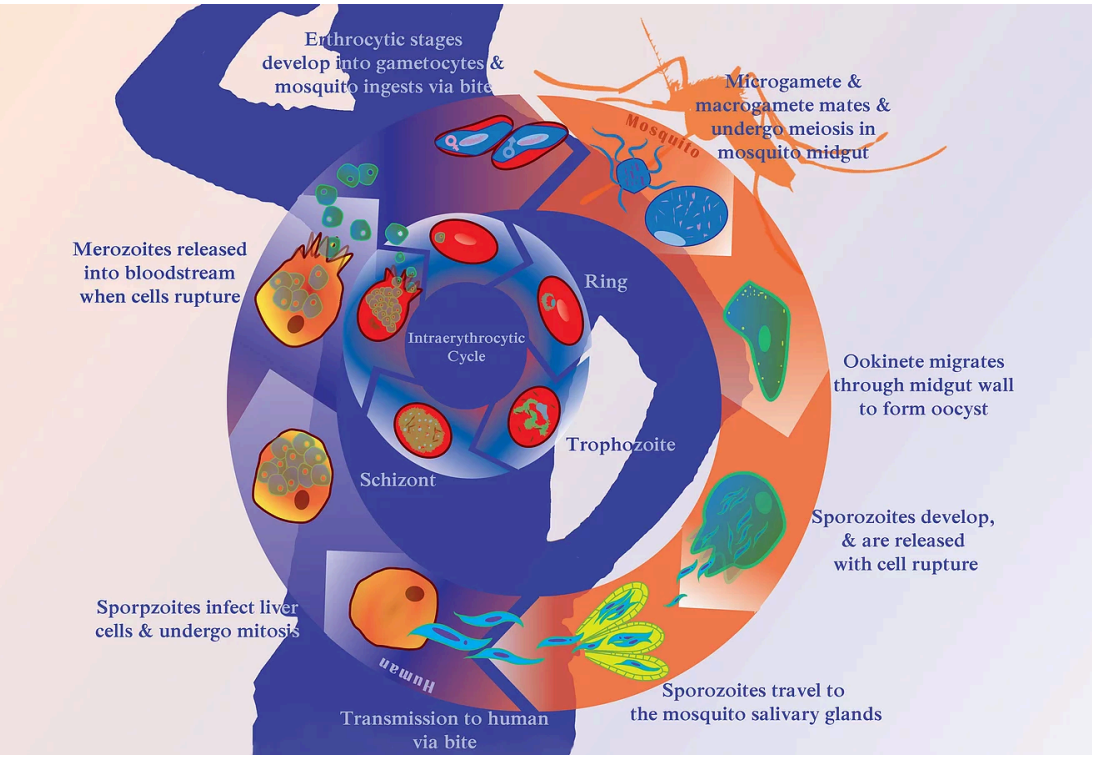

Figure 1.3. The complex lifecycle of *P. falciparum.* Completion of the *Plasmodium* lifecycle requires development in both the mosquito vector (orange) and the human host (blue). The *Plasmodium* genome is haploid throughout most of its lifecycle apart from diploid zygote formation during sexual reproduction within the mosquito. Artwork created by Michelle Warthan, 2017.

without quiescence induction though genetic changes that lead to higher levels of survival under ART pressure, such as mutations in the propeller domain of *Kelch13* [45, 46]. Wild type Kelch13 serves as an adaptor for polyubiquitination of phosphatidylinositol 3-kinase (PI3K), which targets PI3K for degradation. Mutant Kelch13 proteins found in ART resistant parasites have reduced ubiquitination of PI3K leading to accumulation of PI3K protein and its product, phosphatidylinositol 3-phosphate (PI3P) [47]. While it has been shown that increased PI3P levels confer ART resistance, the exact mechanisms are poorly understood. Proposed downstream mechanisms include the unfolded protein response (UPR), and autophagy, which have both been implicated in ability to manage ART damage [48-50]. Activation of autophagy in *P. falciparum* (perhaps through UPR phosphorylation of eIF2a) is a logical mechanism for mitigation of ART damage in parasites as this process has been shown to be induced by ART in a mammalian model [51, 52].

As mentioned above, even prior to the acquisition of resistance conferring mutations, a small proportion of parasites *P. falciparum* enter a reduced metabolic, quiescent state to survive ART treatment [43, 53, 54]. Quiescence induction occurs in parasites with and without ART resistance conferring *Kelch13* mutations [43]. However, only the early blood stage parasites (aka “rings”) are capable of entering into this quiescent state, while ART remains lethal to late blood stage parasites (trophozoites and schizonts, **Figure 1.3.**). Once quiescent rings resume growth and mature into late stages, parasites do not have increased resistance to ART as compared to the original parasite [54-56]. This phenomenon is similar to bacterial persistence in which cells evade antibiotic pressure by entering a quiescent state regardless of genetic resistance status [57, 58]. One benefit of quiescence for *P. falciparum* may be the ability of some parasites to persist during treatment, thereby creating a larger pool in which a beneficial (resistance-conferring) mutation may arise [38, 39, 54, 59].

With the spread of resistance to ART and its partner drugs, there is a renewed effort to both i) find ways to increase the efficacy of current drugs and ii) find novel parasite drug targets. As detailed above, ring stage parasites have the highest propensity to overcome ART treatment. The SLOPE enrichment method presented in Chapter 3, will allow researchers to more accurately study both metabolically active and quiescent ring stage *Plasmodium* leading to improvements in our understanding of parasite biology and how it may be leveraged to improve efficacy of ART treatments.

Chapter 4 explores potential new metabolic drug targets and how manipulation of these target pathways may interact in combination with ART treatment and existing ART resistant genotypes. Due to the practical limitations of collecting clinical samples directly from humans, most malaria research is performed on laboratory adapted parasites *in vitro*. However, as discussed in detail in Chapter 2, there is increasing evidence suggesting the nutrient rich media used for standard *in vitro* culture can alter drug sensitivity. Given this, two potential metabolic drug targets with plausible connections to changes in ART sensitivity were chosen for exploration: nucleotide and thiamine metabolism.

Nucleotide & Thiamine Metabolism

Nucleotide metabolism is a promising drug target in *P. falciparum*; antimalarials are currently being developed to inhibit both purine scavenging and pyrimidine biosynthesis [60-63]. As some of these candidates move closer to being utilized in the clinic, it is imperative that we understand how parasites sense and respond to the stress of nucleotide deprivation. Interestingly, increased survival in response to nutrient deprivation has recently been associated with an increase in *P. falciparum* autophagy [48]. This finding parallels results in mammalian models where autophagy is important for nucleotide substrate recycling [64]. Given the proposed link between autophagy and ART survival (see above, [48]), ART resistance mutations, such as those in *Kelch13,* may impact survival of parasites under nucleotide deprivation as well. Furthermore, ART treatment decreases purine levels and pyrimidine biosynthesis [40, 55]; the reason for this effect remains unknown but it suggests that altered nucleotide levels and ART treatment may have similar downstream effectors. It is intriguing to consider that the effects of ART and nucleotide deprivation are managed by overlapping pathways. If so, the efficacy of antimalarials that target nucleotide metabolism may be at increased risk of treatment failure due to existing ART resistance phenotypes.

A second proposed, metabolic drug target is thiamine metabolism. Thiamine is an essential metabolite used to generate thiamine pyrophosphate (also known as Vitamin B1). Vitamin B1 is a cofactor for diverse enzymes, many with key metabolic functions [65,

Figure 1.4. Thiamine acquisition in *P. falciparum.* The iPfal17 genome-scale metabolic network reconstruction predicts the essentiality of thiamine import in ART resistant, but not ART sensitive, parasites. Figure modified from Carey, *et al*.

66]. While humans are dependent on scavenge of this cofactor from food, wild-type *P. falciparum* has the ability to synthesize Vitamin B1 from either scavenging or biosynthesized thiamine (**Figure 1.4**) [67, 68]. Interestingly, a critical role for thiamine metabolism was indicated in a previous study from the J. Guler lab using metabolic network reconstruction models integrating transcriptome data from both ART sensitive and ART resistant parasites [69]. These data suggest an artemisinin resistant genetic background leads to essentiality of thiamine scavenging, generating a weakness potentially exploitable as a drug target (**Figure 1.4**).

The development of new antimalarial drug targets, such as nucleotide or thiamine metabolism, will play a critical role in the future of malaria control as resistance to currently available treatments spread. Even in 2020, malaria caused by *P. falciparum* led to over half a million deaths; and the availability of effective antimalarial drugs is critical to prevent this number from rising and to work toward malaria eradication. The studies presented here aim to aid in this goal by building the basic biology foundation of how *P. falciparum* responds to drug stressors through the development of new research methods and investigations of malaria metabolism.

Chapter 2:
From Circulation to Cultivation: *Plasmodium in vivo* versus *in vitro*

This chapter has been adapted from the following review article published in *Trends in Parasitology*:

Brown, A. C. and J. L. Guler (2020). "From Circulation to Cultivation: Plasmodium In Vivo versus In Vitro." Trends Parasitol **36**(11): 914-926.

Figures and tables have been renumbered to maintain sequence within this document.

Abstract

Research on *Plasmodium* parasites has driven breakthroughs in reducing malaria morbidity and mortality. Experimental analysis of *in vivo*/*ex vivo* versus *in vitro* samples serve unique roles in *Plasmodium* research. However, these distinctly different environments lead to discordant biology between parasites in host circulation and those under laboratory cultivation. Here, we review how *in vitro* factors, such as nutrient levels and physical forces, differ from those in the human host and the resulting implications for parasite growth, survival, and virulence. Additionally, we discuss the current utility of direct-from-host methodologies, which avoid the potentially confounding effects of *in vitro* cultivation. Finally, we make the case for methodological improvements that will drive research progress of physiologically relevant phenotypes.

Malaria and *Plasmodium* Biology

In humans, five species of *Plasmodium* lead to malaria infections, with *Plasmodium falciparum* being responsible for the majority of malaria morbidity and mortality [70]. Malaria has burdened humanity for millennia. Even as recently as the 20th century, malaria infections accounted for an estimated 2-5% of all deaths [71]. Yet, successful vector control, infection prevention, and antimalarial drug treatments have put malaria elimination in reach for progressively more countries [70]. The advent of a standardized *P. falciparum* continuous laboratory *"in vitro"* culture system in the 1970s has been essential to these successes by accelerating understanding of parasite biology and drug sensitivity.

In vitro culture allows for the continuous cultivation of the **intraerythrocytic developmental cycle** (IDC**;** *see Glossary*) of not only *P. falciparum* but, more recently of *P. knowlesi* as well [72, 73]. Notably, conditions suitable for robust long-term *in vitro* propagation of *P. vivax* have yet to be deciphered, and therefore samples of *P. vivax* and other human malaria species (*P. ovale, P. malariae*) must come directly from human infections. Within the human body, known as "*in vivo"*, the IDC is responsible for all symptoms of malaria, including cyclical fevers and hypoglycemia. Asexual stages that occur late during the IDC, as well as immature **gametocytes,** sequester in the microvasculature and bone marrow [74-76], respectively, to avoid removal by the host's spleen [32, 77]. Thus, a blood sample taken directly from an infected human will contain primarily early stage asexual parasites and mature gametocytes, whereas a sample from *in vitro* culture can contain an asynchronous mix of all stages. Similar to samples directly

from *in vivo*, ***ex vivo*** samples are parasites within the first asexual developmental cycle outside of the host and, like *in vivo* samples, will contain a synchronous population of parasites but at a stage dependent on the time elapsed since phlebotomy.

Implications of the Parasite Environment

While modern *in vitro* culture systems have been wholly necessary for many of the biological breakthroughs in *Plasmodium* biology, no *in vitro* system can perfectly recapitulate an *in vivo* infection. Parasites *in vivo* are subjected to a myriad of physical, nutritional, and immunological factors differing from those found *in vitro*. Pressure exerted by these factors *in vivo* induce dynamic reactions in parasites that are difficult to appreciate *in vitro* but result in meaningful changes affecting virulence, transmissibility, and drug sensitivity. Many of the differences between *in vitro* and *in vivo Plasmodium* environments and their implications were reviewed by LeRoux, *et al*. over a decade ago [78]. Here, we review knowledge that has been gained in the intervening decade on how the differences in nutrient levels and physical forces between *in vivo/ex vivo* and *in vitro* culture environments lead to changes in *Plasmodium* biology. Further, we present various methodologies for studying *Plasmodium* biology directly from the human host, which avoids the impact of the artificial culture environment discussed within this review. Finally, we advocate for methodological improvements that will drive research progress of physiologically relevant parasite phenotypes.

Nutrient Levels Affect Parasite Physiology and Growth

In vitro P. falciparum and *P. knowlesi* culture systems are almost universally maintained in RPMI 1640-based media, supplemented either with 1) 10% human serum, 2) 0.5% AlbuMAX Lipid-Rich BSA (ALB) plus hypoxanthine, or 3) a serum-ALB combination. Reducing human serum usage through ALB-supplemented RPMI media is a popular choice due to lower cost, reduced batch to batch variability, and elimination of the logistical challenge of obtaining non-immune serum in endemic localities. Parasites cultured in ALB-supplemented media have generally demonstrated good growth compared to those grown with human serum supplementation, yet evidence suggests large underlying effects of different media formulations. Through a comparison of human serum-supplemented versus ALB-supplemented *P. falciparum* cultures, close to 1000 genes were significantly differentially expressed between cultivation medium, with the large majority exhibiting increased expression in ALB [79]. Gene ontology terms most enriched in ALB upregulated genes indicate significant metabolic changes (e.g. metal ion transport, DNA

catabolic processes, divalent inorganic transmembrane transport activity, and oxidoreductase activity), which highlights the impacts of differing nutrient environments.

Whether supplemented with ALB or serum, all RPMI 1640-based media formulations provide a source of critical lipids and purines in addition to the abundant glucose, amino acids, cofactors, and salts. The nutrient-rich base media contains many metabolites at levels far higher than those present in the host *in vivo* environment (i.e. 10-fold higher hydroxyproline and 100-fold higher folic [78]). This nutritional strategy serves to promote growth in diverse cell types where specific metabolic needs may be poorly defined; however, divergence in metabolite levels *in vivo* and *in vitro* likely contributes to discordant results discussed throughout this review. For example, reduced cholesterol abundance *in vitro* compared to *in vivo* proved to be impactful for a recently developed method that enriches infected RBCs by selectively lysing uninfected RBCs using a cholesterol-dependent lytic agent (**Figure 2.1A**) [11]. The considerably lower cholesterol levels of *in vitro* media formulations maximizes the cellular discrimination required for this technique but these levels remain adequate to support normal parasite invasion *in vitro* [80].

In vivo, **cytoadherence** can lead to **sequestration** and **rosetting** in *P. falciparum* infections, which serve to avoid parasite removal by splenic filtration and increase immune evasion, respectively [81, 82]. Therefore, accurate knowledge about these phenomena is critical for understanding *Plasmodium* virulence. Factors present in human serum, including lipoproteins and components of the immune system, are necessary *in vitro* for high levels of erythrocyte membrane protein 1 (**PfEMP1**) presentation on the *P. falciparum*-infected RBC surface as well as the formation of rosettes (mediated by *stevor* gene products) [83-85]. However, the presence of serum factors may not be the whole story; transcription of PfEMP1-encoding *var* genes is decreased even in parasites transitioned into human serum supplemented cultures [86, 87]. Thus, it remains unclear to what extent expression of key virulence genes *in vivo* are dependent on human serum factors compared to other host-parasite interactions, such as rheology, interaction with endothelial cells, and febrile temperature (*see Physical Environmental Factors* section; **Box 2.1**).

In addition to nutrient levels and serum factors, the fundamental design of *in vitro* culture alters parasite access to nutrients. RBC cell density is traditionally limited *in vitro* because parasite replication suffers at high **hematocrit** with most experiments performed between 1%-5% hematocrit [78]. This is compared to >30% hematocrit in malaria-infected patients [88, 89]. This limitation *in vitro* is likely due to the local depletion of nutrients and

buildup of waste products in this static environment (i.e. a flask sitting in an incubator) [90]. Parasite density also limits growth, presumably for a similar reason. Using typical *in vitro* static culture methods, parasite growth suffers above 10% **parasitemia** even considering the relatively low hematocrit *in vitro* compared to *in vivo* [90]. However, patients with severe malaria have been reported with parasitemia values over 40% [91]. Gentle shaking of *Plasmodium* cultures can partially overcome the challenges associated with high hematocrit and parasitemia, while also increasing chances for non-motile merozoites to contact and invade uninfected RBCs. Utilization of non-traditional culture systems that allow for continual flow of RBCs through an *in vivo*-like environment, such as **hollow-fiber capillary bioreactors** (HFBR), further overcome this problem; HFBRs allow for high parasite replication at physiological hematocrit levels by not only increasing surface area for nutrient exchange but also by allowing continual addition of fresh medium [92-96]. The pumped fluid flow design of HFBRs has specifically facilitated precise *in vitro* modulation of drug concentrations over time, generating conditions that more closely mimic the pharmacokinetics of *in vivo* drug treatment [92, 93, 95]. HFBR-based studies can also facilitate the collection of parasite antigens within cartridges for assessments of immune evasion or vaccine development [94]. However, the HFBR system requires a considerably more complex setup than flask-based culturing and the polymer used in commercially available cartridges is toxic for *P. falciparum* necessitating custom-made glass cartridges [92].

Physical Environmental Factors Predominantly Impact Cytoadherence

Physical factors apart from nutrient availability play important roles in shaping which parasites survive and proliferate *in vivo*: this makes it prudent to understand the effect of varying these factors. *In vivo P. falciparum* parasites are subjected to the constant shear flow within the vascular system, either while circulating as rings or during sequestration as trophozoites and schizonts. The implications of removing fluid flow as part of *in vitro* culture limits nutrient access as mentioned above, but also alters parasite physiology. For example, maintaining cultures in suspension by shaking, along with other serum factors mentioned previously, contributes to the formation of rosettes *in vitro* [85]. Furthermore, parasites grown in static *in vitro* culture systems were not able to switch between glycan moiety-dependent and independent invasion pathways, whereas counterparts suspended with gentle shaking were able to successfully switch [97].

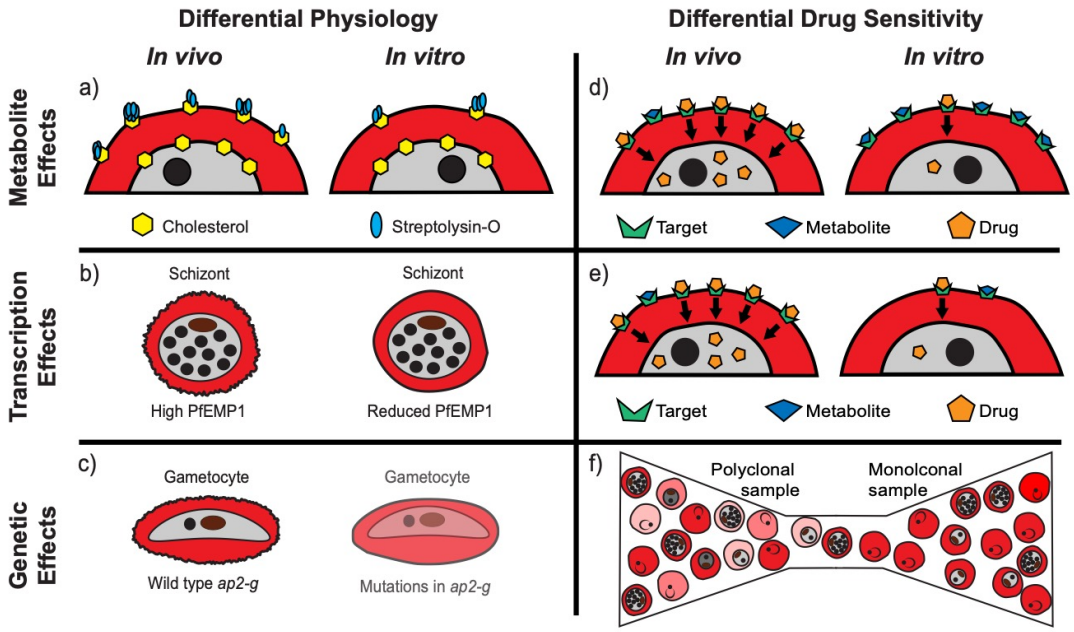

Figure 2.1. Physiology and drug sensitivity differences between *in vivo* and *in vitro* environments can be mediated by metabolic, transcriptional, and genetic changes.
Red areas, RBC; grey areas, parasite. (a) Cholesterol scavenging by parasites leads to lowered RBC membrane cholesterol *in vitro* but not *in vivo*, where exogenous cholesterol is higher and RBC membrane cholesterol is rapidly replenished. Thus cholesterol-dependent streptolysin-O lysis of infected RBCs is lower than uninfected RBC lysis *in vitro*, providing the discrimination for SLOPE [11]. (b) Physical factors *in vivo* lead to high expression of clonally variant RBC surface antigens. Without these factors, formation of PfEMP1-presenting knobs (shown as ridges on the RBC membrane) is reduced *in vitro*. (c) *In vivo*, a fraction of parasites commits to sexual development, forming gametocytes. However, many *in vitro* lines no longer develop sexual forms due to loss of function mutations in the gene, *ap2-g*. (d) 15 μM of the *Plasmodium* surface anion channel inhibitor, ISPA-28, leads to a clear reduction in proliferation when parasites are provided *in vivo* concentrations of isoleucine (~50 μM); however, no such reduction is seen at the *in vitro* culture level of 381 μM isoleucine found in RPMI-1640 [13]. (e) Blasticidin-S exposure leads to decreased sensitivity and regrowth of pre-exposed populations in as little as 6 days [14], meaning drug sensitivity can be altered within the time frame required for *in vitro* adaptation. This change in sensitivity is mediated by decreased transcription of a protein necessary for drug uptake. (f) *In vitro* adaptation leads to reduced genetic heterogeneity. For example, to two-thirds of polyclonal samples became monoclonal during the initial four weeks of adaptation [17].

While cytoadherence is beneficial *in vivo* [81], the parasite's effort to avoid host clearance may reflect a fitness cost in the absence of splenic filtration *in vitro*. Density of PfEMP1 **knobs** on the RBC surface (**Figure 2.1B**), which mediate sequestration in *P. falciparum* to avoid physical filtration by the spleen, was reduced 5-fold upon adaptation of *ex vivo* isolates to *in vitro* culture [98]. Transcription of many *P. vivax* cytoadherence genes were reduced *in vivo* in splenectomized *Aotus* monkeys relative to spleen-intact monkeys demonstrating that *Plasmodium* cytoadherence is likely regulated by many factors, including serum lipoproteins [83], rheology [21], and splenic pressure [99].

Temperature variability presents another physical environmental factor present *in vivo* but not *in vitro*. *In vitro*, incubators allow for continuous, steady temperature maintenance at 37°C. However, *in vivo* temperature fluctuates in a cyclical pattern [30]. Heat shock mimicking host febrile temperatures has been known for many years to lead to phenotypic effects, such as increased cytoadherence to endothelial cells [23, 78]. However, it is only been more recently that the molecular mechanisms underlying these effects have begun to be recognized (**Box 2.1**) [24].

Box 2.1. Mechanistic insight into effects of physical factors on cytoadherence.

Contribution of cellular interactions: Expression of *var* genes in *P. falciparum* grown in serum supplemented media was shown to be further increased by panning selection for endothelial cell binding by Claessens, *et al.* [10]. Physical interaction of infected RBCs with endothelial cells represents a key difference between *in vitro* and *in vivo* environments.

Contribution of rheology: A transcriptomics study by Nyarko, *et al*. utilizing parasites grown statically or in suspension revealed over 200 genes were differentially expressed between, largely representing increases in erythrocyte-binding, rigidity, and invasion-related genes in suspended cultures [21]. These properties enhance *P. falciparum* cytoadherence; thus, studying these phenomena in a static environment plausibly leads to an underappreciation of genes relevant to successful cytoadherence and immune evasion under the shear stress of the vascular system *in vivo*.

Contribution of temperature: Increased PfEMP1 presentation on the infected RBC surface has been observed in response to heat shock by Udomsangpetch, *et al*. but not in more recent studies by Oakley *et al.* nor Zhang, *et al.* These discordant results may be time dependent as levels of PfEMP1 presentation were measured 2h-4h following the onset of febrile temperatures by Zhang, *et al.* and Oakley, *et al.* compared to a ≥4h by Udomsangpetch, *et al.* [23-25]. Other studies have also implicated higher levels of phosphatidylserine (PS) in the outer leaflet of the infected RBC membrane in increased cytoadherence following a 2h pulse of febrile heat shock [27], which is consistent with the observation by Zhang et al. that the adhesion of infected RBCs to mammalian cells was abrogated by the PS-binding protein, Annexin V [24].

- While evidence for heat shock-induced infected RBC adhesion to endothelial cells mounts, others have found a different dynamic occurs between infected RBCs and surrounding uninfected RBCs. Singhaboot, *et al*. detected a significant decrease in rosette formation in all stages of the IDC under febrile temperatures [29]. However, a caveat of this *in vitro* study design is that parasites were subjected to constant elevated temperatures for 48h, contrary to the cyclical tertian fever see *in vivo* with *P. falciparum* infection [30].

Environmental Differences Impact Parasite Drug Sensitivity

In vitro high throughput screening efforts, such as those conducted with the Medicine for Malaria Venture's Pathogen Box, serve as a starting point for the identification and development of new antimalarial drugs through characterization of anti-*Plasmodium* compound attributes [100, 101]. As with any *in vitro* system, the translatability to *in vivo* efficacy presents a critical hurdle. For example, only 8% of compounds that enter preclinical evaluation end up as part of an antimalarial product [102]. Failure of compounds to exert the same effect *in vitro* and *in vivo* may occur due to a variety physiological differences between these environments; such differences can lead to

competitive selection between genetic variants or more transient transcriptional and metabolic regulation (**Figure 2.1D-F**).

Parasite drug susceptibility can be affected by changes in population genetics brought about by the *in vitro* adaptation process itself. Drug resistance within a human host confers a survival advantage but may exert a fitness cost in the absence of drug pressure. Under *in vitro* conditions, more resistant clones may be outcompeted by faster growing clones in instances of multiplicity of infection (**Figure 2.1F**), leading to drug sensitivities that do not accurately reflect the *in vivo* parasite source population [17, 103]. Chaorattanakawee, *et al*. found *in vitro* culture adapted parasites showed a significant decrease in $\mathbf{EC_{50}}$ concentrations compared to *ex vivo* isolates for all commonly used antimalarial drugs tested, with most drugs showing approximately a 50% increase in sensitivity *in vitro* [104]. If shifts in sensitivity upon *in vitro* cultivation represent a consistent pattern, anticipation of this effect can be used to mitigate its impact by estimating true values. However, another similar study of *ex vivo* versus culture adapted isolates yielded mixed results between drugs [105], meriting further research into this phenomenon.

Drug sensitivity changes may be mediated by competitive selection between genetic variants as mentioned above or, additionally, by more transient transcript regulation. Many antimalarial drugs require active uptake (e.g. chloroquine, [106]) or metabolic activation within parasites (e.g. artemisinin, [107]) in order to exert their effect, and the regulation of these processes may be environmentally altered. For example, Sharma, *et al*. demonstrated resistance to Blasticidin S through reversible epigenetic modulation of transcript levels encoding a protein target necessary for drug uptake (**Figure 2.1E**) [14]. Even barring changes in drug pressure, the transition from *in vivo* to *in vitro* environments leads to numerous transcriptional changes (see *Genomics and Transcriptomics* section), which are relevant for drug uptake, activation, and other effects. For example, in *P. knowlesi*, heme biosynthesis and proteolysis genes were found to be upregulated *in vitro* compared to *ex vivo*, which may alter levels of artemisinin activation or resulting mitigation of protein damage, respectively [108]. However, this possibility was outside of the scope of the study and not explored further.

Compounds that affect *Plasmodium* growth by altering nutrient acquisition may be especially predisposed to discordant *in vivo* and *in vitro* results due to the considerable differences in nutrient concentrations between these environments. For example, the efficacy of ISPA-28 and halofuginone have been shown to be modulated by exogenous levels of isoleucine and proline, respectively (**Figure 2.1D**) [13, 109]. Dynamic parasite

drug sensitivity associated with differing provided nutrients has also been observed with respect to oxygen levels and culture medium choice. Duffy and Avery found O_2 gas levels altered sensitivity to artemisinin and lumefantrine with hyperoxic conditions leading to less tolerance compared to normoxic conditions for both drugs [110]. Additionally, parasites grown in ALB were significantly more sensitive to pyrimethamine and lumefantrine at the early ring stage and more tolerant to artemisinin throughout the trophozoite and schizont stages compared to parasites grown in ALB/Serum combination medium [110]. However, it should be noted that another study published one-decade prior did not observe a difference in parasite susceptibility to common antimalarials between ALB- and human serum-supplemented parasites [111]. These discordant results may be attributable to minor changes in study setup (e.g. use of serum-only supplemented RPMI versus ALB/serum combination supplemented RPMI; stringency of parasite stage synchronicity).

Transcriptomics and Genomics Highlight Sets of Genes that are Environmentally Sensitive

In the current age of cost-effective high-throughput sequencing, genomics and transcriptomics have become invaluable to parse out molecular roles. Recent studies found relatively large transcriptional variation within both *in vivo* and *in vitro* groups [112-114], leading to the question of which genes or sets of genes are sensitive to environmental variation? Transcription of clonally variant RBC surface antigens (e.g. *var, rifin, stevor*) represents the most well-documented change between *in vivo* versus *in vitro* conditions. Downregulation of these antigens has been repeatedly observed following the adaptation of parasites to *in vitro* culture from diverse sources and across laboratory-adaptable *Plasmodium* species (**Table 2.1**). Many host factors are likely responsible for effecting such a dynamic response in parasite antigen transcription, including immunity status and heterogeneity of receptors [115]. Less intuitively, the static nature of most *in vitro* culture systems has recently been shown to decrease expression of these exported RBC antigens relative to suspension cultures, indicating an important role for fluid flow *in vivo* [21]. For example, increased expression in a number of ApiAP2 transcription factors has been observed *in vivo/ex vivo* versus *in vitro* [108, 112, 116]; these expression changes appear to be in part induced by fluid flow as similar patterns of ApiAP2 upregulation were observed in suspension versus static cultures [21]. Of note, the gametocyte conversion ApiAP2 transcription factor, *ap2-g*, as well as other sexual stage-related genes, is among those seen downregulated in culture conditions [21, 108, 112, 116].

Table 2.1. Transcriptional and genetic changes observed during *Plasmodium* transition from *in vivo* to *in vitro* environment.

Publication	*Spp.*	*In vivo* Parasite source	*In vitro* cultivation duration*	Detection Method	Interpretation of data
[86]	*Pf*	CHMI[a] (3D7)	16 days	RT-qPCR	Downregulation of *var* gene transcription *in vitro* with *upsA* subtypes exhibiting a faster decline compared to *upsB* or *upsC* subtypes.
[87]	*Pf*	Clinical	16 days	RT-qPCR	Downregulation of *upsA* and *upsB* subtype *var* gene transcription during initial cycles *in vitro* cultivation. Expression was partially recovered by day ~16.
[108]	*Pk*	Rhesus macaque	Information not provided	Microarray	Genes significantly downregulated *in vitro* were related to proteolysis, radical-based catalysis, a putative ApiAP2 transcription factor, and dozens of *SICAvar* genes. A small number of genes expressed at higher levels *in vitro* were related to metabolism and growth.
[112]	*Pf*	CHMI (NF54)	25+ years	Microarray	Genes in gametocyte (e.g. *AP2-g*), transmission, and clonally variant (e.g. *var, rifin*) clusters were expressed at lower levels *in* vitro versus *in vivo*.
[116]	*Pf*	Clinical	2 weeks — 3 months	Microarray; CGH[b]	Traditional laboratory lines showed lower expression of gametocyte-related genes and exportome members compared to recent field isolates while higher expression of mtDNA-encoded genes was observed. (Clonally variant genes (*var, rifin, stevor*) were excluded from the analysis). Significant chromosomal clustering of many differentially expressed gene was determined to be the result of genomic CNVs
[117]	*Pk*	Rhesus macaque	2 months—1.5 years	PacBio WGS[c]	Adaptation to different *in vitro* environments led to the fixation of CNVs of genes encoding *GTP cyclohydrolase I* and the reticulocyte binding protein, *NBPXa*.
[118]	*Pf*	Clinical	3—4.5 months	Illumina WGS	Adaptation to *in vitro* culture led to independent SNP mutation events in one *ApiAP2* gene. Mutations in this *ApiAP2* gene, as well as *AP2-g*, and *Epac* (a guanine nucleotide exchange factor), were found in multiple traditional laboratory lines but never *in vivo*.

*All summarized studies longitudinally tracked changes that occurred in the same parasite population upon *in vitro* adaptation. *Pf* = *P. falciparum*; *Pk* = *P. knowlesi*; [a]CHMI = Controlled human malaria infection; [b]CGH = comparative genomic hybridization. [c]WGS = whole genome sequencing.

Changes in transcript abundance of some of the above affected genes have been tied to mutations in the genome upon adaptation to *in vitro* culture (**Table 2.1**). MacKinnon, *et al*. investigated genomic duplications and deletions, referred to as copy number variations (CNVs), upon discovering significant chromosomal clustering of differentially abundant transcripts in field versus laboratory-adapted strains [116]. Transcript abundance in the identified chromosomal clusters were found to be attributable to CNVs. Others have similarly found mutations within genes commonly differentially expressed in transcriptional studies of parasites upon laboratory adaptation. For example, nonsense mutations in *ap2-g* are well documented to arise spontaneously *in vitro* (**Figure 2.1C**) [118, 119], where transmission of gametocytes to mosquitos is not necessary for survival and asexual propagation is the primary determinant of fitness.

Other instances of convergent evolution upon *in vitro* adaptation provide further indications of differential selective pressures on metabolism and invasion between the host and laboratory environments. First, genomic amplification of the folate pathway rate-limiting enzyme, GTP cyclohydrolase I, has arisen in both *P. falciparum* and *P. knowlesi* samples adapted to laboratory culture in human RBCs [116, 117, 120], plausibly reflecting an increased need for folate biosynthesis in the absence of the human host. Second, nonsense mutations distinct from those found in clinical isolates arose three independent times in laboratory-adapted clinical samples within the same ApiAP2 transcription factor gene, PF3D7_1342900 [118]. This ApiAP2 is a putative regulator of heat shock genes, which may be less essential *in vitro* in the absence of febrile host temperatures. Finally, evidence suggests parasite invasion of RBCs is also under differential selective pressures *in vivo* versus *in vitro*. The study identifying convergent ApiAP2 mutations also identified a nonsynonymous mutation *in vitro* within *DOC2*, a gene affecting RBC invasion [118]; and another study on adaptation of *P. knowlesi* from rhesus macaque RBCs to human and cynomolgus RBCs resulted in superior invasion by amplification of the reticulocyte binding protein gene, *NBPXa* [117].

Direct-from-Host Methodologies Exhibit Distinct Challenges and Benefits

In vitro culture systems have been invaluable for research progress in the malaria field and still have advantages over *in vivo/ex vivo* samples (**Table 2.2**). However, assays on samples isolated directly from malaria-infected patients have the capability to avoid potentially confounding effects of the laboratory culture environment and save the time and materials needed adapt samples to culture (**Table 2.2**). Additionally, declining cost and the improved sensitivity and specificity of many experimental pipelines, such as RNA-

seq and whole genome sequencing, make analyses of direct-from-host samples increasingly tractable. Here we discuss common direct-from-host methodologies that do not require *in vitro* adaptation to study drug sensitivity, transcription, and genetics.

Table 2.2. Characteristics of different *Plasmodium* parasite sources.

In vitro	***Ex vivo/In vivo***
More reliable for steady procurement of parasites and large quantities of sample	Avoids genetic selection that may reduce heterogeneity
Well controlled parasitemia, stage synchronicity, and parasite viability	Avoids shifts in drug sensitivity due to genetic, transcriptional, or metabolic changes
More practical for experiments requiring equipment not readily available in endemic settings (e.g. metabolomics)	Prevents transcriptional changes upon culture adaptation
Necessary for experiments requiring long-term manipulation or observation (e.g. transfection)	More pronounced parasite cytoadherence characteristics (e.g. higher PfEMP1 presentation)
More feasible selection of immune status and blood group of donors (e.g. Duffy-positive blood for *P. knowlesi* propagation)	The only source currently available for *P. vivax*, *P. ovale*, and *P. malariae*.
IRB (or equivalent) approval not needed	Saves time, resources, and expertise needed to adapt samples to *in vitro* culture
Controlled environment limits sample to sample variability (i.e. gas, temperature, semi-defined media, reduced host contribution)	Reduced risk of findings being parasite line-specific/not broadly applicable

Ex vivo testing of field isolates is a technique used frequently for surveillance of drug efficacy. These methods have been employed not only for *P. falciparum* but have been heavily relied upon for studies of *P. vivax*. Conditions to facilitate high rates of successful *in vitro P. vivax* propagation have yet to be determined, thus, necessitating analyses of samples directly from patients. Testing of parasites is most commonly achieved by combining the infected sample with culture medium in a microwell plate containing a pre-dried concentration gradient of antimalarial drug. After incubation in a candle jar or CO_2 gas incubator for 24-72h, parasite growth is measured by a choice of methods to determine drug EC_{50} [121-124]. While widely used, this EC_{50}-based format is not a one-size-fits-all answer to understanding parasite drug susceptibility. For example, Amaratunga, *et al*. noted a poor correlation between EC_{50} and parasite clearance half-life following treatment with artesunate [125]. Subsequently, Witkowski, *et al*. developed the **ring-stage survival assay** (RSA) for testing of artemisinin derivatives [126]. The RSA protocol achieves readouts that strongly correlate to parasite half-life clearance through a design that takes into account the stage dependent susceptibility of parasites to artemisinin and utilizes a high concentration of drug for a short period of time, which

more closely mimics pharmacokinetics parasites experience *in vivo*. Both *ex vivo* EC_{50} and RSA experiments provide standard readouts that can be directly compared to other data sets. However, it should be noted that factors such as parasite viability can vary greatly in *ex vivo* samples, making the data from these assays sometimes difficult to interpret [122].

Drug sensitivity and parasite heterogeneity can also be captured in direct-from-host samples using polymerase chain reaction (PCR)-based methods. Amplification of parasite-specific gene targets by PCR is conducive to the low input and heavy human white blood cell (WBC) contamination typically found in samples collected in low-resource settings, such as in **dried blood spots (DBS).** These attributes make PCR-based methods useful for resistance mutation surveillance and quantification of parasite diversity prior to bottleneck selection of *in vitro* adaptation (**Figure 2.1F**). PCR-based methods offer

Box 2.2. **Mitigation of human genetic material in direct-from-host samples.**

- Following collection, samples may be depleted of WBCs or directly subjected to nucleic acid extraction (**Figure 2.IA**). Various methods are available to remove WBCs ranging from simple methods, such as filtration through CF-11 cellulose [6], Plasmodipur filters [8], or a combination thereof [9], to more complicated techniques, such as fluorescently activated cell sorting of infected RBCs [12] or *ex vivo* maturation to schizonts for magnetic parasite isolation.

- At the stage if isolated nucleic acids, methylation-dependent restriction endonucleases (MDRE) have been used to selectively degrade human DNA on the premise organisms that do no undergo DNA cytosine methylation, such as *Plasmodium*, are not susceptible to digestion (**Figure 2.IB**). This method may be advantageous for samples where parasite species is unknown or mixed because all *Plasmodium* species are theoretically equally resistant to digestion. However, discordant results have been reported on the benefit of MDRE for *Plasmodium* DNA enrichment with some groups experiencing positive results [15, 16] while other saw no benefit [4, 5].

- Hybrid selection may also be used at this stage to enrich parasite DNA/RNA. This method uses RNA "bait" probes complementary to the genome of the species of interest (**Figure 2.IC**). The RNA bait probes contain biotinylated nucleotides allowing them, along with hybridized *Plasmodium* DNA, to be selectively retained while unbound human DNA is washed away. Hybrid selection has been used to enrich *P. falciparum* and *P. vivax* DNA in clinical samples from 0.1% to 1.0% *Plasmodium* DNA to 30% to >80% *Plasmodium* DNA [18-20]. Hybrid selection was also recently employed in a *Plasmodium* transcriptomics study for the first time to select for parasite genetic material once RNA was reverse transcribed to cDNA [22].

Figure 2.I. Workflow of methods for human contamination mitigation.

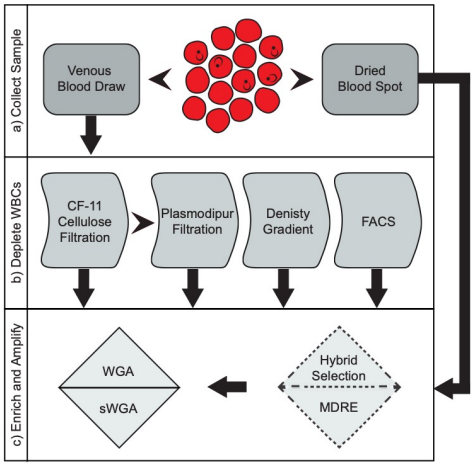

- Finally, parasite nucleic acids can be amplified using either traditional or selective WGA methods (**Figure 2.IC**). Methods for selective amplification of *P. falciparum* [1-4], *P. vivax* [5], and *P. knowlesi* [7] DNA have proven successful at yielding high parasite sequencing coverage from samples with heavy human contamination. Selective whole genome amplification (sWGA) uses specialized polymerases and primers designed to selectively bias amplification of the genome of interest resulting in a higher proportion of reads mapping to the *Plasmodium* genome. This method is particularly useful for samples with low starting DNA where little to no loss of parasite DNA in upstream steps can be tolerated, such as DBS cards [1, 3-5] or single parasites [2].

relatively simple, low-cost analyses of samples, but are limited in utility to the assessment of known targets. For unbiased exploration of parasite samples, 'omics-levels investigations offer an increasing breadth of analysis capabilities. Progressively less material has been required to obtain high quality 'omics results with research groups successfully performing RNA-seq [44, 127, 128] and whole genome sequencing [2, 129-131] on single *P. falciparum* and *P. vivax* parasites. Single-cell approaches are attractive not only because they require less material, which is conducive to *ex vivo/in vivo* sampling, but they also have the ability to capture within population heterogeneity that is frequently missed when analyzing the bulk population. The cost of 'omics methods has decreased considerably in recent years to the point that sample quality, not cost considerations, more frequently limit data acquisition. Abundant "contamination" from human host genetic material hinders the tractability of producing quality, high-coverage results. However, several methods have been developed to reduce the effect of host nucleic acid contamination at the level of both sample preparation and nucleic acid amplification (**Box 2.2**).

For some projects, resources available at collection sites may preclude the depletion of WBCs prior to sample storage; after whole blood samples are stored by cryopreservation or on a dried blood spot card removal of WBCs is no longer an option. Alternatively, in instances of low parasitemia, researchers may wish to forego filtration as some portion of parasite material will be lost during the process. However, additional methods to increase the proportion of *Plasmodium* DNA and RNA in a sample are available (**Box 2.2**). Further selective amplification of the parasite genome can be achieved using a combination of specialized polymerases and primers (**Box 2.2**).

Other 'omics-level methods also suffer from difficulty identifying parasite signal over human host material. Abundance of host proteins and metabolites lead to difficulty, even *in vitro*, generating high quality proteomics [132] and metabolomics [133], respectively. Thus, proteomics and metabolomics on samples directly from hosts have focused on analyzing human serum to infer biology of disease diversity and drug resistance effects through host-parasite interactions [134-139].

Concluding Remarks

Outstanding questions remain about how best to mitigate the effects of environmental differences on experimental design (*see Outstanding Questions*). To better understand the potentially confounding effects of the *in vitro* environment moving forward, the

malaria research community will benefit from the development of more "*in vivo*-like" culturing platforms. A setup similar to the previously used HFBRs, modified for simpler use and made commercially available, would be such an option. More sensitive methods for analyzing the *in vivo* state, such as the ability to purify high numbers of parasites from *in vivo* samples to be analyzed by increasingly sensitive proteomics and metabolomics platforms, will not only drive research progress forward but also allow us to gauge the physiological relevance of specific *in vitro* phenotypes.

Current technologies that have experienced rapid, recent improvement can be strategically used to address remaining questions about parasites reared in different environments. Computational modeling may be employed to help address the lack of uniform control over direct-from-host samples and estimate changes that occur upon transfer from *in vivo* to *in vitro*. For example, mathematical models have been useful to estimate the asexual/sexual blood stage parasite dynamics in a clinical sample, where researcher control over parasite stage makeup is not possible and sequestered subpopulations must be inferred [74, 140]. Additionally, genome-scale metabolic models, informed by transcriptional data collected from clinical parasites, allowed for the appreciation of metabolic characteristics relevant for *in vivo* drug sensitivity [69]. Furthermore, advances in the sensitivity of 'omics-based technology, such as single-cell RNA-seq and whole genome sequencing, may be utilized to quantify and compare levels of heterogeneity within and between *in vitro* and *in vivo* populations (as in [2, 130]). Understanding the diversity within human hosts and comparison to that found *in vitro*, may yield powerful insight on the selective pressures and competition present in each environment.

Outstanding Questions

- Can more *in vivo*-like culture platforms, such as hollow-fiber capillary bioreactors, be designed for simple, wide-spread use?
- Will more *in vivo*-like culture platforms allow faithful recapitulation of physiologically relevant phenotypes seen *in vivo* (i.e. parasite growth, survival, drug sensitivity, and virulence)?
- What are the impacts of the environment on drug uptake, activation, and other effects relevant to parasite drug sensitivity?
- How much genetic and transcriptional heterogeneity exists within *in vivo* parasite populations and how does this compare to levels of heterogeneity *in vitro*?

- Can advances in 'omics technology, such as proteomics and metabolomics, be used to analyze parasite signal in heavily contaminated patient samples to better understand the true *in vivo/ex vivo* parasite state?
- To what extent can computational modeling be used to fill in information gaps about *in vivo* parasite characteristics?

Acknowledgments
Special thanks to Victoria Kelley and Shiwei Liu for assistance with literature curation.

Glossary

Cytoadherence adhesive interactions between an infected RBC and either host endothelial cells or uninfected RBCs leading to sequestration and rosetting, respectively.

Dried Blood Spots an easy, cost-effective method of sample collection where blood is spotted onto filter paper and dried before storage

EC_{50} the concentration of drug required to inhibit 50% of parasite growth relative to an untreated control

Ex vivo typically considered to be the first asexual developmental cycle outside of the host

Gametocytes sexual stages of the *Plasmodium* parasite that are transmissible to the *Anopheles* mosquito vector

Hematocrit the proportion of blood volume occupied by RBCs

Hollow-Fiber Capillary Bioreactors a 3D culture platform that allows continuous perfusion of media and for nutrient/gas exchange through a semi-permeable membrane

Intraerythrocytic Developmental Cycle the portion of the *Plasmodium* lifecycle that takes place within RBCs. One cycle of the asexual IDC in *P. falciparum* takes ~48h.

Knobs small protrusions on the surface of a *P. falciparum* infected RBC that act as sites for PfEMP1-mediated adhesion

Parasitemia the percentage of RBCs infected with a *Plasmodium* parasite

PfEMP1 *a P. falciparum* exported RBC surface protein encode by the multi-copy *var* gene family important for sequestration and antigenic variation

Ring-Stage Survival Assay a standardized assay to assess the percentage of highly synchronous 0-3h post-invasion ring stage parasites that survive a 6h treatment with 700nM dihydroartemisin

Rosettes adhesive aggregation of uninfected RBCs around a *P. falciparum* infected RBC to facilitate immune evasion and thereby increase successful merozoite invasion

Sequestration adhesive interaction of infected RBCs with endothelial cells of the microvasculature leading to removal of parasites from circulation

Chapter 3:
Cholesterol-dependent enrichment of understudied erythrocytic stages of human *Plasmodium* parasites

This chapter has been adapted from the following research article published in *Scientific Reports*:

Brown, A. C., et al. (2020). "Cholesterol-dependent enrichment of understudied erythrocytic stages of human Plasmodium parasites." Sci Rep **10**(1): 4591.

Figures and tables have been renumbered to maintain sequence within this document.

Abstract

For intracellular pathogens, the host cell provides needed protection and nutrients. A major challenge of intracellular parasite research is collection of high parasite numbers separated from host contamination. This situation is exemplified by the malaria parasite, which spends a substantial part of its life cycle inside erythrocytes as rings, trophozoites, and schizonts, before egress and reinvasion. Erythrocytic *Plasmodium* parasite forms refractory to enrichment remain understudied due to high host contamination relative to low parasite numbers. Here, we present a method for separating all stages of *Plasmodium*-infected erythrocytes through lysis and removal of uninfected erythrocytes. The **S**trepto**l**ysin **O**-**Pe**rcoll (SLOPE) method is effective on previously inaccessible forms, including circulating rings from malaria-infected patients and artemisinin-induced quiescent parasites. SLOPE can be used on multiple parasite species, under multiple media formulations, and lacks measurable impacts on parasite viability. We demonstrate erythrocyte membrane cholesterol levels modulate the preferential lysis of uninfected host cells by SLO, and therefore modulate the effectiveness of SLOPE. Targeted metabolomics of SLOPE-enriched ring stage samples confirms parasite-derived metabolites are increased and contaminating host material is reduced compared to non-enriched samples. Due to consumption of cholesterol by other intracellular bacteria and protozoa, SLOPE holds potential for improving research on organisms beyond *Plasmodium*.

Introduction

Malaria, caused by protozoan parasites of the *Plasmodium* genus, is a continuing threat to global health. A total of five *Plasmodium* species cause malaria in humans, with *Plasmodium falciparum* being responsible for the large majority of malaria morbidity and mortality [141]. While the global malaria burden has decreased over the past decade, the emergence and spread of antimalarial resistant *Plasmodium* threatens to undo this progress and emphasizes the dire need to understand more about the biology of this parasite. The current World Health Organization recommendation for treatment of malaria is artemisinin combination therapy [142]. However, clinical resistance has now been reported to both artemisinin and almost all of its partner drugs [38, 39, 143].

All symptoms of malaria, including cyclical fevers and hypoglycemia, occur due to the asexual replication cycle of the parasite within human erythrocytes (**Fig. 3.1A**). Parasites undergo rounds of replication progressing from the ring stage, to trophozoites and schizonts, before rupturing from host erythrocytes to release merozoites, which go on to

invade new erythrocytes and continue the cycle of infection [144]. Many studies aiming to understand the biology of asexual *Plasmodium* are performed only on late stage parasite samples (trophozoites and schizonts). This is due in part to the larger biomass of these stages but also to the existence of effective enrichment methods [145]; erythrocytes infected with late stage parasites can be separated from uninfected erythrocytes by density gradient centrifugation or by using the paramagnetic properties of hemozoin, a byproduct of parasite maturation. The ability to enrich for late stages, thus limiting noise from excess uninfected erythrocytes, has fueled the recent explosion of omics-based studies of late stage *P. falciparum* biology and antimalarial drug action [40, 132, 146-152].

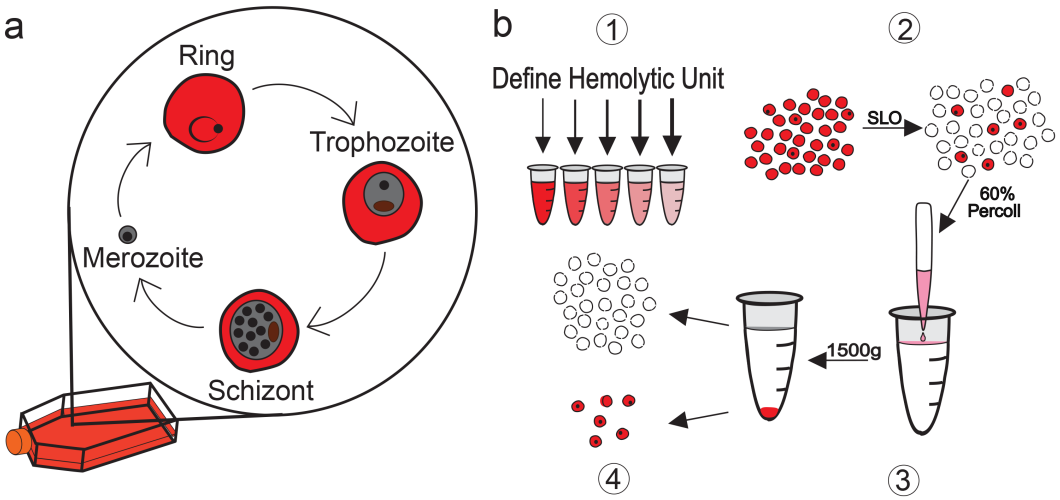

Figure 3.1. SLOPE enrichment overview. (A) The asexual replication cycle of *Plasmodium* occurs inside erythrocytes. Both *P. falciparum* and *P. knowlesi,* which take 48 and 24 hours, respectively, to complete the replication cycle, can be propagated *in vitro* indefinitely. (B1) Hemolytic activity of Streptolysin-O (SLO) was assessed on uninfected erythrocytes to define a unit (the amount of SLO necessary for 50% lysis of 50µl of uninfected erythrocytes at 2% hematocrit in PBS for 30 min at 37°C). (B2) Ring stage synchronized cultures were treated with a defined quantity of SLO units to preferentially lyse uninfected erythrocytes. (B3) SLO treated samples were layered over a 60% Percoll gradient and centrifuged to separate lysed ghosts from intact cells. (B4) The upper layer of Percoll containing lysed ghosts was discarded while the lower, intact, infected erythrocyte enriched fraction was collected. Uninfected erythrocytes, red circles; Infected erythrocytes, red circles with black dots; lysed membranous ghosts, white circle with dashed outline.

The lack of an effective enrichment method dramatically limits our ability to study ring stage parasites, as well as ring-derived forms. For example, recent proteomics and metabolomics studies of this early erythrocytic *P. falciparum* show the heavy influence of host metabolites in non-enriched preparations, which contributes to variability between samples and obscures parasite phenotypes [49, 132, 133]. This limitation is particularly acute when dealing with material directly from malaria patients as only ring forms of *P.*

falciparum are collected during blood draws [77], and there is a high ratio of uninfected host cells to parasite-infected cells (typically 100:<4) [153]. Ample access to clinically-relevant parasites is important for the study of antimalarial resistance especially in the context of artemisinin, which impacts rings differently than later stages through the induction of quiescence [42, 154, 155]. This impactful biological discovery highlights the need to improve upstream purification steps for the study of ring stage biology.

In this study, we present a method for the enrichment of viable asexual *Plasmodium*-infected erythrocytes, including ring stage-infected cells, that is simple to employ, rapid, and non-toxic to the parasite. This method can be scaled to the needs of individual experiments without compromising these attributes. We show that the effective removal of uninfected erythrocytes is unaffected by standard culture media formulations and is conserved across multiple *Plasmodium* species and parasite sources, further highlighting utility for a range of experimental needs. To our knowledge, this is the first enrichment method that is effective on ring stage parasites to increase parasitemia (the percentage of erythrocytes infected with a parasite) and reduce host erythrocyte contamination. The "SLOPE" enrichment method offers a tool to increase research quality in virtually all areas of *Plasmodium* asexual parasite research.

Results

A two-step SLOPE protocol effectively enriches ring-infected erythrocytes

We developed the Streptolysin-O (SLO)–Percoll-based protocol (termed SLOPE) for enrichment of ring stage *P. falciparum* infected erythrocytes (**Fig. 3.1B,** see *Materials and Methods* and **Supplementary Method 3.S1** for protocol details). SLO is a pore forming toxin that preferentially lyses uninfected erythrocytes, leaving the large majority of infected erythrocytes intact [156]. Using the protocol outlined by Jackson, *et al*. with slight modifications, we were able to achieve levels of lysis discrimination for erythrocyte populations that were comparable to this original report (93.4% and 9.9% lysis of uninfected and infected erythrocytes, respectively, **Fig. 3.2A,** yellow highlight). In addition to reproducing lysis levels, we quantified uninfected and infected erythrocyte lysis across a gradient of SLO concentrations. More complete lysis of uninfected cells (>99%) was obtained at the cost of greater infected erythrocyte lysis by increasing SLO quantity. For example, we found that 47U of SLO leads to >99% lysis of uninfected erythrocytes and 40% lysis of infected erythrocytes (**Fig. 3.2A,** grey highlight). Additionally, we show that SLO favors uninfected erythrocyte lysis irrespective of parasite line or culture media (**Fig 3.2A**; **Supplementary Fig. 3.S1**). SLO showed comparable lysis discrimination between uninfected and infected erythrocytes in parasites grown in two common media

formulations, RPMI 1640 supplemented with AlbuMAX II or RPMI 1640 supplemented with 20% human serum (**Fig. 3.2A**, maximum difference between uninfected and infected erythrocyte lysis: AlbuMAX supplementation = 83.5%; serum supplementation = 81.3%). Furthermore, SLO lysis showed considerable discrimination between uninfected and infected erythrocytes for both *P. falciparum* and the zoonotic species, *Plasmodium knowlesi* (**Fig. 3.2A)**.

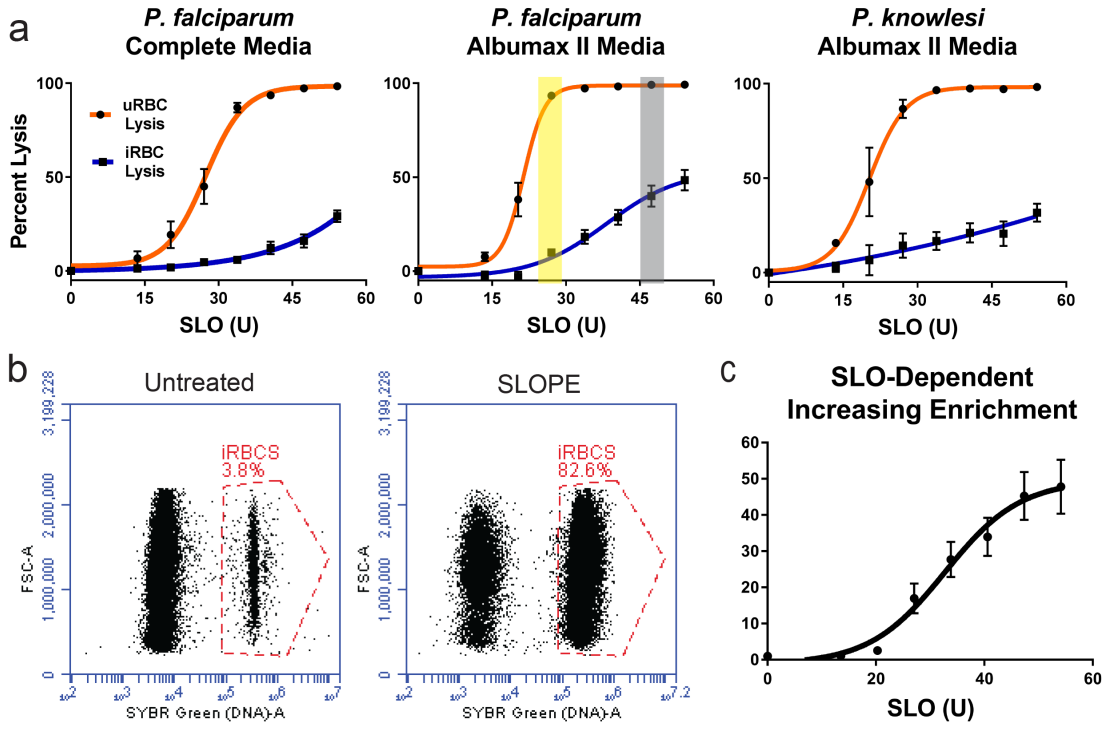

Figure 3.2. SLOPE enriches ring stage *Plasmodium* parasites irrespective of species or media formulation. (A) SLO lysis of uninfected erythrocytes (uRBCs) and infected erythrocytes (iRBCs) from (left) ring-stage synchronized *P. falciparum* grown in RPMI 1640 supplemented with 20% human serum (*N* = 6; 3 replicates each of lines Hb3 and K1), (middle) RPMI 1640 supplemented with Albumax II (*N* = 9; 3 replicates each of lines Hb3, K1, and MRA 1240), and asynchronous *P. knowlesi* grown in RPMI 1640 supplemented with Albumax II (*N*=3). (B) SYBR-Green based flow cytometry measurements before and after SLOPE enrichment. Flow plots show single cells within the erythrocyte size range. The infected erythrocyte fraction ("iRBCs") is denoted within the dashed red gate. (C) Parasitemia fold increase upon treatment with increasing SLO units relative to untreated controls. Represented samples were grown in RPMI 1640 supplemented with Albumax II (*N* = 9; 3 replicates each of lines Hb3, K1, and MRA 1240). All error bars represent S.E.M.

After treatment with SLO, parasite samples contained a mixture of primarily lysed erythrocyte membranes (from uninfected erythrocyte lysis), termed ghosts, and intact erythrocytes (enriched in infected erythrocytes) (**Fig. 3.1B2**). For the second part of the

enrichment protocol, we exploited the difference in density of intact erythrocytes and ghost membranes to separate the two populations (**Fig. 3.1B3**). We found that intact erythrocytes travel through a 60% Percoll gradient during centrifugation while erythrocyte ghosts remained above the Percoll layer (**Fig. 3.1B4**, **Fig. 3.3**). Collection of the intact erythrocyte population leads to a sample with up to a greater than 20-fold increase in the parasite to erythrocyte membrane ratio. In one representative trial, we demonstrate enrichment of ring stage samples to a final parasitemia over 80% (22-fold increase over starting parasitemia, **Fig. 3.2B**). Higher levels of enrichment were attainable with higher amounts of SLO (up to 48-fold with 55 units of SLO, **Fig. 3.2C**) but this is at the cost of parasite material (up to ~40% of infected erythrocytes, **Fig. 3.2A**).

We performed SLOPE on mixed stage populations to determine whether our protocol biases enrichment of certain asexual stages. We found that SLOPE enrichment of lightly synchronized cultures (i.e. contains rings and some residual trophozoites) did not result in any alteration of the ring to trophozoite proportion (**Supplementary Fig. 3.S2**). SLOPE enrichment was also unbiased when performed on asynchronous cultures (includes rings, trophozoites, and schizonts). However, the protocol did result in a non-significant drop in schizont percentage (**Supplementary Fig. 3.S2**). Centrifugation and washes likely lysed fragile schizont-infected erythrocytes resulting in partial loss of the schizont population. Further, SLOPE was effective on rings very early in the erythrocytic cycle (0-3h post-invasion). Early rings showed an average of 16-fold enrichment in parasitemia following SLOPE (Untreated: 0.88% ± 0.061%; SLOPE 13.9% ± 0.64%).

Next, we employed immunofluorescence detection of erythrocyte components to confirm that Percoll gradient density centrifugation removed ghost erythrocyte membranes from SLO treated samples (**Fig. 3.3**). Specifically, we visualized all erythrocyte membranes through detection of an external erythrocyte surface protein (CD235a); we identified ghosts through detection of an intra-erythrocyte protein (spectrin). Untreated (control) samples contain high erythrocyte membrane to parasite ratios (~100:1 due to ~1% parasitemia) as expected, and almost all membranes (>99%) were in the form of intact cells (spectrin negative, **Fig. 3.3A** and **B**). All erythrocyte membranes in samples treated with a nondiscriminatory lytic agent (saponin) were lysed ghosts (spectrin positive); however, the same high erythrocyte membrane to parasite ratio (100:1) that was observed in untreated samples persisted. In samples treated only with SLO (no Percoll gradient centrifugation), a subset of cells enriched for infected erythrocytes remained intact (1 of the 4 erythrocytes in **Fig. 3.3A**). However, the considerable lysed erythrocyte population remained, leaving the erythrocyte membrane to parasite ratio at 100:1. Complete SLOPE enrichment demonstrated the effectiveness of Percoll

centrifugation for separating ghosts and intact cells by removing this lysed erythrocyte population, leaving a >99% intact erythrocyte population that is enriched for parasites (25-fold decrease in the erythrocyte membrane to parasite ratio; starting of 100:1, final of 4:1)**.** Image quantification revealed that <0.2% of erythrocytes in SLOPE enriched samples were ghosts (**Fig. 3.3B**).

Parasites retain full viability after SLOPE enrichment

We sought to test the effect of SLOPE enrichment on parasite metabolism and viability. First, parasites were stained with a mitochondrial membrane potential dependent dye to

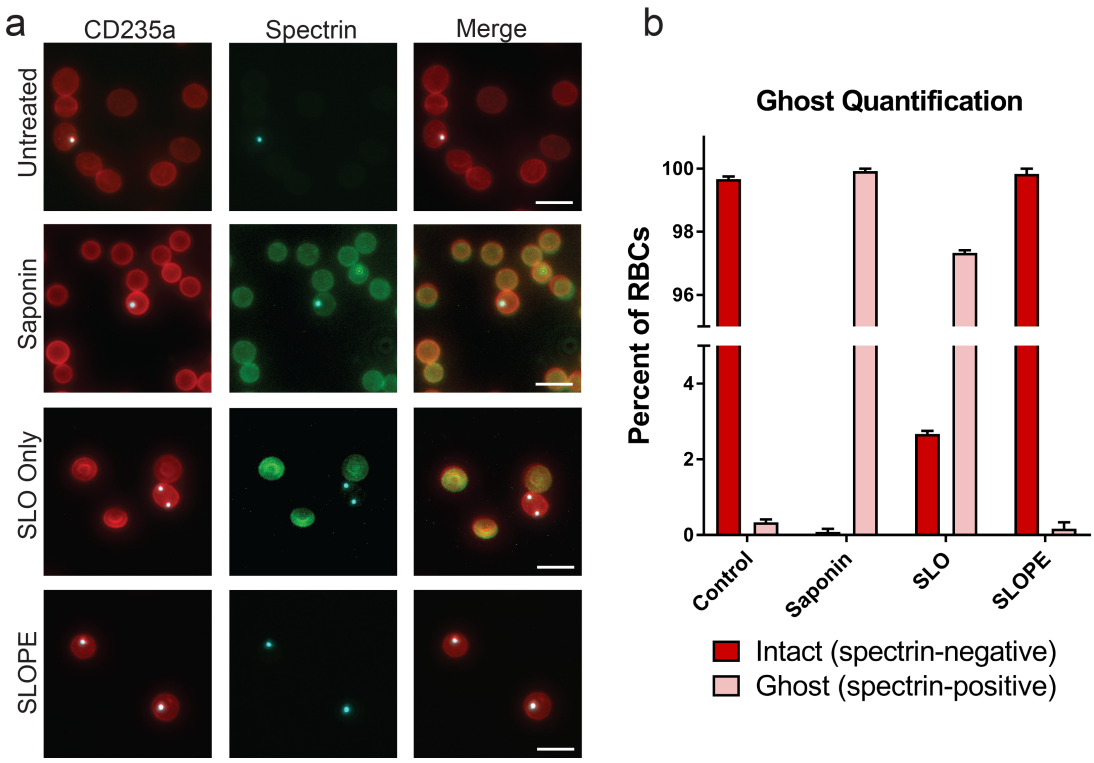

Figure 3.3. Validation of ghost separation from intact erythrocytes by Percoll step. (A) Intact erythrocytes are shown as CD235a (red) positive and spectrin (green) negative. Lysed erythrocytes, termed ghosts, are shown as CD235a and spectrin double positive (yellow in merge). All images show ring-stage *P. falciparum* line MRA 1240 parasites stained with SYBR Green (cyan). 40X Magnification; bar represents 10µm. Saponin samples were treated with 0.15% saponin for 5 minutes. SLO samples were treated with 40U of SLO for 6 minutes but were not centrifuged through a Percoll gradient. SLOPE samples were also treated with 40U SLO but were subjected to Percoll gradient centrifugation (B) Proportions of lysed ghosts and intact erythrocytes quantified from fluorescence microscopy imaging across different treatments using SYBR Green dye and CD235a and spectrin antibodies (*N* = 3; 400 erythrocytes per condition per preparation, error bars represent S.E.M.).

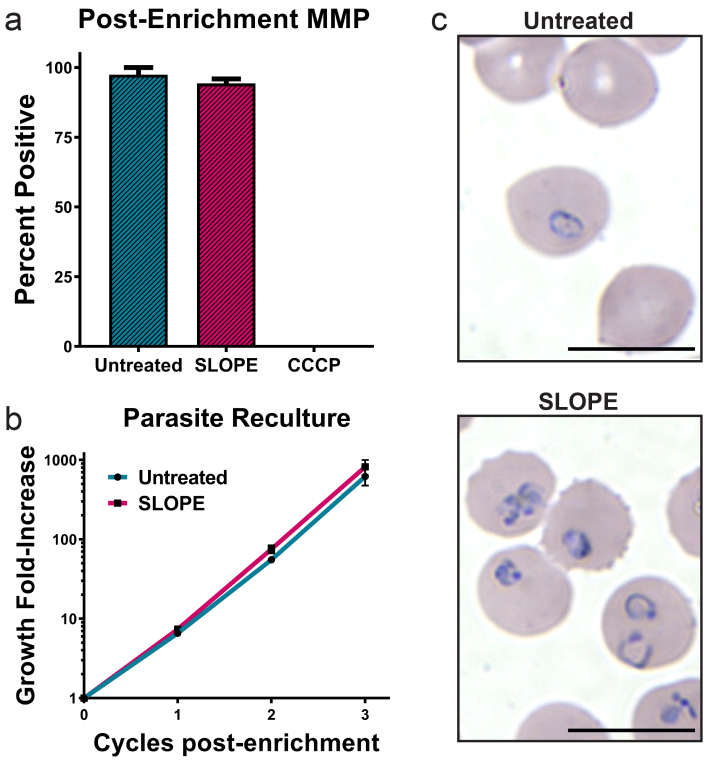

Figure 3.4. SLOPE enriched parasites remain viable. (A) Mitoprobe $DiIC_1$ (5) mitochondrial membrane potential (MMP) measurements obtained by flow cytometry in untreated and SLOPE enriched ring-stage *P. falciparum* line MRA 1240 parasites (*N* = 3, error bars represent S.E.M.). (B) Six days of *P. falciparum* line MRA 1240 parasite growth from untreated controls or SLOPE enriched samples diluted with uninfected erythrocytes (*N* = 4, error bars represent S.E.M.). (C) Ring and early trophozoite stage *P. falciparum* line Dd2 infected erythrocytes visualized by Giemsa-stain at 100X magnification; bar represents 10µm.

determine the fraction of metabolically active parasites. The percentage of parasites with an active mitochondrial membrane potential was not significantly different between SLOPE enriched samples and untreated controls (*untreated*=97%, *SLOPE*=94%, *p*=0.46, **Fig. 3.4A**). To assess parasite viability on a longer-term scale, we monitored parasite growth following SLOPE enrichment. This was accomplished by diluting SLOPE enriched parasites with fresh erythrocytes to reduce parasitemia to appropriate levels for culture (<5%). When compared to that of parasitemia-matched non-enriched, untreated flasks, the growth rate of parasites from SLOPE enriched samples showed no growth defects over the time period measured (6 days for *P. falciparum*; 3 days for *P. knowlesi*) (**Fig. 3.4B; Supplementary Fig. 3.S3**) nor was staging shifted over this time by SLOPE treatment (**Supplementary Fig. 3.S3**). Ring stage parasites retained normal morphology following SLOPE enrichment, further providing evidence that SLOPE enrichment did not damage parasites (**Fig. 3.4C**).

SLOPE-enriched samples exhibit increased parasite metabolites

We hypothesized that a reduction of excess erythrocyte ghosts following SLOPE will lead to increased parasite signal, especially in ring stage samples. In order to investigate this impact, we compared synchronous ring stage *P. falciparum* parasites that were either untreated or SLOPE enriched by 15-fold using a plate-based targeted metabolomics

platform that detects and quantifies up to 180 defined small molecules (*N*=4 per condition, $3x10^8$ erythrocytes per replicate) (**Fig. 3.5A**). One hundred and sixteen metabolites were detected in at least 50% of samples, representing 11 acylcarnitines, 17 amino acids, 5 polyamines, 69 glycerophospholipids, and 14 sphingolipids. Principal component analysis revealed distinct separation of untreated and SLOPE samples indicating a clear contribution of the increased concentration of parasite metabolites (**Fig. 3.5B**). In general, lipids contribute heavily to the separation of untreated and SLOPE groups with phosphatidylcholines having a large impact on the metabolic differentiation of the two groups (**Supplementary Table 3.S1**), which is in line with the observation that this lipid class is dramatically increased in infected erythrocytes [157].

Table 3.1. SLOPE enrichment leads to significant differences in detection of the ring stage metabolome. *Denotes metabolites in the polyamine synthesis pathway.

Metabolites	BH adjusted *p*-value	SLOPE/Control
Polyamines		$\bar{x}$ = 10.3
Putrescine*	0.000848	13.9
Spermidine*	0.000848	11.5
Spermine*	0.00796	5.53
Amino Acids		$\bar{x}$ = 14.8
Alanine	0.0296	13.2
Arginine*	0.0204	6.94
Asparagine	0.0125	12.3
Aspartic Acid	0.0380	20.3
Glutamic Acid	0.0204	25.0
Lysine	0.0380	3.14
Ornithine*	0.0287	2.73
Phenylalanine	0.0204	8.11
Serine	0.0485	8.92
Threonine	0.0204	17.3
Tyrosine	0.0204	20.8
Valine	0.0170	38.7
Glycerophospholipids		$\bar{x}$ = 3.13
lysoPC.a.C16:0	0.0485	1.70
lysoPC.a.C17:0	0.0313	1.40
lysoPC.a.C18:1	0.0249	2.67
lysoPC.a.C18:2	0.0204	3.74
PC.aa.C32.0	0.0290	5.91
PC.aa.C36.1	0.0380	5.29
PC.aa.C38.5	0.0485	3.10
PC.aa.C40.4	0.0289	3.57
PC.ae.C38.0	0.0380	2.36
PC.ae.C38.3	0.0287	2.61
PC.ae.C40.1	0.0447	2.79
PC.ae.C40.4	0.0204	2.40
Sphingolipids		$\bar{x}$ = 5.64
SM.C24.0	0.0290	7.44
SM..OH..C24.1	0.0380	4.58
SM.C24.1	0.0445	4.91
Acylcarnitines		$\bar{x}$ = 2.19
C2	0.0380	3.78
C16	0.0447	0.60

Thirty-two metabolites were significantly different between untreated and SLOPE groups after multiple testing correction (**Table 3.1**). While some conservation of metabolites was expected due to the persistence of erythrocyte membranes, metabolites that significantly differed between groups reflected expected biological differences associated with increased parasite signal. SLOPE enriched samples exhibited a substantial increase in 12 glycerophospholipids and 3 sphingolipids (3.13 and 5.64 average fold change, respectively, **Table 1**), which was likely due to the contribution of parasite membranes and other lipid-containing structures in parasitized erythrocytes

[158]. Twelve amino acids were higher in SLOPE samples (14.8 average fold change, **Table 3.1**), indicative of the breakdown of hemoglobin by the parasite into free amino acids [159]. Additionally, metabolites of the polyamine synthesis pathway, which is active in the parasite [160, 161], were dramatically increased (10.3 average fold change, **Table 3.1**).

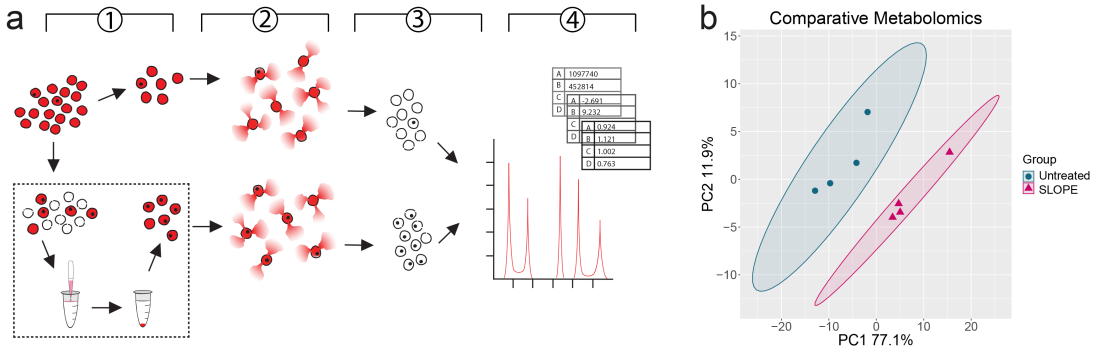

Figure 3.5. SLOPE enrichment increases detection of ring stage parasite metabolome. (A) Pipeline outlining metabolomics sample preparation and analysis. 1) Ring-stage synchronized *P. falciparum* Dd2 cultures were split into two fractions: one portion was taken for the untreated group and one portion was SLOPE enriched. 2) Equal numbers of erythrocytes from untreated and SLOPE groups were saponin lysed and washed to remove cytosolic erythrocyte metabolites. 3) Metabolism of the resulting pellet containing erythrocyte ghosts and parasites was quenched and metabolites were extracted. 4) Metabolites were identified and quantified from extracts using the AbsoluteIDQ p180 kit. These data were log transformed, centered, and scaled prior to statistical analysis. (B) Principal component analysis was performed on all metabolites detected in at least 50% of samples. Significance between untreated and SLOPE groups was determined by perMANOVA: p=0.037. Ellipses show 95% confidence intervals.

SLOPE enriches clinical samples in a cholesterol dependent manner

In order to determine the utility of SLOPE for the enrichment of clinical *P. falciparum* parasites, which predominantly circulate as ring stages, we tested SLO lytic discrimination between infected and uninfected erythrocyte populations directly from human patients. Contrary to results with *in vitro* propagated parasites (**Fig. 3.2A**), patient erythrocytes demonstrated reduced SLO lytic discrimination (**Fig. 3.6A**, left panel). However, short-term (6h) incubation of clinical samples in complete media (RPMI with 20% human serum) greatly increased SLO lytic discrimination, thereby decreasing parasite loss leading to a higher possible final parasitemia (**Fig. 3.6A**, right panel). Restoring SLO discrimination occurred with as little as 4h of *ex vivo* incubation but the benefit peaked at ~6h (**Supplementary Fig. 3.S4**).

We hypothesized that the reduced SLO lytic discrimination observed in samples upon immediate acquisition from patients was due to the increased abundance of cholesterol *in vivo* compared to *in vitro* media formulations. As expected, the *in vivo* environment contained cholesterol at concentrations up to ~250 times higher than those found *in vitro*

(**Supplementary Table 3.S2**). To test the exchange of cholesterol between serum and erythrocyte membranes, we compared the SLO lysis of laboratory *P. falciparum* grown in complete media to parasites grown in complete media supplemented with cholesterol (**Fig. 3.6B**). This artificial addition of cholesterol led to the predicted increase in infected erythrocyte SLO lysis, closely mimicking the reduced SLO lytic discrimination observed upon immediate acquisition of clinical samples from patients (47.5% lysis and 47.8% lysis in clinical *ex vivo* and cholesterol supplemented *in vitro* samples, respectively, when treated with ~30U SLO; **Fig. 6**, black circles).

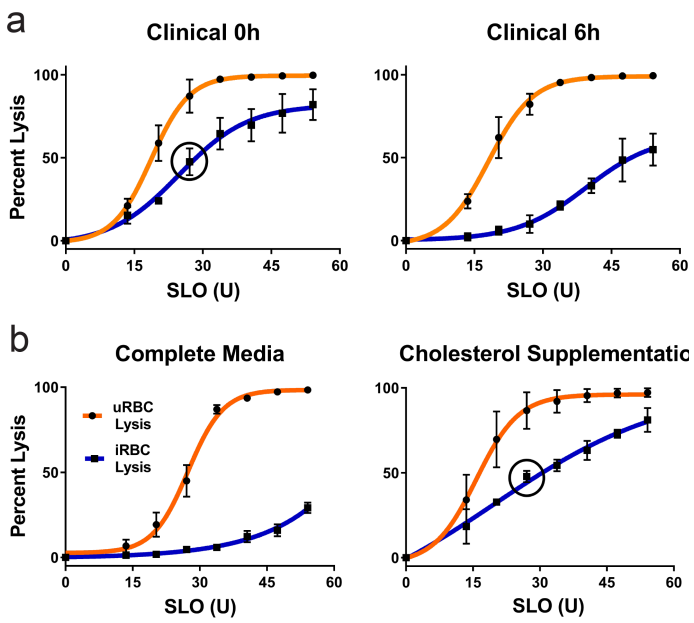

Figure 3.6. SLOPE is effective on clinical samples in a cholesterol dependent manner. (A) SLO lysis of erythrocytes from *P. falciparum* infected patients either directly isolated from the patient (0h) or after 6h of incubation in complete media (RPMI supplemented with 20% serum). *N*=3 patients. Error bars represent S.E.M. (B) SLO lysis of laboratory *P. falciparum* either grown for 48h in complete media or complete media supplemented with 4mM cholesterol saturated mβCD. *N*=6 (left; 3 replicates each of lines Hb3 and K1); *N*=3 (right; line Hb3). Error bars represent S.E.M. Black circles in selected graphs show iRBC lysis at 27U SLO.

SLOPE enriches in vitro-derived quiescent parasites

A low frequency of ring stage *P. falciparum* parasites has been reported to enter a quiescent state upon artemisinin treatment. In order to explore the effectiveness of our enrichment method on non-traditional erythrocytic forms of the parasite, we treated parasites with dihydroartemisinin (DHA), removed actively growing parasites daily, and then performed SLOPE to enrich the remaining metabolically quiescent parasites. When quiescent parasites were quantified using flow cytometry (SYBR-Green positive/MitoProbe positive), we detected an enrichment in quiescent parasites by >100-fold (pre-enrichment: undetectable but estimated based on previous studies to be ~0.005 quiescent parasites/100 erythrocytes [43]; post-enrichment: 1 quiescent parasite/100 erythrocytes). Quiescent parasites were also readily visually identifiable in SLOPE enriched samples under microscopy (**Fig. 3.7A,** SYBR-Green/MitoTracker Red positive). When compared to untreated rings, quiescent parasites showed reduced MMP staining area, indicative of the condensed cytoplasm and

reduced metabolism seen in quiescence [162, 163]. While quiescent parasites were enriched by the removal of uninfected erythrocyte material, erythrocytes containing dead parasites were also enriched by this process (**Fig. 3.7A and B**, SYBR-Green positive, Mitotracker/Mitoprobe negative parasites). However, live, quiescent parasites appeared to be enriched at considerably higher rates compared to their dead counterparts. Specifically, the dead parasite population experienced less than 10-fold enrichment (1.2% immediately pre-SLOPE versus 9.1% post-SLOPE), whereas mentioned above, quiescent-infected erythrocytes were enriched by >100-fold. Overall, ~one-tenth of total enriched parasites (SYBR-Green positive events) were quiescent (Mitoprobe positive events) (**Fig. 3.7B**), despite estimates that <<1% of all parasites enter quiescence upon DHA treatment [43].

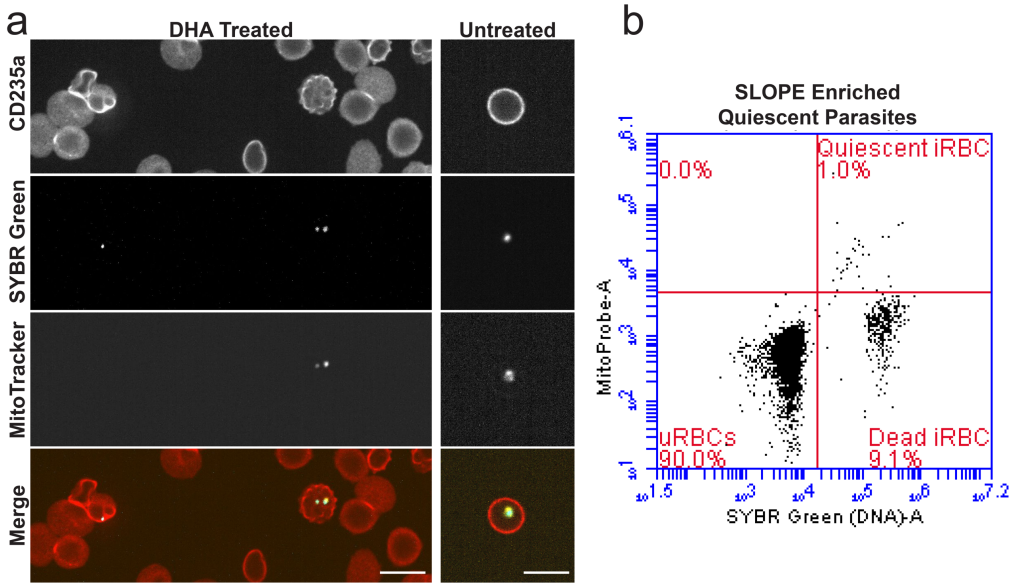

Figure 3.7. SLOPE is effective on DHA-induced quiescent parasites. (A) Erythrocytes are shown by CD235a staining and *P. falciparum* MRA 1238 parasites are shown by SYBR Green. Within the DHA-treated image, a dead parasite (left) failed to accumulate MitoTracker Deep Red, while two quiescent parasites accumulated MitoTracker Deep Red. 63X magnification; bar represents 10µm. (B) Flow cytometry plot measuring quiescent parasites as SYBR Green and Mitoprobe double positive events. Dead parasites are SYBR Green positive, but Mitoprobe negative; uninfected erythrocytes (uRBCs) are SYBR Green and Mitoprobe double negative. iRBC = infected erythrocyte.

Discussion

For the first time, we can achieve considerable parasite enrichment of all asexual stages, including rings, that is effective across a variety of conditions and *Plasmodium* species (**Fig. 3.1**; **Fig. 3.2**), as well as on understudied ring-related populations (clinical isolates, **Fig. 3.6**; quiescent forms, **Fig. 3.7**). Our two-part SLOPE enrichment relies on the

cholesterol-dependent lysis of uninfected erythrocytes, followed by the exploitation of density differences between a parasite-rich intact population and a ghost population of primarily uninfected erythrocyte membranes (**Fig. 3.3; Fig. 3.6**). Importantly, resulting enriched infected erythrocytes maintain active metabolism and growth (**Fig. 3.4; Fig. 3.5; Table 3.1**).

The SLOPE method expands on a discovery made over a decade ago[156] and integrates our metabolic knowledge about the parasite. *Plasmodium* species lack the ability to synthesize cholesterol *de novo* and therefore, the parasite scavenges this lipid from host erythrocyte membranes [164]. This scavenging likely leads to the lower levels of cholesterol observed in infected erythrocyte plasma membranes [158]. Upon discovery of the preferential action of SLO on uninfected erythrocytes, reduced levels of cholesterol in the membranes was proposed as the mechanism of discrimination [156]. Our study on parasites from a cholesterol rich environment and the impact of cholesterol addition on SLOPE effectiveness add validity to this hypothesis (**Fig. 3.6B**). We showed that when parasites were isolated from the human patient (100% serum), SLO discrimination was nominal. Since cholesterol is readily exchanged between the serum environment and erythrocyte membranes [165], we predict that this result is due to the replenishment of parasite-scavenged cholesterol in the erythrocyte membrane (**Fig. 3.8**). While enrichment of parasites directly from the bloodstream of a patient is possible, this is at the expense of parasite number (**Fig. 3.6A**, **Supplementary Fig. 3.S4**). Fortunately, parasite loss can be minimized with a short-term incubation in the laboratory to reduce erythrocyte membrane cholesterol levels; the limited duration (≤6h) and use of 20% human serum during this step will likely allow parasites to maintain *in vivo* qualities (e.g. transcription and metabolic program). Further studies will be required to determine if this is the case. Additionally, our demonstration of SLOPE enrichment on rings within 3 hours of invasion indicates cholesterol changes on the host erythrocyte membrane occur upon invasion or shortly thereafter, further revealing the dynamics of cholesterol exchange in this system.

SLOPE shows utility for the enrichment of non-traditional populations of *Plasmodium* parasites that were previously understudied due to limited accessibility. In previous studies, clinical parasites were often fully adapted to *in vitro* culture to generate enough material for characterization [47, 126]. This is not ideal considering parasite populations are altered by the selective pressure and environmental changes upon transition to *in vitro* culture [118, 166, 167]. Further, a sizeable portion of clinical isolates fail entirely to adapt to *in vitro* conditions [168]. With the direct enrichment of parasites from patients, many studies can now be performed with minimal perturbations (see above) or without culture adaptation entirely.

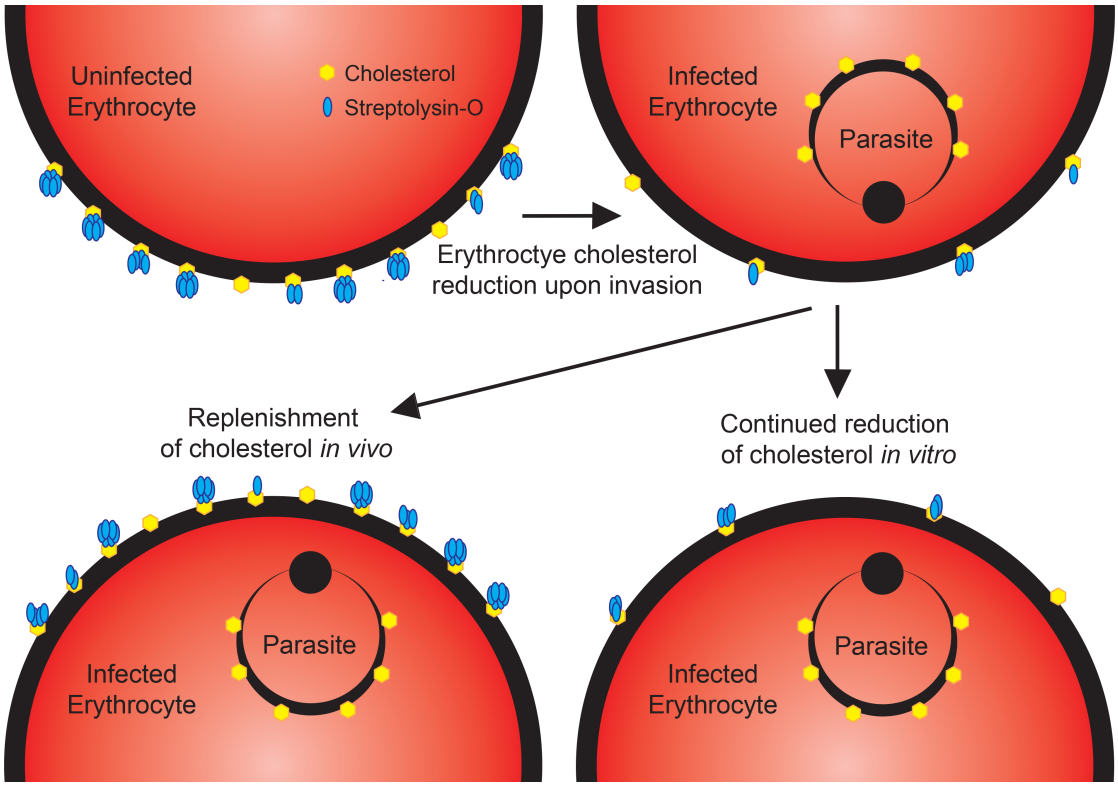

Figure 3.8. Proposed mechanism for decreased susceptibility of infected erythrocytes to SLO lysis. Upon invasion of an erythrocyte, the parasite salvages host membrane cholesterol leading to lower cholesterol levels on the infected erythrocyte surface (top of diagram). During *in vitro* incubation in conditions with sub-physiological cholesterol levels, cholesterol remains low via continued parasite scavenging. Upon exposure physiological levels of cholesterol, such as *in vivo,* the exchange of cholesterol between plasma and erythrocytes restores erythrocyte cholesterol to near pre-invasion levels.

Another form of *P. falciparum* that remains understudied is the artemisinin-induced quiescent state that is somewhat analogous to persister cells seen in bacteria [169]. Populations of both quiescent parasites and bacterial persisters demonstrate arrested growth leading to decreased susceptibility in the face of stressful conditions, such as drug treatment. Quiescent and persister metabolic states share similarities as well, including downregulation of DNA replication, tRNA synthesis, and oxidative metabolism but maintenance of fatty acid synthesis [53]. Following stressor removal, both populations have the ability to resume growth leading to a recrudescent infection. Parasite recrudescence following quiescence presents a challenge to the efficacy of antimalarial therapies. Yet, the rarity of quiescent parasites following drug treatment (<<1% of all parasites, [43]) limits the study of this phenomenon. Excitingly, SLOPE enrichment increases the parasitemia of quiescent parasites to readily detectable levels (~1%) through both the reduction of uninfected erythrocytes and the partial reduction of erythrocytes containing dead parasites (**Fig. 3.7**). At detectable levels, it is feasible to

further enrich quiescent parasite populations using other methods (i.e. fluorescence activated cell sorting). The increased enrichment preference for live, quiescent parasites over dead parasites is likely due to the loss of cholesterol metabolism in parasites upon death. While quiescent parasites down-regulate many aspects of metabolism [162], these data indicate that quiescent parasites continue the utilization of cholesterol.

The utility of SLOPE enrichment in increasing access to both *in vitro* rings and non-traditional parasite forms (quiescent parasites and clinical rings) will reduce many of the previous barriers to high-quality *Plasmodium* research. Lack of an effective enrichment method for ring stage *Plasmodium* has led to considerable host-contributed noise in samples, limiting the success of sensitive downstream analyses such as proteomics and metabolomics. Specifically, our previous work demonstrated that characteristics of the erythrocyte batch contributed to the resultant ring parasite metabolome as heavily as drug treatment [133]. Additionally, erythrocyte noise stymied previous ring stage metabolomics and proteomics experiments as parasite-derived signals could not reliably be determined over the host erythrocyte contribution [49, 132, 133]. Since parasitemia was low in these studies (~1-5 parasites per 100 erythrocytes), this was undoubtedly due to the high number of erythrocyte ghost membranes that remained in the preparations. SLOPE significantly reduces the number of ghosts in our preparations, thus drastically increasing parasitemia (up to >80% in some cases, **Fig. 3.2B**). We directly observed this increase in parasite specific metabolites over the host erythrocyte noise using targeted metabolomics (**Fig. 3.5B**, **Table 3.1**). Most notably, we detected an increase in metabolites of the polyamine synthesis pathway that was proportional to the parasite enrichment level (mean of ~10-fold and 15-fold, respectively). Uninfected erythrocytes lack the machinery necessary for polyamine synthesis and contain only low levels of putrescine, spermidine, and spermine [170]. However, polyamine levels are much higher in proliferating cell, such as *Plasmodium*, which both scavenge and synthesize polyamines [160, 161]. Given the association between parasite number and polyamine concentration, we propose to use this group of metabolites as a quality control marker for parasite-derived metabolites in future metabolomics investigations.

The SLOPE method has several advantages for the isolation of material to be used for sensitive downstream analyses. Firstly, our method can be performed rapidly (~30-40 min). This is equal to or faster than the amount of time needed to perform the field-accepted purification method for isolation of late stage parasites by magnetic column purification (~30min to 1hr). The rapid purification ensures the cellular state of samples is as close as possible to the true phenotype. Secondly, this method is highly scalable and can be used on culture amounts that range from a fraction of a milliliter to combined

pools of many flasks (hundreds of milliliters). Finally, SLOPE enrichment is facile and only requires access to a few reagents and a standard centrifuge. While a fluorescence-based flow cytometer and an automated brightfield cell counter were used to perform the experiments in this paper, less costly devices, such as a microscope and hemocytometer, respectively, can be used. The addition of SLOPE to our laboratory toolset will be useful not only for proteomic and metabolomics studies (see above) but also genomic and transcriptomic analyses. Reduction of contaminating host DNA and RNA that remain associated with erythrocytes relative to parasite material will lead to increased sequencing coverage particularly in clinical samples, which contain a considerable human contribution [171].

One caveat of this method may be the cost of SLO lytic agent. Researchers seeking to regularly enrich large quantities of parasites may consider in-house isolation of SLO from *Streptococcus pyogenes* culture or recombinant SLO expression in *Escherichia coli* in place of purchasing commercially available SLO. An additional caveat of SLOPE enrichment is the loss of parasite material. However, due to the scalability of this method, starting material can be increased to compensate for this loss. When sample material is limited, researchers may wish to use lower quantities of SLO to minimize lysis of infected erythrocytes. The efficacy of SLOPE enrichment on multiple *Plasmodium* species, increases the utility of this method. However, only infected human erythrocytes were tested in this study. The use of SLOPE on non-human erythrocytes, such as *P. knowlesi*-infected macaque erythrocytes, may require additional optimization.

With SLOPE enrichment as a tool, researchers can more accurately study the ring stage of the *Plasmodium* erythrocytic cycle. Improvements in our understanding of parasite biology will lead to more effective treatments for this deadly disease. Beyond this use, SLOPE has the potential to be extended to other intracellular parasites and cell types. Many Apicomplexan parasites scavenge cholesterol from host cells. For example, asexual replication of *Toxoplasma gondii* within nucleated cells requires cholesterol scavenging with cholesterol being transferred from the host cell membrane to the parasitophorous vacuole immediately upon invasion [172]. This presents the possibility that other cells types infected with cholesterol scavenging parasites will also display increased resistance to SLO lysis. Further, SLO causes cholesterol dependent membrane lysis in cell types other than erythrocytes [173, 174]. Thus, the SLOPE method shows potential for the enrichment of cells infected with other intracellular, cholesterol-scavenging pathogens, including *Toxoplasma*, *Cryptosporidium*, *Theileria, Chlamydia,* and *Mycobacterium.*

Materials and Methods

Parasites and growth

Plasmodium falciparum lines (MRA-155 (Hb3), MRA-159 (K1), MRA 150 (Dd2), MRA 1240, and MRA 1238, use of respective lines are indicated in figure legends) were obtained from the Malaria Research and Reference Reagent *Resource* Center (MR4, BEI Resources); The human erythrocyte-adapted *Plasmodium knowlesi* line (yH1, [175]) was a gift from Manoj Duraisingh (Harvard University T.H. Chan School of Public Health). *Plasmodium* cultures were maintained in A+ human erythrocytes (Valley Biomedical, Winchester, VA) at 3% hematocrit in RPMI 1640 HEPES (Sigma Aldrich, St Louis, MO) supplemented with either 0.5% Albmumax II Lipid-Rich BSA (Sigma Aldrich, St Louis, MO) and 50 mg/L hypoxanthine (Thermo Fisher Scientific, Waltham, MA) or with 20% heat inactivated human serum (cRPMI) (Valley Biomedical, Winchester, VA). Cultures were grown at 37^{o}C under 5% oxygen, 5% carbon dioxide, 90% nitrogen gas [176]. Dilution of cultures with uninfected erythrocytes to maintain parasitemia at <5% was performed every other day as was changing of culture medium. Parasitemia was determined by flow cytometry using SYBR-Green staining [177]. Cultures were confirmed negative for mycoplasma monthly using a LookOut Mycoplasma PCR detection kit (Sigma Aldrich, St Louis, MO).

Parasites from infected patients were obtained from adults admitted to the University of Virginia Health System with clinical malaria. All patients had a recent history of travel to a malaria-endemic African country, and *P. falciparum* infection was clinically determined by a positive rapid diagnostic test and peripheral blood smear analysis. Samples were obtained within 24h of phlebotomy and washed twice with RPMI 1640 HEPES to remove white blood cells. Erythrocytes were then either immediately used for experiments or kept under short-term *in vitro* culture conditions in cRPMI.

Ethical Approval and Waiver for Informed Consent

Ethical approval for this study was provided by the University of Virginia Institutional Review Board for Health Sciences Research. All samples were handled in accordance with approved protocols and carried out in agreement with ethical standards of the Declaration of Helsinki. A waiver for informed consent was provided by the University of Virginia Institutional Review Board for Health Sciences Research as our study design met the following criteria: 1) The research involves minimal risk to subjects. 2) The waiver will not adversely affect the rights and welfare of subjects. 3) The research could not practicably be carried out without the waiver. 4) Where appropriate, subjects will be provided with additional information.

SLO activation and storage

Streptolyisn-O (SLO, Sigma Aldrich, St Louis, MO) activation was performed as previously described [156]. Following activation, SLO was stored in aliquots at -20^{o}C until use. Hemolytic units (U) of each SLO batch were quantified from a stored aliquot; one unit equals the amount of SLO necessary for 50% lysis of 50μl uninfected erythrocytes at 2% hematocrit in PBS for 30 min at 37^{o}C. Hemolytic activity was recurrently assessed (approximately monthly) in triplicate to control for SLO degradation over time and varying cholesterol levels contributed by different media batches.

SLOPE enrichment

When required, *P. falciparum* cultures were synchronized to the ring stage prior to enrichment using one round of 5% D-sorbitol (Sigma Aldrich, St Louis, MO) [178]. SLO lysis was performed as previously described but with modifications [156] (**Fig. 3.1B; Supplementary Method 3.S1**). Briefly, erythrocyte density was measured using a Cellometer Auto T4 (Nexcelom Biosciences, Lawrence, MA). Cell density was adjusted to 2x10^{9} erythrocytes/mL. The desired amount of SLO (between 0U and 55U) was added in a ratio of 2 parts SLO solution to 5 parts erythrocytes. Samples were mixed well by pipetting and incubated at room temperature for precisely 6 min. Five-10 volumes of 1X PBS or non-cholesterol containing media (ex. RPMI 1640 HEPES) were added and cells were centrifuged at 2,500xg for 3 min. After removal of the supernatant, cells were washed twice more with 1X PBS or non-cholesterol containing media. Following SLO lysis, cells suspended in 1X PBS were layered onto a 60% Percoll gradient (Sigma Aldrich, St Louis, MO) and centrifuged at 1,500xg for 5-10 min depending on the volume of the gradient. The top layer of Percoll was discarded while the lower cell pellet was collected and washed twice with 1X PBS or media.

SLO lysis curves

Plasmodium were treated with a range of SLO units as described above. Flow cytometry was used to assess equal volumes of each sample for every experiment on a BD Acurri C6 flow-cytometer (BD Biosciences, San Jose, CA.). Total erythrocyte values were obtained by gating for intact erythrocytes based on forward and side scatter. Infected erythrocyte values were obtaining by gating for SYBR-Green positive intact erythrocytes. Uninfected erythrocyte values were obtained by subtracting infected erythrocyte values from total erythrocyte values. Percent lysis of uninfected and infected erythrocyte populations were determined by comparing the infected and uninfected erythrocyte values for each SLO-treated sample in an experiment to the untreated control.

Ghost Quantification

CD235a is constitutively present on the erythrocyte outer surface and thus, both intact erythrocytes and lysed ghosts are CD235a+. Conversely, spectrin is located in the erythrocyte cytoskeleton meaning anti-spectrin cannot access the antibody target in intact erythrocytes. However, pores in lysed erythrocyte membranes (saponin or SLO treated) allow passage of antibodies into the erythrocyte cytosolic compartment making these cells spectrin+. For fluorescent imaging, unfixed samples (average parasitemia of 1%) were blocked with 2% BSA followed by staining in suspension with a 1:100 dilution of mouse anti-alpha I spectrin antibody (Abcam, Cambridge, MA) at $2x10^7$ erythrocytes/mL. Samples were washed then incubated with the fluorescently conjugated secondary antibody, goat anti-mouse Alexa Fluor 594 (Abcam, Cambridge, MA) at 1:1000 dilution. Following additional washes, samples were incubated with the fluorescently conjugated CD235a-PE antibody (Thermo Fisher Scientific, Waltham, MA) at 1:100 and SYBR Green (Thermo Fisher Scientific, Waltham, MA) at 1:10,000. A wet mount was prepared on microscope slides, and samples were immediately imaged. Images were acquired on an EVOS FL Cell Imaging System (Thermo Fisher Scientific, Waltham, MA) using RFP, GFP, and Texas Red light cubes.

Brightfield Microscopy

Slides for brightfield imaging were prepared by fixation in methanol for 1 minute prior to the addition of Giemsa stain for 20 minutes (Sigma Aldrich, St Louis, MO). Brightfield images were obtained on an Eclipse Ci microscope (Nikon, Melville, NY) using an ImagingSource microscope camera and NIS Elements Imaging Software (Nikon, Melville, NY). For parasite stage quantification, slides were prepared for brightfield microscopy as described above both prior to and after SLOPE enrichment. Parasites were categorized by eye as either a ring, trophozoite, or schizont. In the case of a multiply infected erythrocytes, all parasites were counted separately. Gametocytes were excluded from counting.

Enrichment of 0-3h post-invasion rings

Cultures containing only parasites within 3 hours of invasion were generated using a modified version of the "*Preparation of 0-3h post-invasion rings*" protocol [179]. Briefly, 35-mL cultures of *P. falciparum* line Dd2 were grown *in vitro* at 4% hematocrit with media changes daily to 4% parasitemia with ≥50% rings. Cultures were synchronized with 5% D-sorbitol and allowed to progress until the culture was determined by Giemsa stain to be ≥0.5% schizonts. Schizonts were isolated by layering 4mL of culture over 4mL 75% Percoll, centrifugation, and collection of the intermediate band. Isolated schizonts were washed with media then added to uninfected erythrocytes. Exactly three hours later, a rapid D-

sorbitol synchronization was performed (10m at 37 ^{o}C followed by 5s vortex) to remove any uninvaded late stage parasites. Cultures were then SLOPE enriched using 40U SLO. Data mentioned in the text are mean ± SEM.

Re-culturing of SLOPE enriched parasites

P. falciparum cultures were synchronized using 5% D-sorbitol immediately prior to use. *P. knowlesi* parasite cultures were left asynchronous. A fraction of culture was split to <1% parasitemia and 3% hematocrit to generate an untreated control flask, while the remaining volume of culture was enriched according to the SLOPE protocol described above. Following enrichment, the parasite density was measured by SYBR-Green based flow cytometry and a "SLOPE" flask was seeded with the number of the enriched cells necessary to match the parasite density of the respective untreated control flask. Uninfected erythrocytes were added to the SLOPE flask to bring hematocrit up to 3%. The parasitemia of the flasks was measured every replication cycle for 3 replication cycles. Untreated and SLOPE flasks were diluted every 48h to maintain parasitemia levels under 5%. For each dilution event, both flasks were subjected to the same dilution factor. Percentage of rings in *P. falciparum* re-culture experiments was determined by SYBR Green-based flow cytometry and confirmed by microscopy of Giemsa stained smears. The stage makeup of *P. knowlesi* re-cultures was determined solely by microscopy of Giemsa stained smears. The significance between groups was calculated in Graphpad Prism using a paired t-test or a two-way ANOVA where appropriate.

Mitochondrial membrane potential measurements

The mitochondrial membrane potential (MMP) was assessed using the MitoProbe DiIC1(5) kit (Thermo Fisher Scientific, Waltham, MA). MitoProbe DiIC1(5) accumulates in eukaryotic mitochondria in a mitochondrial membrane potential-dependent manner [180]. The effect of SLOPE enrichment on MMP was tested using ring stage synchronized *P. falciparum* cultures. Following SLOPE enrichment, parasites were incubated with 50nM Mitoprobe $DiIC_1$ (5) in media at ~$1x10^6$ parasites/mL for 30 min at 37^{o}C. Negative controls were treated with the oxidative phosphorylation uncoupler, Carbonyl cyanide m-chlorophenyl hydrazone (CCCP) (Thermo Fisher Scientific, Waltham, MA). Untreated positive controls and were assayed alongside enriched samples. Samples were co-stained with SYBR Green and analyzed using 488nm (for SYBR-Green) and 640nm (for Mitoprobe) filters on a BD Accuri C6 flow cytometer. The percentage of MMP positive parasites was determined as the ratio of Mitoprobe positive to SYBR-Green positive events. The significance between SLOPE treated and untreated groups was calculated in Graphpad Prism using a paired t-test.

Targeted Metabolomics

P. falciparum parasites were synchronized using D-sorbitol 40h prior to sample collection and again, immediately prior to sample collection. Synchronized cultures at 3% parasitemia were either taken directly from culture for untreated samples or were SLOPE enriched to 45% parasitemia. $3.5x10^8$ erythrocytes were taken per sample. Samples were lysed in 0.15% saponin as previously described [181]. A series of three wash steps was then performed on all samples using PBS to remove soluble erythrocyte metabolites. Metabolites were immediately extracted from the lysed pellet according to the Biocrates p180 Cell Lysis standard operating procedures. Briefly, pellets were resuspended in ice-cold ethanol/0.01 M phosphate buffer (85:15, v/v). Samples were sonicated for 3 minutes, then snap frozen in liquid nitrogen for 30 seconds. Sonication and freezing were repeated followed by a final sonication and centrifugation to pellet insoluble material. The supernatant was taken and stored at -80^{o}C until the day of use (<2 weeks from extraction).

Metabolite extracts were run using the AbsoluteIDQ p180 kit according to the user manual (Biocrates Life Sciences AG, Innsbruck, Austria). Samples were added to filter spots in each well along with provided internal standards and placed under a gentle stream of nitrogen gas to dry. Fresh phenyl isothiocyanate was then used for derivatization of amines, followed again by plate drying under nitrogen gas. Samples were extracted off of the filter spots using 5mM ammonium acetate in methanol. Sample extracts were either diluted 1:2 with water for LC-MS/MS analysis or diluted 1:50 with the provided flow injection analysis (FIA) mobile phase for FIA-MS/MS analysis. Liquid chromatography and mass spectrometry analysis were performed by the University of Virginia Lipidomics and Metabolomics Core. Chromatographic separation was performed using ACQUITY UPLC system (Waters Corporation, Milford, MA) with an ACQUITY 1.7 µm, 2.1 mm×75 mm BEH C18 column with an ACQUITY BEH C18 1.7 µm, 2.1mm×5mm VanGuard pre-column. Samples for both LC-MS/MS and FIA-MS/MS were analyzed on a Xevo TQ-S Mass Spectrometer (Waters Corporation, Milford, MA) according to the standard operating procedure provided by Biocrates for the AbsoluteIDQ p180kit. All metabolites were identified and quantified against the isotopically labeled internal standards. Raw data was computed in MetIDQ version Nitrogen (Biocrates Life Sciences AG, Innsbruck, Austria).

Statistical analysis and visualization of results was performed in R version 3.5.3 with tidyverse, vegan, and broom [182-184]. Only metabolites detected in at least 50% of samples were analyzed (116 metabolites; **Supplementary Data 3.S1**). Concentration

values were not normalized *post-hoc* as equal cell numbers were input for each sample. Missing values were replaced with half of the lowest detected value for each metabolite. Values were then log transformed, centered, and scaled [185]. Statistically significant metabolites between SLOPE and untreated groups were determined using paired t-tests and the Benjamini and Hochberg method for multiple testing correction. Metabolite data and code are available at https://github.com/gulermalaria/SLOPE_Analysis.

Cholesterol manipulation and measurement

Methyl-β-cyclodextrin (mβCD) pre-saturated with cholesterol was purchased from Sigma Aldrich and dissolved in RPMI 1640 HEPES (Sigma Aldrich, St Louis, MO) to a concentration of 5mM. The solution was filtered then diluted with human serum (Valley Biomedical, Winchester, VA) to make a final "cholesterol-rich media" with 20% human serum and a final concentration of 4mM cholesterol saturated mβCD. *P. falciparum* parasites were incubated in this cholesterol-rich media for 48h. Samples were then taken for SLO lysis curve experiments as described above. Cholesterol levels in media formulations were quantified using the Amplex Red Cholesterol Assay Kit (Thermo Fisher Scientific, Waltham, MA) according to the manufacturer's instructions. The assay was read using a SpectraMax i3x microplate reader (Molecular Devices, San Jose, CA) with Invitrogen black-walled, clear-bottom 96-well microplates (Thermo Fisher Scientific, Waltham, MA). Each replicate measurement of media cholesterol represents a separate heat inactivated batch of human plasma (Valley Biomedical, Winchester, VA) or a separate 0.5% AlbuMAX II Lipid Rich BSA preparation (Sigma Aldrich, St Louis, MO).

Quiescent Parasite Analysis

Quiescent parasites were generated using the modified Teuscher, *et al*. protocol as described by Breglio, *et al.* [42, 43]. Briefly, synchronized *P. falciparum* cultures were treated with 700nM dihydroartemisinin (Sigma Aldrich, St Louis, MO) in DMSO for 6h. Cells were washed three times with RPMI to remove drug before being resuspended in media and returned to culture conditions. Cultures were then treated with D-sorbitol every 24 hours for the following 72 hours to remove any actively growing parasites that did not enter quiescence. Immediately following the final sorbitol treatment, flasks were split into two aliquots. One aliquot was left unenriched to serve as the control, while the second aliquot was SLOPE enriched with 55 SLO units as described above. A portion of both untreated and SLOPE samples was then stained with SYBR-Green and MitoProbe DiIC1(5) as described above for flow cytometry analysis. The remainder of each untreated and SLOPE sample was stained for fluorescence microscopy as described below.

Fluorescence Microscopy

Unenriched and SLOPE enriched samples containing quiescent parasites were stained with anti-CD235a-PE antibody, (Thermo Fisher Scientific, Waltham, MA) at 1:100 and 50nM MitoTracker Red (Thermo Fisher Scientific, Waltham, MA) at 37°C under 5% CO_2 for 30 min. SYBR-Green (Thermo Fisher Scientific, Waltham, MA) was added for the last 15 min of incubation at 1:10,000. Erythrocytes were washed three times with PBS. A wet mount was immediately prepared on microscope slides, and samples were imaged using a Nikon Eclipse Ti spinning disk confocal microscope at 63X magnification using 488nm, 561nm, and 649nm lasers and the Nikon NIS Elements Software.

Acknowledgements

Special thanks to Michelle Warthan for culturing support and to the UVA Lipidomics and Metabolomics Core for targeted metabolomics run support.

Author Contributions

ACB and JLG conceptualized and designed experiments. ACB and CCM acquired data. ACB performed data analysis. ACB and JLG wrote the manuscript. ACB, CCM, and JLG edited the manuscript.

Additional Information

This project was supported with funding through the National Institute of Allergy and Infectious Disease R21AI119881 and the University of Virginia 3Cavaliers Grant (to JLG and CCM). ACB is supported by an institutional training grant (5T32GM008136-33). The authors declare no competing interests.

Data Availability

All metabolomics data is available at https://github.com/gulermalaria/SLOPE_Analysis. All other data is available upon request.

Supplemental Materials

Supplementary Materials not included in this document:

Supplementary Data 3.1. Complete p180 Metabolite Data (separate .csv attachment)

All other Supplementary Materials are included below:

Supplementary Table 3.1. 10 most influential metabolites for principal components 1 and 2

PC1	PC2
PC.aa.C34.1	*C18*
PC.aa.C38.5	*C18.2*
PC.aa.C38.6	*C18.1*
PC.aa.C32.2	*C16.1.OH*
PC.aa.C36.5	*SM.C16.1*
PC.aa.C30.0	*lysoPC.a.C28.1*
PC.aa.C32.1	*C16*
PC.aa.C34.2	*SM.C20.2*
PC.aa.C36.3	*PC.aa.C28.1*
PC.ae.C38.0	*lysoPC.a.C24.0*

Supplementary Table 3.2. Quantification of cholesterol from human plasma and AlbuMAX II Lipid Rich BSA

Source	Average	S.E.M.	*N*
Human Plasma	3300 µM	650 µM	4
AlbuMAX II	13.5 µM	1.43 µM	4

Supplementary Figure 3.1. SLOPE enrichment is effective irrespective of parasite line. SLOPE enrichment performed on three different ring stage synchronized *P. falciparum* lines grown in the same blood and AlbuMAX II media batches. For each graph: *N*=3. Error bars represent S.E.M.

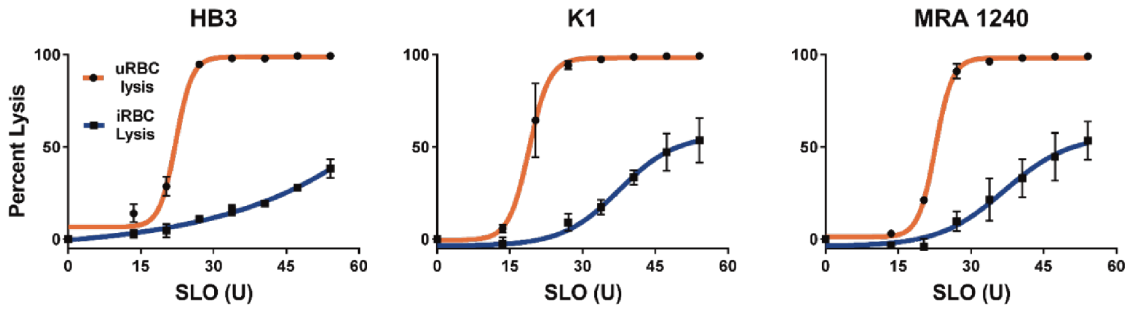

Supplementary Figure 3.2. SLOPE enrichment shows no bias across stages of the intraerythrocytic cycle. *P. falciparum* line MRA 1240 cultures either (A) synchronized by one sorbitol treatment or (B) left asynchronous were staged by microscopy before and after SLOPE enrichment. For each graph: *N*=3 (200 parasites counted per replicate). Error bars represent S.E.M.

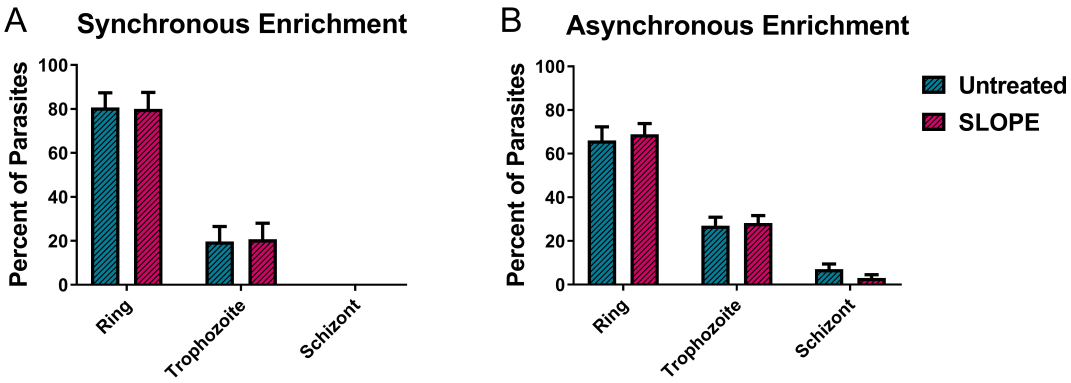

Supplementary Figure 3.3. SLOPE enrichment does not affect growth or staging over multiple replication cycles. (A) Three days of *P. knowlesi* line yH1 parasite growth from untreated controls or SLOPE enriched samples diluted with uninfected erythrocytes (*N* = 3, error bars represent S.E.M.). (B) Stage distribution for asynchronous Untreated and SLOPE enriched *P. knowlesi* line yH1 every 24h during 3 days of re-culture growth. (*N* = 3, error bars represent S.E.M.). R = ring; T = trophozoite; S = schizont. (C) The percentage of parasites in the ring stage for synchronized Untreated and SLOPE enriched *P. falciparum* line MRA 1240 every 48h during 6 days of re-culture growth. (*N* = 3, error bars represent S.E.M.).

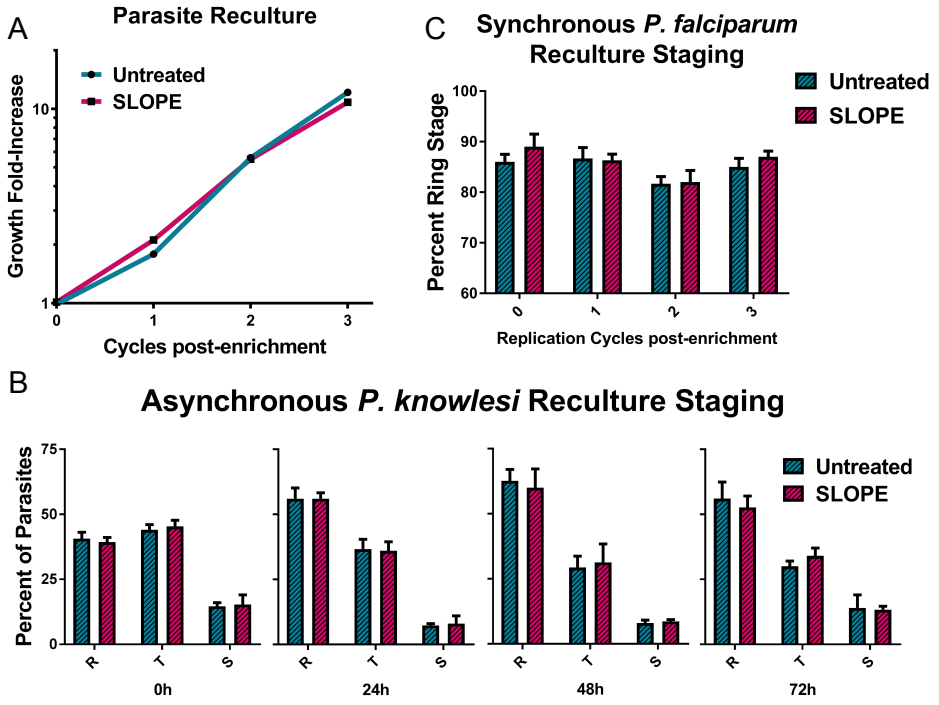

Supplementary Figure 3.4. SLOPE enrichment is effective irrespective of parasite line. SLOPE enrichment performed on clinical erythrocytes incubated in cRPMI for differing lengths of time. For infected erythrocytes (iRBCs), each line represents one trial; for uninfected erythrocytes (uRBCs), lysis curves from all time points were combined as no change was observed over time: *N*=4. Error bars represent SEM.

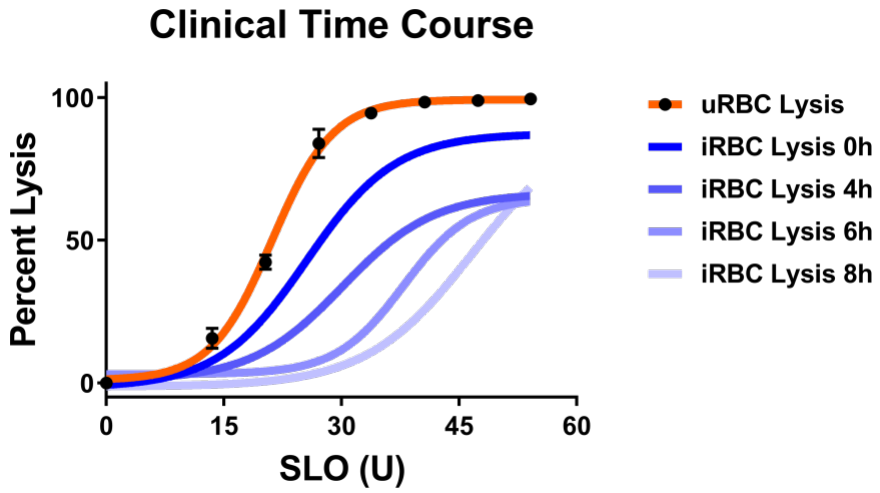

Supplementary Method 3.1. Detailed SLOPE Protocol.

Protocol Developed and Written by Audrey Brown
PI: Jennifer Guler, University of Virginia

SLO activation

Once a new vial of SLO has been received from a vendor (ex. Sigma-Aldrich S5265), the lyophilized powder should be activated according the following protocol (adapted from Jackson, *et al*. *Biochem J.* 2007).

1. Make activation solution: 1X PBS + 0.1% BSA + 5mM DTT
2. Resuspend lyophilized powder in 5ml of activation solution. Mix well by pipetting or inverting.
3. Incubate solution at 37C for 2 hours.
4. Mix the solution well by pipetting or inverting.
5. Divide into aliquots and store at -20C.

Defining a Hemolytic Unit (U)

Testing to determine the SLO solution volume which constitutes a U should be done in triplicate every time a new shipment of SLO has been received and activated.

1. Preincubate uRBCs in growth media at 37C for at least 4h. (This allows uRBC cholesterol levels to accurately reflect the cholesterol levels that will occur in *in vitro* culture and accounts for cholesterol level variation between media batches).
2. Suspend uRBCs at 2% hematocrit in 1X PBS.
3. Label a series of eppendorfs with the given SLO volumes you wish to test. (We recommend testing 6-8 points between 0µl SLO and 1.5µl SLO.
4. Aliquot 50µl of 2% uRBCs into each tube.
5. Make the appropriate dilutions of SLO in 1X PBS so that equal volumes can be added to each tube. (Also add the equivalent volume of PBS to the "0µl SLO" control tube).
6. Mix each tube by pipetting.
7. Incubate at 37C for 30min.
8. Remove tubes from heat and quickly mix by pipetting.
9. Add 10µl from each tube into 990µl of 1X PBS to generate a 1:100 dilution. Dilution aids in stopping lysis. (We suggest preparing tubes for dilutions during the 30min incubation period so that this step can proceed immediately following the end of the incubation).
10. Use the Cellometer T4 to count the intact RBC cell density of each sample.

*If a Cellometer T4 is not available, intact cells can be counted by flow cytometry. Alternatively, lysis can be measured spectrophotometrically by centrifuging (undiluted) tubes and taking aliquots of supernatant. Then measure samples at 412nm to determine hemoglobin release. Finally, normalize against a sample subjected to hypo-osmotic lysis (see Jackson, *et al. Biochem J*. 2007).

11. Determine the fraction of cells lysed by subtracting the cell density of each SLO-containing sample from the cell density of the "0µl SLO" control tube. Then divide this value by the "0µl SLO" control cell density.
12. Plot cell lysis as a function of SLO amount to determine the amount of SLO which causes 50% lysis. This is 1 hemolytic unit.

SLOPE enrichment

1. Count the cell density of your sample using a flow cytometer, hemocytometer, or Cellometer T4.

*__Note__: SLOPE enrichment will uniformly enrich for all asexual blood stages. If you wish to enrich a specific stage, such as only ring stage parasites, utilize your synchronization method of choice prior to this step.

2. Spin down the sample and remove cell culture media. Add the volume of non-cholesterol containing solution (ex. PBS, RPMI) required to yield a concentration of $2x10^9$ RBCs/ml.
3. For every 5 volumes of RBCs you wish to SLOPE enrich, SLO and 1X PBS should be added to a total of 2 volumes.
    a. Ex. Given an SLO stock of 2U/µl, a desired SLO activity of 30U, and cell amount of $1x10^8$ RBCs for enrichment: to 50µl RBCs (at $2x10^9$ RBCs/ml), add 15µl SLO (30U) and 5µl PBS (SLO + PBS = 20µl total aka "2 volumes").
4. Mix by pipetting and incubate at room temperature for exactly 6 min.
5. Add >5-10 volumes of PBS or RPMI and mix by pipetting
6. Spin at 2,500xg for ~3 min, remove supernatant

*Delaying the initial wash may lead to over lysis.

7. Add PBS or RPMI to wash, spin at 2,500xg for 3 min, remove supernatant.
8. Repeat step 7 for a total of 3 washes.

*The wash step can be repeated again if lysis appears to still be occurring as evidenced by hemoglobin in the supernatant. (Even though the free SLO has been removed, lysis may continue to take place for a few minutes). Ensure lysis has finished before proceeding to the Percoll gradient step.

9. Resuspend cells in desired volume of PBS or media (cholesterol containing solutions, such as serum-supplemented RPMI, may now be used).
10. Slowly layer cells on top of a 60% Percoll gradient.
    a. To make Percoll: take 9 parts Percoll and add 1-part 10X PBS to make stock isotonic Percoll (SIP).
    b. Dilute from SIP to make 60% Percoll using 1X PBS (2-parts SIP plus 1-part 1X PBS)
11. Spin the Percoll gradient at 1500xg for 5min using a swinging bucket rotor. (Spin may need to be extended for >5min, if you are using a large Percoll gradient, ex. 50ml).
12. Carefully remove and discard the upper fraction of Percoll, which contains lysed RBC ghosts. Keep the pipette tip at the top of the Percoll as you are removing this fraction to ensure ghosts are removed effectively.
13. Using a new pipette tip to avoid cross-contamination of ghosts, remove the lower, intact RBC fraction and place these cells into a clean tube.
14. Wash cells twice in >10 volumes of PBS or media.
15. Optional: Take a small aliquot to assess parasitemia by Giemsa staining a blood smear or by SYBR Green-based flow cytometry.

*Parasites can now be used for downstream applications.

Chapter 4:
Broad metabolic nutrient stress increases *P. falciparum* survival of artemisinin

Audrey C. Brown, Michelle D. Warthan, Anush Aryal, Shiwei Liu, Jennifer L. Guler*
Department of Biology, University of Virginia, Charlottesville, VA.

This chapter has been adapted from a manuscript in preparation for publication.

Figures and tables have been renumbered to maintain sequence within this document.

Abstract

Mounting evidence demonstrates that nutritional environment can alter pathogen drug sensitivity. While the nutrient-rich media used for standard *in vitro* culture contains supraphysiological metabolite concentrations, pathogens encounter a relatively restrictive environment *in vivo*. However, research has revealed that nutrient restriction does not always have a negative effect on pathogen fitness. The adaptive benefits of mild environmental stress can overshadow adverse effects in a phenomenon termed, hormesis. We assessed the potential for hormesis in the protozoan parasite that causes malaria and demonstrated that short-term growth under physiologically-relevant mild nutrient stress (or "metabolic priming") triggers tolerance of the potent antimalarial drug dihydroartemisinin (DHA). We observed beneficial effects using both short term survival assays and longer-term proliferation studies, where metabolic priming increases parasite survival to a level previously defined as DHA resistance (>1% survival). We performed these assessments by either decreasing single metabolites that have distinct roles in parasite metabolism (i.e. hypoxanthine or thiamine) or using a media formulation with reductions in many metabolites that simulates the human plasma environment. We determined that priming-induced tolerance was restricted to parasites that had newly invaded the host red blood cell but the effect was not dependent on genetic background. As evidence of the biphasic nature of hormesis, we identified the level of stress that was essential to elicit beneficial effects. Our investigations into the molecular mechanisms of this effect revealed that metabolic priming stimulates changes that mimic aspects of genetic artemisinin resistance, including translational repression, autophagy, and vesicle transport. This finding suggests that, regardless of the impact on survival rates, environmental stress could stimulate changes that ultimately directly contribute to resistance. Furthermore, the observation that DHA sensitivity is not solely determined by genetics is an important consideration as we develop ways to prevent resistance development. Finally, we presume that metabolic stress occurs more frequently *in vivo* compared to the stable *in vitro* environment; therefore, our observation that a physiological environment increases drug tolerance has ramifications for how in vitro results translate to in vivo studies. Improving our understanding of how pathogens adjust their metabolism to impact survival of current and future drugs is an important avenue of research to prevent and slow the spread of resistance.

Introduction

In vitro culture provides microbes with a stable environment for growth with relatively little challenge to organismal homeostasis. For example, the supra-physiological concentrations of nutrients *in vitro* largely protect cultured organisms from the stress of starvation conditions. Yet, nutrient limitation occurs frequently *in vivo* [186-189]. Therefore, the consequences of dynamic adaptation to these stressors, such as nutrient limitation, are largely missed by standard *in vitro* experimental designs.

Interestingly, data from across the tree of life has shown that the relationship between stress and negative fitness consequences is not necessarily linear. The adaptive benefits of low doses of mild environmental stress overwhelm the adverse effects from the stressor in a biphasic dose response phenomenon termed, hormesis ([190, 191]; **Fig. 4.1A**). Given this, adjustment of metabolism in response to homeostatic challenge from mild nutrient stress may increase pathogen fitness and survival of subsequent stressors, such as drug pressure.

Indeed, metabolic adjustability to varied nutritional environments has been shown to alter drug sensitivity across diverse pathogens [192, 193]. For example, in *Trypanasoma cruzi* reduction of exogenous glutamine decreases flux through the sterol synthesis pathway rendering parasites sensitive to azole drugs [194]. Meylan, *et al*. found *Pseudomonas aeruginosa* supplementation with specific carbon sources increased susceptibility to tobramycin [195]. Increasing proline concentration confers halofuginone resistance in *P.falciparum* [109]. The nutritional environment *in vitro* is highly divergent from conditions pathogens are exposed to in the context of human infection, with metabolite concentrations frequently found at considerably higher levels in culture [78, 196, 197]. Discrepancies in metabolic activity between *in vitro* and *in vivo* environments brought about by non-physiological conditions can lead to reduced translatability of findings from culture-based experiments when metabolic flux through pathways is altered [13, 198]. For example, glycerol metabolism sensitizes *Mycobacterium tuberculosis* to pyrimidine-imidazoles through accumulation of toxic metabolites [198]. However, these drugs are ineffective *in vivo* where changes in nutrient availability lead to differences in carbon metabolism.

Previously characterized changes in pathogen drug sensitivity as a consequence of varied nutritional environment typically depend on either 1) changes in flux through a specific metabolic pathway relevant to a given drug target or 2) a general slowing of growth leading to decreased uptake and activation of drug. Here, we present a case where

nutrient stress induces a change in drug sensitivity of the human malaria parasite, *Plasmodium falciparum*. We demonstrate that short-term growth under mild, physiologically relevant nutrient stress leads to superior recovery from drug treatment. We observe this effect under distinct conditions that impact the parasites differently; therefore, it is not dependent on a change in flux within a specific metabolic pathway nor an overall decrease in growth rate. Importantly, the increased survival rates achieve a level that reaches the field's definition of "resistance," yet no genetic resistance mutations are necessary. We determined that the induction of stress response pathways within the parasite occurs during nutrient stress, which prime the parasite to better withstand drug treatment. This study emphasizes the link between nutrient limitation, stress response pathways, and survival of drug treatment and could have important implications for the selection of drug resistant pathogens.

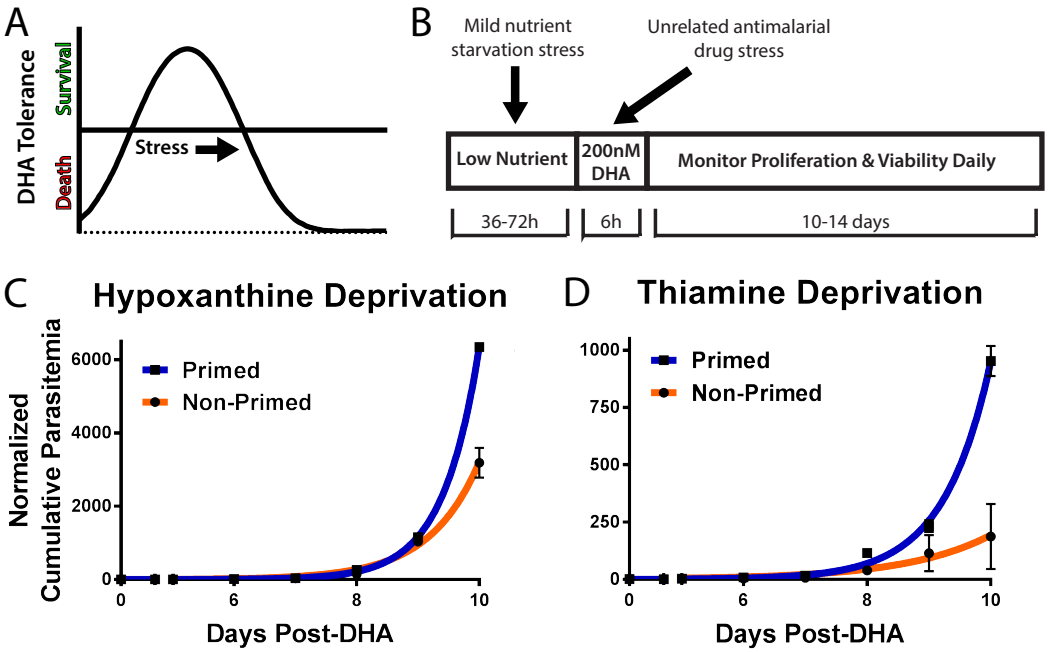

Figure 4.1. Mild nutrient stress prior to DHA treatment increases post-drug recovery. A) The biphasic dose response to stress characteristic of hormesis. B) Paradigm used for metabolic priming followed by DHA challenge and recovery. C-D) Post-DHA recovery in standard media of *P. falciparum* primed in either low hypoxanthine or zero thiamine media. Bars represent S.E.M. of technical replicates within one independent experiment.

Results

Metabolic priming increases parasite recovery from DHA

We sought to determine the effect of mild nutrient stress on the survival of *P. falciparum*. Asynchronous parasite cultures were subjected to short-term (36-72h) incubation in

media restricted of either hypoxanthine or thiamine (**Table 4.1**, termed "metabolic priming"). *Plasmodium* lack the ability to *de novo* synthesize purines, instead requiring scavenging from the environment. In serum-free malaria cultures, the purine derivative, hypoxanthine, is a standard additive to fulfill this requirement. In contrast, *Plasmodium* can both *de novo* synthesize or scavenge thiamine; however, recent metabolic network reconstruction data suggests drug resistance status can alter metabolism, making parasites reliant on thiamine import for survival [69]. In addition to different modes of acquisition for these nutrients, hypoxanthine and thiamine represent distinct metabolite classes: nucleoside and cofactor, respectively. The duration of incubation and level of nutrient restriction for these metabolites were optimized to induce stress while keeping the majority of the parasite population viable (**Supplemental Fig. 4.1**).

We treated parasites grown in either metabolic priming conditions or standard media (formulations detailed in *Methods*) with a rapid-acting, highly potent antimalarial drug (200nM dihydroartemisinin (DHA) for 6h, **Fig. 4.1B**). DHA is an artemisinin derivative, which causes widespread damage within parasites by promiscuously alkylating different classes of biomolecules, including heme and numerous proteins, thereby disrupting multiple biological pathways [107, 199, 200]. Following removal of drug and continued culture for ten days in standard media, metabolically primed parasites showed an increase in cumulative proliferation compared to non-primed controls (**Fig 4.1C-D**). We detected this effect in both priming conditions despite the restricted metabolites in each condition being of unrelated classes, irrespective of the parasite line (**Supplemental Table 4.1**, *Dd2* originally from Southeast Asia and *NF54* from Africa). Additionally, increased cumulative proliferation is driven by altered response to DHA treatment; we only observed this effect in primed parasites that were subjected to DHA treatment but not in those treated with vehicle alone (**Supplemental Fig. 4.2**).

During metabolic priming experiments, the level of stress applied to the parasites impacted whether we observed increased cumulative proliferation. For example, a 10-50% growth reduction of over the course of low hypoxanthine metabolic priming was found to facilitate the phenotype (**Fig. 4.1C**), while <10% or >50% growth reduction during hypoxanthine priming was detrimental to post-DHA cumulative proliferation (**Supplemental Fig. 4.3**). These data support a biphasic dose response to metabolic priming characteristic of hormesis. However, in other conditions growth during priming did not serve as a proxy for estimating dose response. For example, thiamine deprivation metabolic priming did not lead to growth reduction but still led to increased cumulative proliferation following DHA treatment (**Fig. 4.1D**). The different effect of priming

treatments on growth is likely due to parasite ability to scavenge or *de novo* synthesize thiamine, whereas *P. falciparum* are strictly purine auxotrophs.

Nutrient Restricted	Class of Restricted Nutrient	Conc. of Restricted Nutrient	Length of Restriction
Hypoxanthine*	Purine	0.5uM	48-72h
Thiamine**	Cofactor	0.0uM	36h
Multiple (HPLM)**	Multiple	Variable	≥ 7d

Table 1. Length and concentration of nutrient restrictions for metabolic priming. *Priming was considered successful when an approximately 10-50% growth decrease occurred, there was little to no decrease in mitochondrial membrane potential (MMP) (approx. <10% drop), and ring stage percentages were within <10% ± non-primed. **Priming was considered successful when the latter two above conditions were met but no growth reduction criteria were required.

Metabolic priming is stage-specific and facilitates increased DHA survival rates

Because our priming conditions alter the parasites' response to DHA (**Fig. 4.1C-D**), and DHA survival patterns are known to be dependent on the parasite life cycle stage [126], we next investigated 1) stage effects of metabolic priming and 2) stage-specificity of the proliferation effect. We were particularly interested the proportion of young ring stage parasites, the earliest stage following erythrocyte invasion (0-3hr, **Fig. 4.2A**, as they are innately less sensitive to DHA treatment [126].

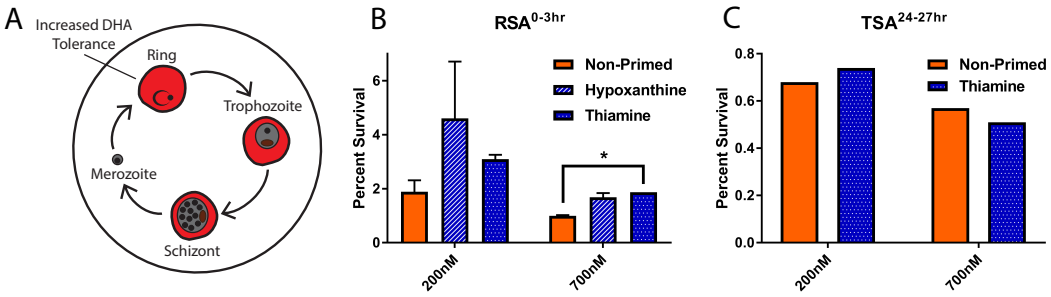

Figure 4.2. Increases in DHA survival are mediated by rings. A) *P. falciparum* asexual blood stage replication cycle. B-C) *Dd2* survival assay values for early rings (B) or trophozoites (C) 66h following 6h treatment with 200 or 700nM DHA. Bars represent S.E.M.

First, we compared parasite stage distribution in primed and non-primed populations to assess if subtle changes in lifecycle stage distribution take place in low-nutrient conditions (i.e. stage effects). We did not detect any significant differences in the percentage of ring-stage parasites in non-primed compared to primed samples (Non-primed: 61.6% ± 2.1%, Primed: 61.3% ± 2.3% (mean ± S.E.M); p=0.67), (**Supplemental Table 4.1**). Therefore, stage-dependent effects of starvation-induced alteration of cell cycle progression is not contributing to altered proliferation following DHA treatment.

Second, we performed shorter term DHA survival assays on highly synchronous parasite populations to determine if changes in parasite proliferation are stage-specific. To assess the behavior of early stage parasites (**Fig. 4.2A**), we performed "ring stage survival assays" (RSAs) on highly synchronous populations of 0-3h rings [126]. Metabolic priming prior to DHA treatment increased ring stage survival (**Fig. 4.2B-C**). The fold increase depended on the level of DHA used; we observed an 2.12-fold increase when treated with 200nM DHA, which is the concentration used for our study (**Fig. 4.1C-D**), and ~2.05-fold for 700nM, the standard concentration for DHA RSAs. Notably, metabolic priming increased survival percentages to a level that is considered resistant (<1%, [126]). Additionally, we tested later stage parasites (24-27h) in a modified RSA that assesses trophozoite survival (TSA). We detected no significant increase in DHA survival following metabolic priming, indicating the benefit of metabolic priming is ablated in trophozoites (**Fig. 2D**). In addition to showing stage-specificity of the effect, these experiments also showed that higher cumulative proliferation in primed samples post-DHA is a result of an increased percentage of parasites surviving DHA treatment, as opposed to, increased proliferation per parasite post-drug.

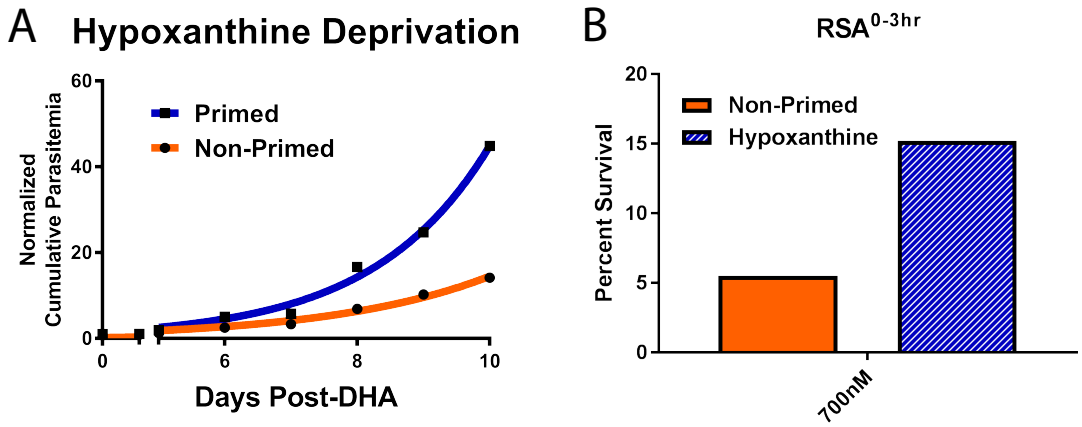

Figure 4.3. Increases in DHA survival occurs in genetically resistant parasites. A) Post-DHA recovery of line MRA-1238 in standard media primed in low hypoxanthine media. Bars represent S.E.M. of technical replicates within one independent experiment. B) Line MRA-1238 survival assay values for early rings 66h following 6h treatment with 700nM DHA.

Metabolic priming increases survival in parasites with genetic DHA resistance

Next, we sought to assess if the survival benefits of metabolic priming are limited to DHA sensitive parasites (RSA <1%; [126]). Our prior studies (**Fig. 4.1C-D** and **Fig. 4.2B-C**) utilized laboratory parasite lines with no genetic resistance to artemisinin derivatives. To assess the interaction between priming and genetic resistance, we first performed a preliminary growth curve on DHA recovery of metabolically primed on a moderately DHA resistant

parasite strain that harbors a mutation in the *kelch13* gene (**Fig. 4.3A**; MRA-1238, RSA: 6.2%, *kelch13* I543T mutant [201]). Following this, we performed RSA testing with and without metabolic priming Survival of this parasite line in RSAs with a high amount of DHA (700mM) increased 2.75-fold following metabolic priming. This parasite line was not tested at the lower 200nM concentration as in (**Fig. 4.3B-C**) due to the known resistance status; other DHA resistant lines (i.e. MRA 1240, RDA: 88.2%, *kelch 13* R539T) could not be assessed because of their high tolerance to even 700nM DHA levels. These data in combination with data generated using DHA sensitive lines (**Figure 4.1C-D** and **Fig. 4.2B-C** , *Dd2* and *NF54*), indicate that increased DHA survival following metabolic priming is not dependent on genetic background.

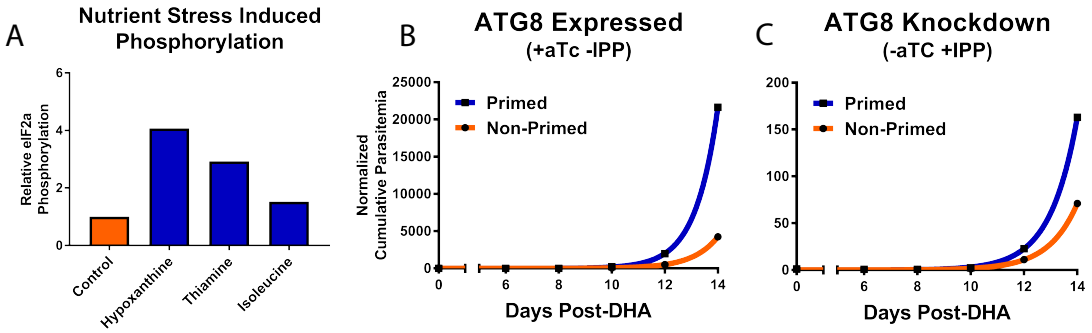

Figure 4.4. Metabolic priming induced translation inhibition and autophagy. A) Quantification of phosphorylation increase for priming conditions. B-C) Post-DHA recovery in a paired experiment of hypoxanthine primed ATG8 TetR-Dozi parasites with ATG8 expression on (B) or off (C).

Metabolic priming-induced translation inhibition and autophagy correspond to DHA survival

Phosphorylation of the translation initiation factor eIF2a is known to occur in *Plasmodium* in response to nutritional stress [202, 203]. Additionally, increased levels of eIF2a phosphorylation have been shown to be protective of DHA treatment [50]. We assessed whether eIF2a phosphorylation was altered following metabolic priming and detected an increase of ~3.5-fold (**Fig. 4.4A**). This level is slightly higher than DHA treatment itself (200nM for 2h), indicating that metabolic priming could initiate cellular changes that promote survival of DHA treatment.

Previously, isoleucine starvation was shown to trigger eIF2a phosphorylation in *P. falciparum* [202, 203]. When we assessed a low-isoleucine priming condition (60% reduction relative to non-primed control), we did not detect increase in phosphorylation (**Fig. 4.4A**). The discrepancy between our results and previous work is likely due to the difference in both the length and severity of deprivation used in our study (i.e. 0uM for

6-24h in [147] compared to 152uM for 72h here). The lack of anticipated eIF2a phosphorylation may indicate a lower than expected degree of nutrient stress in isoleucine primed parasites compared to our other priming conditions. Given our data that inadequate metabolic priming stress places parasites outside of the beneficial range of the biphasic dose response curve of hormesis (in **Supplemental Fig. 4.3**), we next determined whether isoleucine priming leads to differing DHA survival as well. Interestingly, isoleucine priming was not beneficial for DHA survival (**Supplemental Fig. 4.4**). This result, combined with the lack of an impact on eIF2a, provides further evidence nutrient stress-induced eIF2a phosphorylation is contributing to increased DHA survival in our studies.

In higher eukaryotes, phosphorylation of eIF2a can promote activation of the PI3K complex and increase transcription of autophagy-related genes [204, 205]. In *Plasmodium*, increased PI3K activity is a known mediator of artemisinin resistance [47]. Further, polymorphisms in autophagy-related genes, such as ATG18 and ATG7, are associated with decreased artemisinin sensitivity in Southeast Asian parasite populations [48, 206]. While it is unclear if the role of eIF2a phosphorylation in promoting autophagy is conserved in *Plasmodium*, we reasoned that, like the eIF2a phosphorylation (**Fig. 4.4A)**, autophagy may be activated by our metabolic priming in a manner associated with DHA survival.

To test this, we used a parasite strain with conditional regulation of ATG8 expression by a TetR-DOZI system [207]. Removal of the small molecule, anhydrotetracycline (aTc), leads to knockdown of ATG8, which is the essential for autophagosome formation and therefore essential for successful macroautophagy [207]. When we compared cumulative proliferation post-DHA between parasites with low versus normal levels of ATG8 expression (**Supplemental Fig. 4.5**), we detected a reduction in the effect of metabolic priming on survival when ATG8 is repressed (**Fig 4.4B-C.**). Along with eIF2a, autophagy plays a role in the priming-induced pro-survival phenotype.

Physiological growth conditions promote increased DHA survival

Nutrient limitation is a physiologically relevant stress that parasites must adapt to in the context of human infection. Our low hypoxanthine and thiamine-free metabolic priming conditions mimic nutrient stress from a single metabolite deficiency. While this type of sole micronutrient deficiency occurs *in vivo* (refs, beriberi etc.), this is not the only relevant nutritional difference between in vitro cultures and clinical infections. For example, even when human hosts are not suffering micronutrient deficiencies, *in vivo*

levels of not just one, but many, metabolites are dramatically lower compared to the supraphysiological levels in standard RPMI-media based formulations [78, 196, 197].

We hypothesized that the nutritional differences between RPMI and human plasma is sufficient to induce a metabolic priming-like effect similar to that seen with our established conditions. To test this, we utilized Human Plasma-Like Media (HPLM) as a base for *P. falciparum* culture [208]. Under routine propagation conditions, parasites maintained in HPLM grew equivalent to those in RPMI based media across two independent experiments of 5 replication cycles (**Fig. 4.5A**). HPLM and RPMI based cultures increased an average of 18 ± 1.9 and 19 ± 2.5 fold (mean ± S.E.M) per replication cycle, respectively.

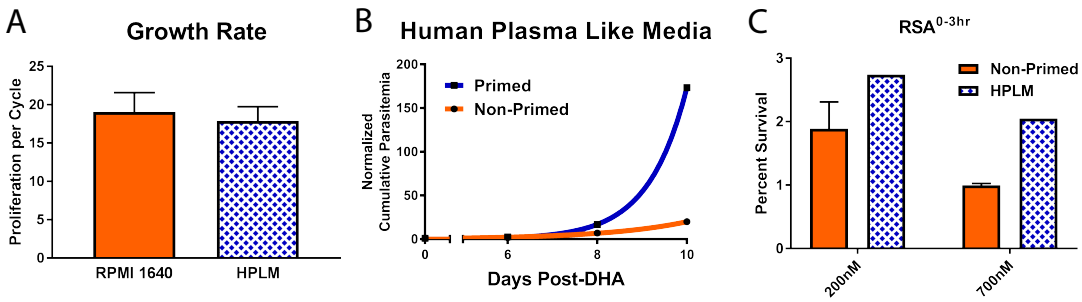

Figure 4.5. Increased DHA survival induced by physiologic nutrient media. A) Average growth rate of *Dd2* parasites propagated in RPMI 1640 versus HPLM based media. B) Post-DHA recovery in standard media of *P. falciparum* primed in either low hypoxanthine or zero thiamine media. Bars represent S.E.M. of technical replicates within one independent experiment. C) *Dd2* survival assay values for early rings 66h following 6h treatment with 200 or 700nM DHA. Parasites were adapted to HPLM based media at least 7 days prior to drug treatment and maintained in HPLM through the RSA reading. Bars represent S.E.M.

We adapted parasites to HPLM-based culture for at least 7 days prior to treating with DHA and kept parasites in HPLM based media for 10 days of recovery. Propagation in HPLM prior to DHA pulse led to increased cumulative proliferation during recovery from drug compared parasites in RPMI based media (**Fig. 4.5B**). As with low hypoxanthine and thiamine-free priming conditions, growth in HPLM also increased DHA survival in highly synchronous RSAs (**Fig. 4.5C**). These data provide evidence that related pro-survival changes are occurring in response to both single metabolite deficiency and broader reductions of environmental metabolites.

RNAseq of metabolically primed parasites

We performed RNAseq on synchronous ring stage non-primed parasites and parasites primed with low hypoxanthine, thiamine-free, or HPLM conditions to identify global transcriptional changes in response to nutritional environment. Principal component

analysis revealed each group had a distinct transcriptional profile, with hypoxanthine primed parasites clustering separate from the other three groups on PC1, while the remaining groups separate on PC2 (**Fig. 4.6A**). This pattern is paralleled in the number of significantly deferentially expressed (DE) genes detected in experimental groups compared to non-primed, RPMI-based control samples with hypoxanthine primed parasites yielding by far the largest number of DE results (**Fig. 4.6B**).

Due to the large number of DE genes in hypoxanthine samples, it was necessary to limit the complexity of results from this group in our analyses. First, we took a targeted approach to determine if regulation of autophagy is altered in our samples given the impact of ATG8 on our phenotype (**Fig. 4.4B-C)**. Autophagy genes were upregulated in hypoxanthine primed parasites (upregulated ATG genes: *pi3k*, *atg8*4CD *atg4*, *atg7*). However, this pattern was not conserved in thiamine free and HPLM groups, indicating the autophagy pathway is unlikely to be the primary driver of observed increased DHA survival.

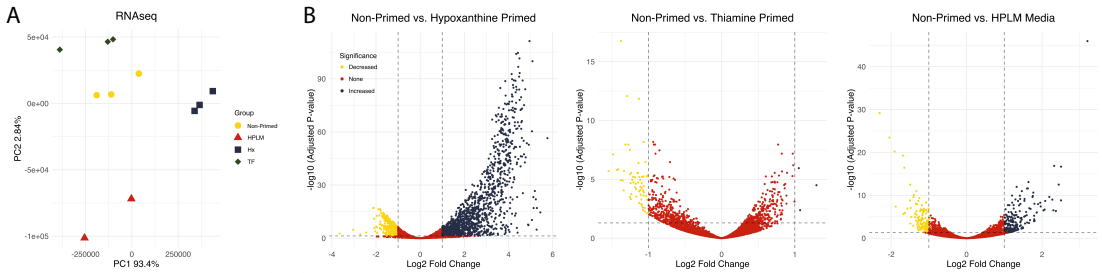

Figure 4.6. Metabolic Priming induced expression changes. A) PCA plot of gene expression from each condition. Volcano plots of differentially expressed genes for each condition. Log2 fold change thresholds set at -1 and +1. Adjusted p-value set to ≤0.05.

To better assess genes within the dataset contributing to our phenotype, we chose to focus specifically the top 15 up- and down-regulated genes in each group as determined by lowest adjusted p-values. This yielded 37 up- and 42 down-regulated unique genes across the three treatment conditions as there was some overlap between groups. Of these genes which had an adjusted p-value of ≤0.05 in all groups were used to generate our curated list of 17 up- and 12 down-regulated genes of interest. Strikingly, this curated list contained many genes implicated in artemisinin genetic resistance, such as *coronin* (PF3D7_1251200), a gene known to be sufficient to induce artemisinin resistance when mutated [209] (**Table 4.2**). In fact, when compared to a list of 151 genes known to be basally altered (not under active DHA treatment; **Supplemental Table 4.2**) in artemisinin resistant parasites, 10 of the 29 genes in **Table 4.2** were present [132, 155, 209-211].

These data indicate nutrient priming remodels metabolism in parasites to induce a non-genetic artemisinin resistant-like state.

Gene ID	***Product Description***
Upregulated	
*PF3D7_0214600**	serine/threonine protein kinase STK2, putative
PF3D7_0402200	surface-associated interspersed protein 4.1 (SURFIN 4.1), pseudogene
*PF3D7_0402300**	reticulocyte binding protein homologue 1
PF3D7_0613900	myosin E, putative
PF3D7_0707300	rhoptry-associated membrane antigen
*PF3D7_0722200**	rhoptry-associated leucine zipper-like protein 1
PF3D7_0724900	kinesin-20, putative
*PF3D7_0822900**	PhIL1-interacting candidate PIC2
PF3D7_0911100	START domain-containing protein, putative
PF3D7_1026600	conserved Plasmodium protein, unknown function
*PF3D7_1126700**	conserved Plasmodium protein, unknown function
PF3D7_1138000	conserved Plasmodium protein, unknown function
*PF3D7_1145200**	serine/threonine protein kinase, putative
*PF3D7_1251200**	coronin
*PF3D7_1310700**	PhIL1-interacting candidate PIC5
PF3D7_1327300	conserved Plasmodium protein, unknown function
PF3D7_1335400	reticulocyte binding protein 2 homologue a
PF3D7_1356800	serine/threonine protein kinase ARK3, putative
Downregulated	
PF3D7_0402000	Plasmodium exported protein (PHISTa), unknown function
*PF3D7_0500800**	mature parasite-infected erythrocyte surface antigen
PF3D7_0510100	KH domain-containing protein, putative
PF3D7_0711000	AAA family ATPase, CDC48 subfamily
PF3D7_0731600	acyl-CoA synthetase
PF3D7_0801100	28S ribosomal RNA
PF3D7_0802200	1-cys peroxiredoxin
PF3D7_1016300	GBP130 protein
*PF3D7_1324300**	conserved Plasmodium membrane protein, unknown function
PF3D7_1359600	conserved Plasmodium protein, unknown function
PF3D7_1371800	Plasmodium exported protein, unknown function
PF3D7_1433400	PHD finger protein PHD2, putative

Table 4.2. Genes of Interest Curated from Differentially Expressed Gene Lists. Asterisk indicates genes found basally altered in artemisinin mutants.

Discussion

In 2020 alone, malaria was responsible for over 200 million cases and 600,000 [212]. While the over half a million deaths due to malaria is a staggering figure, this is only a fraction of the number reported just two decades ago. The reduction in malaria deaths since the turn of the century was in large part due to the effectiveness of potent

antimalarial drugs, namely artemisinin derivatives. The emergence and spread of genetic resistance to artemisinin threatens to undo the progress made in malaria mortality reduction and makes it clear there is a dire need to understand and combat parasite drug resistance. How parasites adjust their metabolism in ways that impact survival of artemisinin, and future drugs, is an important avenue of research to prevent and slow the spread of drug resistant pathogens.

The supraphysiological concentrations of metabolites found in common media formulations, such as RPMI 1640, can potentiate genetic, transcriptional, and metabolic changes in parasite biology [78, 196]. We assessed the effect of nutrient restriction on the *P. falciparum* response to artemisinin treatment to better understand how parasites respond when not protected by this supraphysiological glut of metabolites. To induce starvation in nutrient rich RPMI 1640 based malaria culture, many groups simply dilute media, producing a blanket reduction in metabolite levels. This is somewhat akin to our use of HPLM based cultures, which mimics the concentrations of metabolites in the human blood stream, consequently reducing concentrations of many metabolites [197]. To our knowledge we present the first use of human plasma like media as a base for the propagation of *P. falciparum*.

Other groups have chosen to induce nutrient stress by reduction or elimination of a single metabolite [147]. This is akin to our hypoxanthine or thiamine limited metabolic priming conditions. These metabolites were chosen in part due to contrasting metabolic attributes outlined in the *Results* section, but also in part due to potential relevance to conditions *P. falciparum* may experience *in vivo*. Nucleotide metabolism is a potential future drug target in *P. falciparum*; antimalarials are currently being developed to inhibit both purine scavenging and pyrimidine biosynthesis [60-63]. As some of these candidates move closer to being utilized in the clinic, it is imperative to understand how parasites respond to the stress of nucleotide deprivation. Similarly, thiamine restriction has potential physiological relevance to *P. falciparum* infection as clinical thiamine deficiency is common in malaria endemic regions, such as Southeast Asia [213, 214], and evidence suggests malaria infection exacerbates this deficiency [215].

Our data indicate increased DHA survival after metabolic priming has a similar stage specificity profile to previous observation of DHA survival with early rings surviving to a greater extent than later stages (ex. trophozoites; **Fig. 4.2**) [126]. Interestingly, previous investigations of the molecular mechanism of artemisinin survival have shown that resistant induce basal eIF2a phosphorylation in early rings, but not trophozoites, and that this is protective of DHA treatment [50]. Further, phosphorylation of eIF2a in *Plasmodium*

occurs in response to nutritional stress [202, 203]. However, nutrient deprivation conditions have not been previously shown to induce metabolic changes prior to artemisinin treatment that subsequently confer increased survival. Our data demonstrating increases in eIF2a phosphorylation during metabolic priming conditions which enhance DHA survival, but not during priming conditions with inadequate nutrient stress for DHA survival benefits, establishes a link between nutrient restriction and DHA survival.

Phosphorylation of eIF2a leads to preferential translation of stress responsive genes, including transcription factors, in higher eukaryotes. These factors can promote activation of the PI3K complex, which is required for nucleation of the pre-autophagosomal structure and increase transcription of autophagy related genes needed for elongation of the phagophore, such as ATG5 and ATG12 [204, 205] . Given this, it is not surprising that activation of stress-induced autophagy in higher eukaryotes is partially dependent on eIF2a phosphorylation [216]. To what extent the role of eIF2a phosphorylation in autophagy is conserved from higher eukaryotes to *Plasmodium* is unclear, but we reasoned that autophagy may also be activated by metabolic priming in a manner associated with DHA survival. Inhibition of autophagy via knockdown of a key autophagy protein did indeed also knockdown the magnitude of DHA survival benefit from metabolic priming in hypoxanthine deprivation conditions, providing support for the link between eIF2a and autophagy in *Plasmodium* (**Fig. 4.4B**).

In addition to post-transcriptional regulation, such as eIF2a phosphorylation, RNAseq data showed a clear link between nutrient restriction and priming induced DHA tolerance. The adaptive response to nutrient deprivation led to a metabolic state mimicking that of genetically DHA resistant parasites (**Table 4.2**). Future investigation should determine the longevity of metabolic priming changes for DHA survival and whether these adaptive changes facilitate development of genetic resistance, such as seen in the development of antibiotic resistant bacteria [217].

A biphasic hormetic dose-response curve is seen across biology to adverse conditions [190, 191]. Yet how this phenomenon may unexpectedly affect experiments performed on organisms outside of native environment remains limited. Metabolic driven changes in pathogen drug sensitivity due to nutritional environment can lead to discordance between *in vitro* results and *in vivo* responses. Our data provide evidence a hormetic effect from nutritional environment is affecting *P. falciparum* DHA survival differentially between standard *in vitro* culture conditions and more *in vivo*-like environments.

To our knowledge, this is the first demonstration of *P. falciparum* propagation using HPLM as a media. Future use of the media may be appropriate for selected assessments on the translatability of findings from culture conditions to clinical cases. Future studies should also investigate if hormesis-driven changes in survival is relevant to other antimalarial drugs and how the benefits of hormesis may be targeted to enhance the killing potential of malaria drug treatments.

Materials and Methods

Parasites and growth

Plasmodium falciparum lines MRA 150 (Dd2), MRA 1000 (NF54), and MRA 1238 were obtained from the Malaria Research and Reference Reagent *Resource* Center (MR4, BEI Resources). The ATG8 conditional TetR-Dozi knockdown line was a gift from Ellen Yeh (Stanford University, Stanford, CA). *Plasmodium* cultures were maintained in A+ human erythrocytes (Valley Biomedical, Winchester, VA) at 3% hematocrit in RPMI 1640 HEPES (Sigma Aldrich, St Louis, MO) supplemented with 0.5% Albumax II Lipid-Rich BSA (Sigma Aldrich, St Louis, MO) and 50 mg/L hypoxanthine (Thermo Fisher Scientific, Waltham, MA). This formulation is referred to as "standard media" throughout. ATG8 TetR-DOZI parasites were maintained with 0.5μM anhydrotetracycline (Sigma Aldrich, St Louis, MO) or supplemented with isopentyl pyrophosphate (Isoprenoids LC, Tampa, FL) as previously described (Walczak 2018). Cultures were grown at 37°C and individually flushed with 5% oxygen, 5% carbon dioxide, 90% nitrogen gas. Dilution of cultures with uninfected erythrocytes and changing of culture medium was performed every other day. Parasitemia was determined by flow cytometry using SYBR-Green staining. Cultures were confirmed negative for mycoplasma approximately monthly using a LookOut Mycoplasma PCR detection kit (Sigma Aldrich, St Louis, MO).

Metabolic Priming

Media for hypoxanthine metabolic priming was made using RPMI 1640 HEPES base with reduced exogenous hypoxanthine addition to a final concentration of 0.5 μM. Thiamine free media was custom ordered to be identical to RPMI 1640 HEPES without the addition of thiamine hydrochloride. Hypoxanthine was added to thiamine free media to 50 mg/L. Reduced isoleucine media was made using isoleucine deficient RPMI 1640 base powder (US Biologicals, Salem, MA) with the addition of 50 mg/L hypoxanthine and 25mM HEPES. HPLM (Thermo Fisher Scientific, Waltham, MA) was used without added HEPES or exogenous hypoxanthine. All media formulations were supplemented with 0.5% Albumax II Lipid-Rich BSA.

Uninfected erythrocytes were pre-incubated prior to use in priming experiments in the appropriate low nutrient medium for 48h at 37°C, 3-6% hematocrit, and 5% oxygen, 5% carbon dioxide, 90% nitrogen gas. Pre-incubated uninfected erythrocytes were seeded with infected erythrocyte culture to a starting parasitemia of <0.5% and resuspended in control medium for non-primed samples or low nutrient medium for primed samples. Culture were allowed to incubate for the prescribed period of time dependent on the nutrient deprived (**Table 4.1**). For 72h incubations, media was refreshed at 48h.

Aliquots were taken for flow cytometry measurement with SYBR Green I and MitoProbe DiIC1(5) kit (both Thermo Fisher Scientific, Waltham, MA). Primed samples were compared to non-primed counterparts for reduction in growth, mitochondrial membrane potential (MMP), and percentage of ring stage parasites. Priming was considered successful when the following conditions were met for hypoxanthine and isoleucine primed samples compared to non-primed: 1) an approximately 10-50% growth decrease in growth, 2) little to no decrease in MMP (approx. <10% drop??), and 3) ring stage percentages within 10% of non-primed. Priming in low thiamine and HPLM conditions was considered successful if both conditions "2" and "3" were met. Following successful priming, both primed and non-primed samples were treated with either 200nM dihydroartemisinin (Sigma Aldrich, St Louis, MO) or DMSO for 6h. To remove drug, cultures were washed three times in media and all samples were resuspended in normal, full-nutrient RPMI + Albumax media and returned to the incubator. Cultures were measured every other day with SYBR Green and MitoProbe for 10-14 days post drug treatment.

Ring and Trophozoite Stage Survival Assays

Survival assays were performed as previously described with minor modifications (ref to Witkowski Method, SLOPE paper?). Briefly, all metabolically primed samples were suspended in the relevant media at 36h, 72h, or ≥7d prior to drug treatment for thiamine, hypoxanthine, and HPLM primed conditions, respectively. Approximately 30 h prior to 0-3h ring generation, 35-mL cultures were synchronized with 5% D-sorbitol and allowed to progress until the culture was predominantly schizonts. Schizonts were isolated by layering 4 mL of culture over 4 mL of 75% Percoll, centrifugation, and collection of the intermediate band. Isolated schizonts were washed then added to uninfected erythrocytes in the appropriate media formulation. Exactly three hours later, a rapid D-sorbitol synchronization was performed (10m at 37 °C followed by 5s vortex) to remove any uninvaded late-stage parasites. Parasites for TSAs were returned to the incubator for exactly 24h before drug treatment, whereas parasites for RSAs were immediately pulsed with either DMSO or DHA (200nM or 700nM) for 6h. Following drug treatment, all cells

were washed multiple times and returned to RPMI + ALB media for 66h prior to assessment of survival by flow cytometry measurement with SYBR Green I and MitoProbe DiIC1(5) kit.

Immunoblotting

Rabbit primary antibodies against total eIF2a (Abcam, city) or phospho-specific eIF2a (Cell Signaling Technology, city) were used in conjunction with IRDye® 800CW Goat anti-Rabbit IgG Secondary Antibody (LI-COR Biotechnology, city). Anti-ATG8 was a gift from Ellen Yeh (Stanford University, Stanford, CA). Anti-ATG8 was used in conjunction Goat Anti-Guinea pig IgG H&L (Alexa Fluor® 488) (abcam) with Bound antibodies were detected on a Biorad Imager and quantified using Image Lab Software.

RNAseq

Ring stage samples were generated by synchronization with 5% sorbitol 88h and 44h prior to harvest to accommodate the ~44h erythrocytic cycle duration of Dd2 (Reilly 2007). Primed sample groups were grown as described above in their designated media for 72h, 36h, and 7d prior to extraction for hypoxanthine, thiamine, and HPLM groups, respectively. Starting 24h prior to RNA extraction, smears were made every 3 hours until reinvasion was observed to approximate the age of rings in final samples. At sample collection, erythrocytes were lysed in 0.15% saponin before RNA was extracted from parasite pellets using a Direct-zol RNA Miniprep Kit (Zymo Research) according to the manufacturer's instructions. An aliquot of each sample was taken for later assessment with a 2100 Bioanalyzer using the RNA 6000 Pico assay (Agilent Technologies, USA) before the remainder of sample was snap frozen in liquid nitrogen and stored at -80C.

Samples were shipped to Genewiz, Inc. for standard RNAseq with polyA selection. Results were analyzed using the "DESeq2 Workflow for paired-end unstranded reads (v.6)" on the Galaxy instance hosted by VEuPathDB. Genes were considered significantly differentially expressed if the following criteria were met 1) Benjamini-Hochberg adjusted p-value of ≤0.05 and 2) log2-fold change of ≥1.0 or ≤ -1.0. Gene annotation information was pulled from PlasmoDB (Release 55). Visualizations were generated in R version 4.1.2 using Tidyverse packages.

Supplemental Materials

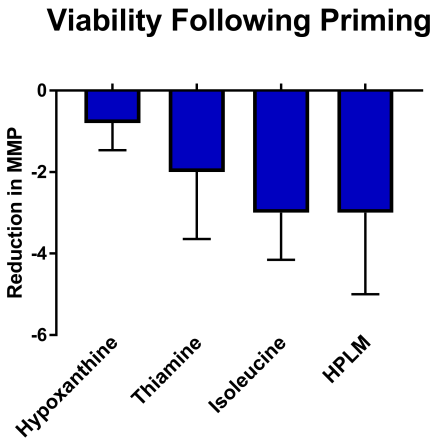

Supplementary Figure 4.1. Metabolic priming leads to minimal drops in MMP. Low nutrient metabolic priming leads to very small drops in MMP compared to standard media, non-primed controls.

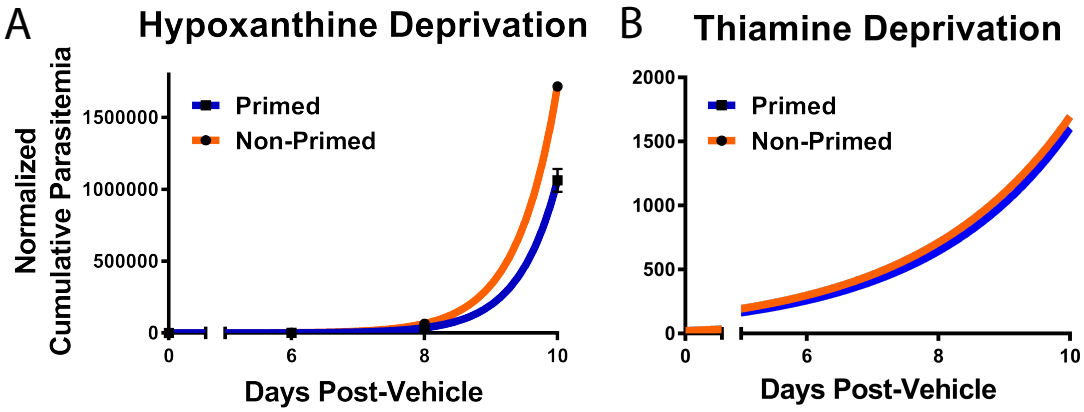

Supplementary Figure 4.2. Metabolic priming has no growth benefit without DHA challenge. A-B) Growth in standard media following A) low hypoxanthine or B) thiamine free metabolic priming without a DHA drug pulse. Bars represent S.E.M. of technical replicates within one independent experiment.

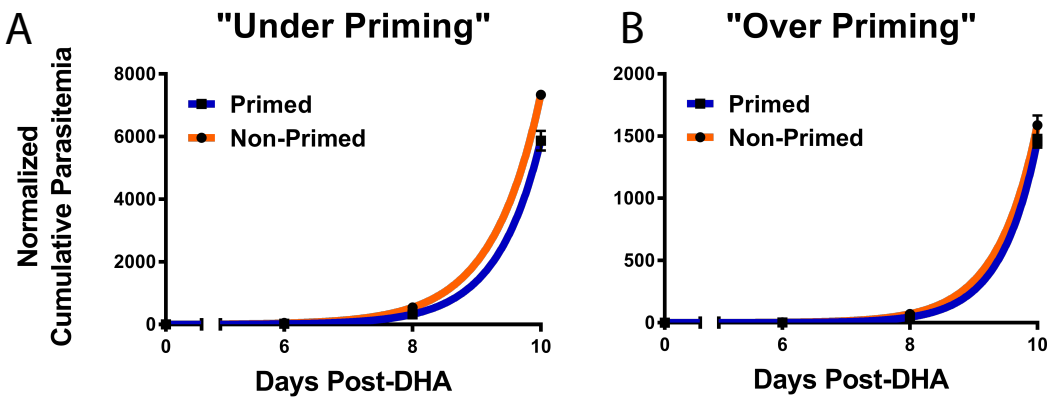

Supplementary Figure 4.3. Metabolic priming is not beneficial outside of the hermetic range. A-B) Post-DHA recovery in standard media following low hypoxanthine metabolic priming where priming led to A) less than 10% growth reduction or B) greater than ~50% growth reduction compared to non-primed controls. Bars represent S.E.M. of technical replicates within one independent experiment.

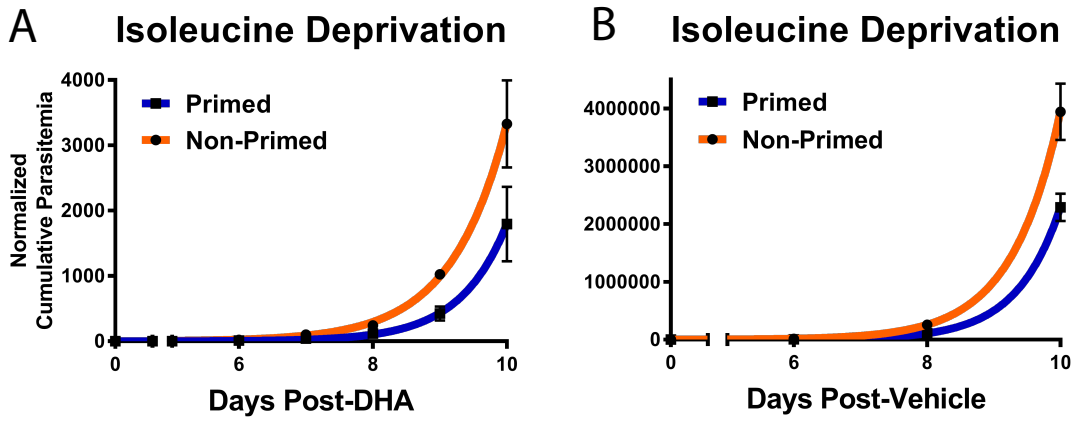

Supplementary Figure 4.4. Isoleucine priming conditions used did not induce increased post-DHA proliferation. A-B) Recovery in standard media of isoleucine primed parasites which A) received a 6h 200nM DHA pulse or B) a vehicle control pulse. Bars represent S.E.M. of technical replicates within one independent experiment.

Supplemental Table 4.1. Data for all recovery post-DHA or post-vehicle control experiments.

LINE	PRIMING STRESS	DRUG STRESS	D10% DIFFERENCE	NON-PRIMED %RINGS	PRIMED %RINGS	PRIMING GROWTH RED.	PRIMING MMP CHANGE	BLOOD AGE (DAYS)
DD2	Hypoxanthine	DHA	200	53.5	59	30	n.d.	14
DD2	Hypoxanthine	DHA	99	58.5	53.5	42	-3	24
DD2	Thiamine Free	DHA	104	72.5	68.5	-69	-18	14
DD2	Thiamine Free	DHA	137	56.5	57	-1	1	18
DD2	Isoleucine	DHA	-46	56	54.5	39	-5	11
DD2	Isoleucine	DHA	25	58.5	66.5	30	-1	9
DD2	HPLM	DHA	676	73.5	74.5	-4	-7	28
DD2	HPLM	DHA	151	76	78	0	-1	16
NF54	Hypoxanthine	DHA	20	47.5	45.5	14	-3	27
NF54 (ATG8 ON)	Hypoxanthine	DHA	304	61	54	60	2	24
NF54 ATG8 OFF	Hypoxanthine	DHA	85	67	61	36	2	24
MRA1238	Hypoxanthine	DHA	142	66.5	63	36	n.d.	9
NF54	Thiamine Free	DHA	195	68.5	67.5	10	1	18
NF54	Thiamine Free	DHA	257	44.5	47	17	-2	18
NF54	Hypoxanthine	No Drug	-30	47.5	45.5	14	-3	27
NF54	Hypoxanthine	No Drug	-27	68.5	75	45	0	9
DD2	Hypoxnathine	No Drug	-38	60	56	24	-1	12
NF54	Hypoxnathine	No Drug	-9	60.5	58.5	37	-3	27
DD2	Thiamine Free	No Drug	-5	48.5	44.5	7	-2	16
DD2	Isoleucine	No Drug	-42	59	64.5	48	-3	19
DD2	HPLM	No Drug	111	76	76	-14	n.d.	21
DD2	HPLM	No Drug		76	78	0	-1	16
NF54 (ATG8 ON)	Hypoxanthine	DHA	-20	72	68	9	0	16
D6	Hypoxanthine	DHA	-8	62	32	66	1	20

Supplemental Table 4.2. Papers measuring basal differences between artemisinin resistant and sensitive parasites using 'Omics level approaches.

Publication	Level	No. Genes Used
Demas, et al. 2018 PNAS	Genome	7
Rocamora, et al. 2018 PloS Pathogens	Genome; Transcript	47
Mok, et al. 2021 Nature Comm.	Transcript	80
Siddiqui, et al. 2017 J. Infectious Disease	Protein	12
Witkowksi, et al. 2010 AAC.	Transcript	9
	Total	**154**
	Unique Genes	**151**

Gene ID	Publication
PF3D7_1454700	Rocamora, et al. 2018 PloS Path
PF3D7_1457200	Rocamora, et al. 2018 PloS Path
PF3D7_1457000	Rocamora, et al. 2018 PloS Path
PF3D7_0704800	Rocamora, et al. 2018 PloS Path
PF3D7_0730300	Rocamora, et al. 2018 PloS Path
PF3D7_1115700	Rocamora, et al. 2018 PloS Path
PF3D7_1141800	Rocamora, et al. 2018 PloS Path
PF3D7_1427100	Rocamora, et al. 2018 PloS Path
PF3D7_0420300	Rocamora, et al. 2018 PloS Path
PF3D7_0528300	Rocamora, et al. 2018 PloS Path
PF3D7_0617100	Rocamora, et al. 2018 PloS Path
PF3D7_0810600	Rocamora, et al. 2018 PloS Path
PF3D7_1230000	Rocamora, et al. 2018 PloS Path
PF3D7_1368400	Rocamora, et al. 2018 PloS Path
PF3D7_1478100	Rocamora, et al. 2018 PloS Path
PF3D7_1200800	Rocamora, et al. 2018 PloS Path
PF3D7_0702300	Rocamora, et al. 2018 PloS Path
PF3D7_1030100	Rocamora, et al. 2018 PloS Path
PF3D7_1300300	Rocamora, et al. 2018 PloS Path
PF3D7_1479000	Rocamora, et al. 2018 PloS Path
PF3D7_0933500	Rocamora, et al. 2018 PloS Path
PF3D7_0812500	Rocamora, et al. 2018 PloS Path
PF3D7_0113400	Rocamora, et al. 2018 PloS Path
PF3D7_1110400	Rocamora, et al. 2018 PloS Path
PF3D7_1116800	Rocamora, et al. 2018 PloS Path
PF3D7_1235300	Rocamora, et al. 2018 PloS Path
PF3D7_1351000	Rocamora, et al. 2018 PloS Path
PF3D7_0609900	Rocamora, et al. 2018 PloS Path
PF3D7_1406200	Rocamora, et al. 2018 PloS Path
PF3D7_0400400	Rocamora, et al. 2018 PloS Path

PF3D7_0600200	Rocamora, et al. 2018 PloS Path
PF3D7_1001200	Rocamora, et al. 2018 PloS Path
PF3D7_0400500	Rocamora, et al. 2018 PloS Path
PF3D7_0712900	Rocamora, et al. 2018 PloS Path
PF3D7_1139100	Rocamora, et al. 2018 PloS Path
PF3D7_0201600	Rocamora, et al. 2018 PloS Path
PF3D7_0302300	Rocamora, et al. 2018 PloS Path
PF3D7_0600400	Rocamora, et al. 2018 PloS Path
PF3D7_1208400	Rocamora, et al. 2018 PloS Path
PF3D7_1470800	Rocamora, et al. 2018 PloS Path
PF3D7_1245500	Rocamora, et al. 2018 PloS Path
PF3D7_0409100	Rocamora, et al. 2018 PloS Path
PF3D7_0617400	Rocamora, et al. 2018 PloS Path
PF3D7_0918300	Rocamora, et al. 2018 PloS Path
PF3D7_0906400	Rocamora, et al. 2018 PloS Path
PF3D7_0107900	Rocamora, et al. 2018 PloS Path
PF3D7_0315000	Rocamora, et al. 2018 PloS Path
PF3D7_0701900	Mok, et al. 2021 Nat Comm
PF3D7_1252600	Mok, et al. 2021 Nat Comm
PF3D7_0702100	Mok, et al. 2021 Nat Comm
PF3D7_1341700	Mok, et al. 2021 Nat Comm
PF3D7_1343700	Mok, et al. 2021 Nat Comm
PF3D7_1218500	Mok, et al. 2021 Nat Comm
PF3D7_1252900	Mok, et al. 2021 Nat Comm
PF3D7_0102200	Mok, et al. 2021 Nat Comm
PF3D7_0401900	Mok, et al. 2021 Nat Comm
PF3D7_1352900	Mok, et al. 2021 Nat Comm
PF3D7_1002100	Mok, et al. 2021 Nat Comm
PF3D7_0933000	Mok, et al. 2021 Nat Comm
PF3D7_1108000	Mok, et al. 2021 Nat Comm
PF3D7_1461600	Mok, et al. 2021 Nat Comm
PF3D7_1006800	Mok, et al. 2021 Nat Comm
PF3D7_0612900	Mok, et al. 2021 Nat Comm
PF3D7_0901900	Mok, et al. 2021 Nat Comm
PF3D7_1000800	Mok, et al. 2021 Nat Comm
PF3D7_1361900	Mok, et al. 2021 Nat Comm
PF3D7_0317200	Mok, et al. 2021 Nat Comm
PF3D7_1304100	Mok, et al. 2021 Nat Comm
PF3D7_1320100	Mok, et al. 2021 Nat Comm
PF3D7_0811600	Mok, et al. 2021 Nat Comm
PF3D7_0315900	Mok, et al. 2021 Nat Comm
PF3D7_1246200	Mok, et al. 2021 Nat Comm
PF3D7_0935800	Mok, et al. 2021 Nat Comm

PF3D7_1223100	Mok, et al. 2021 Nat Comm
PF3D7_1252100	Mok, et al. 2021 Nat Comm
PF3D7_0104200	Mok, et al. 2021 Nat Comm
PF3D7_1128900	Mok, et al. 2021 Nat Comm
PF3D7_1467900	Mok, et al. 2021 Nat Comm
PF3D7_1145200	Mok, et al. 2021 Nat Comm
PF3D7_1335100	Mok, et al. 2021 Nat Comm
PF3D7_0831600	Mok, et al. 2021 Nat Comm
PF3D7_0722200	Mok, et al. 2021 Nat Comm
PF3D7_1140400	Mok, et al. 2021 Nat Comm
PF3D7_1206300	Mok, et al. 2021 Nat Comm
PF3D7_1452000	Mok, et al. 2021 Nat Comm
PF3D7_0810300	Mok, et al. 2021 Nat Comm
PF3D7_0419700	Mok, et al. 2021 Nat Comm
PF3D7_1021700	Mok, et al. 2021 Nat Comm
PF3D7_0628100	Mok, et al. 2021 Nat Comm
PF3D7_0905500	Mok, et al. 2021 Nat Comm
PF3D7_0802600	Mok, et al. 2021 Nat Comm
PF3D7_1022500	Mok, et al. 2021 Nat Comm
PF3D7_0817600	Mok, et al. 2021 Nat Comm
PF3D7_1035300	Mok, et al. 2021 Nat Comm
PF3D7_1035900	Mok, et al. 2021 Nat Comm
PF3D7_1104900	Mok, et al. 2021 Nat Comm
PF3D7_1028700	Mok, et al. 2021 Nat Comm
PF3D7_0614700	Mok, et al. 2021 Nat Comm
PF3D7_1246400	Mok, et al. 2021 Nat Comm
PF3D7_1229800	Mok, et al. 2021 Nat Comm
PF3D7_1344300	Mok, et al. 2021 Nat Comm
PF3D7_0407900	Mok, et al. 2021 Nat Comm
PF3D7_1133400	Mok, et al. 2021 Nat Comm
PF3D7_0822900	Mok, et al. 2021 Nat Comm
PF3D7_0210600	Mok, et al. 2021 Nat Comm
PF3D7_1036000	Mok, et al. 2021 Nat Comm
PF3D7_1468400	Mok, et al. 2021 Nat Comm
PF3D7_1243700	Mok, et al. 2021 Nat Comm
PF3D7_0308300	Mok, et al. 2021 Nat Comm
PF3D7_1251200	Mok, et al. 2021 Nat Comm
PF3D7_0821400	Mok, et al. 2021 Nat Comm
PF3D7_1310700	Mok, et al. 2021 Nat Comm
PF3D7_0515400	Mok, et al. 2021 Nat Comm
PF3D7_1036500	Mok, et al. 2021 Nat Comm
PF3D7_0424100	Mok, et al. 2021 Nat Comm
PF3D7_1125700	Mok, et al. 2021 Nat Comm

PF3D7_0214600	Mok, et al. 2021 Nat Comm
PF3D7_0828800	Mok, et al. 2021 Nat Comm
PF3D7_1227700	Mok, et al. 2021 Nat Comm
PF3D7_0402300	Mok, et al. 2021 Nat Comm
PF3D7_1238800	Mok, et al. 2021 Nat Comm
PF3D7_0731500	Mok, et al. 2021 Nat Comm
PF3D7_0408000	Mok, et al. 2021 Nat Comm
PF3D7_1230700	Mok, et al. 2021 Nat Comm
PF3D7_1433500	Mok, et al. 2021 Nat Comm
PF3D7_0410000	Mok, et al. 2021 Nat Comm
PF3D7_1240100	Mok, et al. 2021 Nat Comm
PF3D7_1251200	Demas, et al. 2018 PNAS
PF3D7_1433800	Demas, et al. 2018 PNAS
PF3D7_1126100	Demas, et al. 2018 PNAS
PF3D7_0209600	Demas, et al. 2018 PNAS
PF3D7_1121900	Demas, et al. 2018 PNAS
PF3D7_1324300	Demas, et al. 2018 PNAS
PF3D7_1422400	Demas, et al. 2018 PNAS
PF3D7_1343700	Siddiqui, et al. 2017 JID
PF3D7_0500800	Siddiqui, et al. 2017 JID
PF3D7_1116700	Siddiqui, et al. 2017 JID
PF3D7_0406200	Siddiqui, et al. 2017 JID
PF3D7_0702500	Siddiqui, et al. 2017 JID
PF3D7_1343700	Siddiqui, et al. 2017 JID
PF3D7_1364800	Siddiqui, et al. 2017 JID
PF3D7_0209800	Siddiqui, et al. 2017 JID
PF3D7_1447000	Siddiqui, et al. 2017 JID
PF3D7_0204500	Siddiqui, et al. 2017 JID
PF3D7_1206200	Siddiqui, et al. 2017 JID
PF3D7_0320700	Siddiqui, et al. 2017 JID
PF3D7_0202000	Wikowski, et al. 2010 AAC
PF3D7_1372500	Wikowski, et al. 2010 AAC
PF3D7_1372600	Wikowski, et al. 2010 AAC
PF3D7_0818900	Wikowski, et al. 2010 AAC
PF3D7_1012400	Wikowski, et al. 2010 AAC
PF3D7_0202100	Wikowski, et al. 2010 AAC
PF3D7_0300900	Wikowski, et al. 2010 AAC
PF3D7_0301700	Wikowski, et al. 2010 AAC
PF3D7_0528400	Wikowski, et al. 2010 AAC

References

1. Guggisberg, A.M. et al. (2016) Whole-Genome Sequencing to Evaluate the Resistance Landscape Following Antimalarial Treatment Failure With Fosmidomycin-Clindamycin. J Infect Dis 214 (7), 1085-91.

2. Liu, S. et al. (2020) Single cell sequencing of the small and AT-skewed genome of malaria parasites. bioRxiv, 2020.02.21.960039.

3. Oyola, S.O. et al. (2016) Whole genome sequencing of Plasmodium falciparum from dried blood spots using selective whole genome amplification. Malar J 15 (1), 597.

4. Shah, Z. et al. (2020) Optimization of parasite DNA enrichment approaches to generate whole genome sequencing data for Plasmodium falciparum from low parasitaemia samples. Malar J 19 (1), 135.

5. Cowell, A.N. et al. (2017) Selective Whole-Genome Amplification Is a Robust Method That Enables Scalable Whole-Genome Sequencing of Plasmodium vivax from Unprocessed Clinical Samples. mBio 8 (1).

6. Venkatesan, M. et al. (2012) Using CF11 cellulose columns to inexpensively and effectively remove human DNA from Plasmodium falciparum-infected whole blood samples. Malar J 11, 41.

7. Benavente, E.D. et al. (2019) Whole genome sequencing of amplified Plasmodium knowlesi DNA from unprocessed blood reveals genetic exchange events between Malaysian Peninsular and Borneo subpopulations. Sci Rep 9 (1), 9873.

8. Nag, S. et al. (2018) Direct whole-genome sequencing of Plasmodium falciparum specimens from dried erythrocyte spots. Malar J 17 (1), 91.

9. Auburn, S. et al. (2011) An effective method to purify Plasmodium falciparum DNA directly from clinical blood samples for whole genome high-throughput sequencing. PLoS One 6 (7), e22213.

10. Claessens, A. et al. (2012) A subset of group A-like var genes encodes the malaria parasite ligands for binding to human brain endothelial cells. Proceedings of the National Academy of Sciences 109 (26), E1772.

11. Brown, A.C. et al. (2020) Cholesterol-dependent enrichment of understudied erythrocytic stages of human Plasmodium parasites. Sci Rep 10 (1), 4591.

12. Boissière, A. et al. (2012) Isolation of Plasmodium falciparum by flow-cytometry: implications for single-trophozoite genotyping and parasite DNA purification for whole-genome high-throughput sequencing of archival samples. Malar J 11, 163.

13. Pillai, A.D. et al. (2012) Solute restriction reveals an essential role for clag3-associated channels in malaria parasite nutrient acquisition. Mol Pharmacol 82 (6), 1104-14.

14. Sharma, P. et al. (2013) An epigenetic antimalarial resistance mechanism involving parasite genes linked to nutrient uptake. J Biol Chem 288 (27), 19429-40.

15. Flaherty, B.R. et al. (2018) Restriction enzyme digestion of host DNA enhances universal detection of parasitic pathogens in blood via targeted amplicon deep sequencing. Microbiome 6 (1), 164.

16. Oyola, S.O. et al. (2013) Efficient depletion of host DNA contamination in malaria clinical sequencing. J Clin Microbiol 51 (3), 745-51.

17. Chen, K. et al. (2014) Competition between Plasmodium falciparum strains in clinical infections during in vitro culture adaptation. Infect Genet Evol 24, 105-10.

18. Bright, A.T. et al. (2012) Whole genome sequencing analysis of Plasmodium vivax using whole genome capture. BMC Genomics 13, 262.

19. Hupalo, D.N. et al. (2016) Population genomics studies identify signatures of global dispersal and drug resistance in Plasmodium vivax. Nat Genet 48 (8), 953-8.

20. Melnikov, A. et al. (2011) Hybrid selection for sequencing pathogen genomes from clinical samples. Genome Biol 12 (8), R73.

21. Nyarko, P.B. et al. (2020) Investigating a Plasmodium falciparum erythrocyte invasion phenotype switch at the whole transcriptome level. Sci Rep 10 (1), 245.

22. Gural, N. et al. (2018) In Vitro Culture, Drug Sensitivity, and Transcriptome of Plasmodium Vivax Hypnozoites. Cell Host Microbe 23 (3), 395-406.e4.

23. Udomsangpetch, R. et al. (2002) Febrile temperatures induce cytoadherence of ring-stage Plasmodium falciparum-infected erythrocytes. Proc Natl Acad Sci U S A 99 (18), 11825-9.

24. Zhang, R. et al. (2018) Febrile Temperature Elevates the Expression of Phosphatidylserine on Plasmodium falciparum (FCR3CSA) Infected Red Blood Cell Surface Leading to Increased Cytoadhesion. Sci Rep 8 (1), 15022.

25. Oakley, M.S.M. et al. (2007) Molecular factors and biochemical pathways induced by febrile temperature in intraerythrocytic Plasmodium falciparum parasites. Infection and immunity 75 (4), 2012-2025.

26. Prevention, T.C.f.D.C.a. About Malaria. https://www.cdc.gov/malaria/about/, (accessed).

27. Engelbrecht, D. and Coetzer, T.L. (2013) Turning up the heat: heat stress induces markers of programmed cell death in Plasmodium falciparum in vitro. Cell death & disease 4 (12), e971-e971.

28. Price, R.N. et al. (2020) Plasmodium vivax in the Era of the Shrinking P. falciparum Map. Trends in Parasitology 36 (6), 560-570.

29. Singhaboot, Y. et al. (2019) Temperature Dependence of Plasmodium falciparum Erythrocytic Stage Development. The American journal of tropical medicine and hygiene 100 (5), 1191-1195.

30. Oakley, M.S. et al. (2011) Clinical and molecular aspects of malaria fever. Trends Parasitol 27 (10), 442-9.

31. Hawadak, J. et al. (2021) Global trend of Plasmodium malariae and Plasmodium ovale spp. malaria infections in the last two decades (2000–2020): a systematic review and meta-analysis. Parasites & Vectors 14 (1), 297.

32. Blasco, B. et al. (2017) Antimalarial drug resistance: linking Plasmodium falciparum parasite biology to the clinic. Nature Medicine 23 (8), 917-928.

33. Sahu, S. et al. (2010) Spectrum of malaria complications in an intensive care unit. Singapore Med J 51 (3), 226-9.

34. Seydel, K.B. et al. (2015) Brain Swelling and Death in Children with Cerebral Malaria. New England Journal of Medicine 372 (12), 1126-1137.

35. Fowkes, F.J. et al. (2016) Immunity to malaria in an era of declining malaria transmission. Parasitology 143 (2), 139-53.

36. Gonzales, S.J. et al. (2020) Naturally Acquired Humoral Immunity Against Plasmodium falciparum Malaria. Frontiers in Immunology 11.

37. World Health, O. (2015) Guidelines for the treatment of malaria, 3rd ed edn., World Health Organization.

38. Dondorp, A.M. et al. (2009) Artemisinin Resistance in Plasmodium falciparum Malaria. New England Journal of Medicine 361 (5), 455-467.

39. Lu, F. et al. (2017) Emergence of Indigenous Artemisinin-Resistant Plasmodium falciparum in Africa. New England Journal of Medicine 376 (10), 991-993.

40. Cobbold, S.A. et al. (2016) Metabolic Dysregulation Induced in Plasmodium falciparum by Dihydroartemisinin and Other Front-Line Antimalarial Drugs. J Infect Dis 213 (2), 276-86.

41. Mok, S. et al. (2015) Drug resistance. Population transcriptomics of human malaria parasites reveals the mechanism of artemisinin resistance. Science 347 (6220), 431-5.

42. Teuscher, F. et al. (2010) Artemisinin-induced dormancy in plasmodium falciparum: duration, recovery rates, and implications in treatment failure. J Infect Dis 202 (9), 1362-8.

43. Breglio, K.F. et al. (2018) Kelch Mutations in Plasmodium falciparum Protein K13 Do Not Modulate Dormancy after Artemisinin Exposure and Sorbitol Selection In Vitro. Antimicrob Agents Chemother 62 (5).

44. Sà, J.M. et al. (2020) Single-cell transcription analysis of Plasmodium vivax blood-stage parasites identifies stage- and species-specific profiles of expression. PLoS biology 18 (5), e3000711-e3000711.

45. Ariey, F. et al. (2014) A molecular marker of artemisinin-resistant Plasmodium falciparum malaria. Nature 505 (7481), 50-55.

46. Ashley, E.A. et al. (2014) Spread of artemisinin resistance in Plasmodium falciparum malaria. N Engl J Med 371 (5), 411-23.

47. Mbengue, A. et al. (2015) A molecular mechanism of artemisinin resistance in Plasmodium falciparum malaria. Nature 520 (7549), 683-7.

48. Breglio, K.F. et al. (2018) A single nucleotide polymorphism in the Plasmodium falciparum atg18 gene associates with artemisinin resistance and confers enhanced parasite survival under nutrient deprivation. Malar J 17 (1), 391.

49. Dogovski, C. et al. (2015) Targeting the cell stress response of Plasmodium falciparum to overcome artemisinin resistance. PLoS Biol 13 (4), e1002132.

50. Zhang, M. et al. (2017) Inhibiting the Plasmodium eIF2α Kinase PK4 Prevents Artemisinin-Induced Latency. Cell Host Microbe 22 (6), 766-776.e4.

51. Wang, L. et al. (2019) Antimalarial Dihydroartemisinin triggers autophagy within HeLa cells of human cervical cancer through Bcl-2 phosphorylation at Ser70. Phytomedicine 52, 147-156.

52. Wang, Z. et al. (2012) Dihydroartemisinin induces autophagy and inhibits the growth of iron-loaded human myeloid leukemia K562 cells via ROS toxicity. FEBS Open Bio 2, 103-112.

53. Chen, N. et al. (2014) Fatty acid synthesis and pyruvate metabolism pathways remain active in dihydroartemisinin-induced dormant ring stages of Plasmodium falciparum. Antimicrobial agents and chemotherapy 58 (8), 4773-4781.

54. Cheng, Q. et al. (2012) Artemisinin resistance in Plasmodium falciparum: A process linked to dormancy? International journal for parasitology. Drugs and drug resistance 2, 249-255.

55. Ittarat, W. et al. (2003) Recrudescence in artesunate-treated patients with falciparum malaria is dependent on parasite burden not on parasite factors. Am J Trop Med Hyg 68 (2), 147-52.

56. Looareesuwan, S. et al. (1997) Open randomized trial of oral artemether alone and a sequential combination with mefloquine for acute uncomplicated falciparum malaria. Am J Trop Med Hyg 56 (6), 613-7.

57. Amato, S.M. et al. (2014) The role of metabolism in bacterial persistence. Front Microbiol 5, 70.

58. Harms, A. et al. (2016) Mechanisms of bacterial persistence during stress and antibiotic exposure. Science 354 (6318).

59. Tucker, M.S. et al. (2012) Phenotypic and genotypic analysis of in vitro-selected artemisinin-resistant progeny of Plasmodium falciparum. Antimicrobial agents and chemotherapy 56 (1), 302-314.

60. Cassera, M.B. et al. (2011) Purine and pyrimidine pathways as targets in Plasmodium falciparum. Current topics in medicinal chemistry 11 (16), 2103-2115.

61. Evans, G.B. et al. (2018) Immucillins in Infectious Diseases. ACS Infect Dis 4 (2), 107-117.

62. Phillips, M.A. et al. (2015) A long-duration dihydroorotate dehydrogenase inhibitor (DSM265) for prevention and treatment of malaria. Science translational medicine 7 (296), 296ra111-296ra111.

63. Sulyok, M. et al. (2017) DSM265 for Plasmodium falciparum chemoprophylaxis: a randomised, double blinded, phase 1 trial with controlled human malaria infection. The Lancet Infectious Diseases 17 (6), 636-644.

64. Guo, J.Y. et al. (2016) Autophagy provides metabolic substrates to maintain energy charge and nucleotide pools in Ras-driven lung cancer cells. Genes Dev 30 (15), 1704-17.

65. Chan, X.W.A. et al. (2013) Chemical and genetic validation of thiamine utilization as an antimalarial drug target. Nature Communications 4 (1), 2060.

66. Müller, I.B. et al. (2010) Vitamin B metabolism in Plasmodium falciparum as a source of drug targets. Trends Parasitol 26 (1), 35-43.

67. Eschbach, M.L. et al. (2006) The human malaria parasite Plasmodium falciparum expresses an atypical N-terminally extended pyrophosphokinase with specificity for thiamine. Biol Chem 387 (12), 1583-91.

68. Wrenger, C. et al. (2006) Vitamin B1 de novo synthesis in the human malaria parasite Plasmodium falciparum depends on external provision of 4-amino-5-hydroxymethyl-2-methylpyrimidine. Biol Chem 387 (1), 41-51.

69. Carey, M.A. et al. (2017) Novel Plasmodium falciparum metabolic network reconstruction identifies shifts associated with clinical antimalarial resistance. BMC Genomics 18 (1), 543.

70. WHO, World malaria report 2019, World Heath Organization Geneva, 2019.

71. Carter, R. and Mendis, K.N. (2002) Evolutionary and historical aspects of the burden of malaria. Clinical microbiology reviews 15 (4), 564-594.

72. Lim, C. et al. (2013) Expansion of host cellular niche can drive adaptation of a zoonotic malaria parasite to humans. Nature Communications 4 (1), 1638.

73. Moon, R.W. et al. (2013) Adaptation of the genetically tractable malaria pathogen Plasmodium knowlesi to continuous culture in human erythrocytes. Proceedings of the National Academy of Sciences 110 (2), 531.

74. Cao, P. et al. (2019) Modeling the dynamics of Plasmodium falciparum gametocytes in humans during malaria infection. Elife 8.

75. Neveu, G. et al. (2018) Plasmodium falciparum gametocyte-infected erythrocytes do not adhere to human primary erythroblasts. Scientific Reports 8 (1), 17886.

76. Obaldia, N. et al. (2018) Bone Marrow Is a Major Parasite Reservoir in Plasmodium vivax Infection. mBio 9 (3), e00625-18.

77. David, P.H. et al. (1983) Parasite sequestration in Plasmodium falciparum malaria: spleen and antibody modulation of cytoadherence of infected erythrocytes. Proceedings of the National Academy of Sciences of the United States of America 80 (16), 5075-5079.

78. LeRoux, M. et al. (2009) Plasmodium falciparum biology: analysis of in vitro versus in vivo growth conditions. Trends Parasitol 25 (10), 474-81.

79. Tilly, A.K. et al. (2015) Type of in vitro cultivation influences cytoadhesion, knob structure, protein localization and transcriptome profile of Plasmodium falciparum. Sci Rep 5, 16766.

80. Dluzewski, A.R. et al. (1985) Relation of red cell membrane properties to invasion by Plasmodium falciparum. Parasitology 91 (2), 273-280.

81. Henry, B. et al. (2020) The Human Spleen in Malaria: Filter or Shelter? Trends Parasitol 36 (5), 435-446.

82. Niang, M. et al. (2014) STEVOR is a Plasmodium falciparum erythrocyte binding protein that mediates merozoite invasion and rosetting. Cell Host Microbe 16 (1), 81-93.

83. Frankland, S. et al. (2007) Serum lipoproteins promote efficient presentation of the malaria virulence protein PfEMP1 at the erythrocyte surface. Eukaryot Cell 6 (9), 1584-94.

84. Luginbühl, A. et al. (2007) Complement factor D, albumin, and immunoglobulin G anti-band 3 protein antibodies mimic serum in promoting rosetting of malaria-infected red blood cells. Infect Immun 75 (4), 1771-7.

85. Ribacke, U. et al. (2013) Improved in vitro culture of Plasmodium falciparum permits establishment of clinical isolates with preserved multiplication, invasion and rosetting phenotypes. PLoS One 8 (7), e69781.

86. Peters, J.M. et al. (2007) Differential changes in Plasmodium falciparum var transcription during adaptation to culture. J Infect Dis 195 (5), 748-55.

87. Zhang, Q. et al. (2011) From in vivo to in vitro: dynamic analysis of Plasmodium falciparum var gene expression patterns of patient isolates during adaptation to culture. PLoS One 6 (6), e20591.

88. Chotivanich, K. et al. (2000) The mechanisms of parasite clearance after antimalarial treatment of Plasmodium falciparum malaria. J Infect Dis 182 (2), 629-33.

89. Price, R.N. et al. (2001) Factors contributing to anemia after uncomplicated falciparum malaria. Am J Trop Med Hyg 65 (5), 614-22.

90. Ferrer, J. et al. (2008) Effect of the haematocrit layer geometry on Plasmodium falciparum static thin-layer in vitro cultures. Malar J 7, 203.

91. Branco, A. and Melo-Cristino, J. (2018) Extreme parasitemia in P falciparum malaria. Blood 132 (8), 868-868.

92. Bakshi, R.P. et al. (2013) Model system to define pharmacokinetic requirements for antimalarial drug efficacy. Sci Transl Med 5 (205), 205ra135.

93. Caton, E. et al. (2016) Hollow-Fiber Methodology for Pharmacokinetic/Pharmacodynamic Studies of Antimalarial Compounds. Curr Protoc Chem Biol 8 (1), 29-58.

94. Li, T. et al. (2003) A new method for culturing Plasmodium falciparum shows replication at the highest erythrocyte densities. J Infect Dis 187 (1), 159-62.

95. Meyer, K.J. et al. (2018) Model System Identifies Kinetic Driver of Hsp90 Inhibitor Activity against African Trypanosomes and Plasmodium falciparum. Antimicrob Agents Chemother 62 (8).

96. Preechapornkul, P. et al. (2010) Optimizing the culture of Plasmodium falciparum in hollow fiber bioreactors. Southeast Asian J Trop Med Public Health 41 (4), 761-9.

97. Awandare, G.A. et al. (2018) Plasmodium falciparum strains spontaneously switch invasion phenotype in suspension culture. Sci Rep 8 (1), 5782.

98. Quadt, K.A. et al. (2012) The density of knobs on Plasmodium falciparum-infected erythrocytes depends on developmental age and varies among isolates. PLoS One 7 (9), e45658.

99. Fernandez-Becerra, C. et al. (2020) Plasmodium vivax spleen-dependent genes encode antigens associated with cytoadhesion and clinical protection. Proc Natl Acad Sci U S A 117 (23), 13056-13065.

100. Dans, M.G. et al. (2020) Screening the Medicines for Malaria Venture Pathogen Box for invasion and egress inhibitors of the blood stage of Plasmodium falciparum reveals several inhibitory compounds. Int J Parasitol 50 (3), 235-252.

101. Dennis, A.S.M. et al. (2018) Diverse antimalarials from whole-cell phenotypic screens disrupt malaria parasite ion and volume homeostasis. Sci Rep 8 (1), 8795.

102. Burrows, J.N. et al. (2017) New developments in anti-malarial target candidate and product profiles. Malaria journal 16 (1), 26-26.

103. Ochong, E. et al. (2013) Fitness Consequences of Plasmodium falciparum pfmdr1 Polymorphisms Inferred from Ex Vivo Culture of Ugandan Parasites. Antimicrob Agents Chemother 57 (9), 4245-4251.

104. Chaorattanakawee, S. et al. (2015) Attenuation of Plasmodium falciparum in vitro drug resistance phenotype following culture adaptation compared to fresh clinical isolates in Cambodia. Malaria Journal 14 (1), 486.

105. Akala, H.M. et al. (2011) Antimalarial drug sensitivity profile of western Kenya Plasmodium falciparum field isolates determined by a SYBR Green I in vitro assay and molecular analysis. Am J Trop Med Hyg 85 (1), 34-41.

106. Juge, N. et al. (2015) Plasmodium falciparum chloroquine resistance transporter is a H+ -coupled polyspecific nutrient and drug exporter. Proceedings of the National Academy of Sciences 112 (11), 3356.

107. Wang, J. et al. (2015) Haem-activated promiscuous targeting of artemisinin in Plasmodium falciparum. Nature communications 6, 10111-10111.

108. Lapp, S.A. et al. (2015) Plasmodium knowlesi gene expression differs in ex vivo compared to in vitro blood-stage cultures. Malaria Journal 14 (1), 110.

109. Herman, J.D. et al. (2014) A genomic and evolutionary approach reveals non-genetic drug resistance in malaria. Genome Biol 15 (11), 511.

110. Duffy, S. and Avery, V.M. (2017) Plasmodium falciparum in vitro continuous culture conditions: A comparison of parasite susceptibility and tolerance to anti-malarial drugs throughout the asexual intra-erythrocytic life cycle. Int J Parasitol Drugs Drug Resist 7 (3), 295-302.

111. Singh, K. et al. (2007) Growth, drug susceptibility, and gene expression profiling of Plasmodium falciparum cultured in medium supplemented with human serum or lipid-rich bovine serum albumin [corrected]. J Biomol Screen 12 (8), 1109-14.

112. Hoo, R. et al. (2019) Transcriptome profiling reveals functional variation in Plasmodium falciparum parasites from controlled human malaria infection studies. EBioMedicine 48, 442-452.

113. Rovira-Graells, N. et al. (2012) Transcriptional variation in the malaria parasite Plasmodium falciparum. Genome Res 22 (5), 925-38.

114. Tarr, S.J. et al. (2018) Schizont transcriptome variation among clinical isolates and laboratory-adapted clones of the malaria parasite Plasmodium falciparum. BMC Genomics 19 (1), 894.

115. Lee, H.J. et al. (2018) Transcriptomic Studies of Malaria: a Paradigm for Investigation of Systemic Host-Pathogen Interactions. Microbiol Mol Biol Rev 82 (2).

116. Mackinnon, M.J. et al. (2009) Comparative transcriptional and genomic analysis of Plasmodium falciparum field isolates. PLoS Pathog 5 (10), e1000644.

117. Moon, R.W. et al. (2016) Normocyte-binding protein required for human erythrocyte invasion by the zoonotic malaria parasite <em>Plasmodium knowlesi</em&gt. Proceedings of the National Academy of Sciences 113 (26), 7231.

118. Claessens, A. et al. (2017) Culture adaptation of malaria parasites selects for convergent loss-of-function mutants. Scientific Reports 7 (1), 41303.

119. Kafsack, B.F. et al. (2014) A transcriptional switch underlies commitment to sexual development in malaria parasites. Nature 507 (7491), 248-52.

120. Kidgell, C. et al. (2006) A systematic map of genetic variation in Plasmodium falciparum. PLoS Pathog 2 (6), e57.

121. Chaorattanakawee, S. et al. (2017) Measuring ex vivo drug susceptibility in Plasmodium vivax isolates from Cambodia. Malar J 16 (1), 392.

122. Rangel, G.W. et al. (2018) Enhanced Ex Vivo Plasmodium vivax Intraerythrocytic Enrichment and Maturation for Rapid and Sensitive Parasite Growth Assays. Antimicrob Agents Chemother 62 (4).

123. Russell, B. et al. (2013) Field-based flow cytometry for ex vivo characterization of Plasmodium vivax and P. falciparum antimalarial sensitivity. Antimicrob Agents Chemother 57 (10), 5170-4.

124. WHO, IN VITRO MICRO-TEST (MARK III) FOR THE ASSESSMENT OF THE RESPONSE OF Plasmodium falciparum TO CHLOROQUINE, MEFLOQUINE, QUININE, AMODIAQUINE, SULFADOXINE/PYRIMETHAMINE AND ARTEMISININ, in: Diseases, D.o.C.o.T. (Ed.) 2001.

125. Amaratunga, C. et al. (2012) Artemisinin-resistant Plasmodium falciparum in Pursat province, western Cambodia: a parasite clearance rate study. Lancet Infect Dis 12 (11), 851-8.

126. Witkowski, B. et al. (2013) Novel phenotypic assays for the detection of artemisinin-resistant Plasmodium falciparum malaria in Cambodia: in-vitro and ex-vivo drug-response studies. Lancet Infect Dis 13 (12), 1043-9.

127. Ngara, M. et al. (2018) Exploring parasite heterogeneity using single-cell RNA-seq reveals a gene signature among sexual stage Plasmodium falciparum parasites. Experimental Cell Research 371 (1), 130-138.

128. Walzer, K.A. et al. (2019) Latent transcriptional variations of individual Plasmodium falciparum uncovered by single-cell RNA-seq and fluorescence imaging. PLOS Genetics 15 (12), e1008506.

129. Nair, S. et al. (2014) Single-cell genomics for dissection of complex malaria infections. Genome research 24 (6), 1028-1038.

130. Nkhoma, S.C. et al. (2020) Co-transmission of Related Malaria Parasite Lineages Shapes Within-Host Parasite Diversity. Cell Host Microbe 27 (1), 93-103.e4.

131. Trevino, S.G. et al. (2017) High-Resolution Single-Cell Sequencing of Malaria Parasites. Genome Biol Evol 9 (12), 3373-3383.

132. Siddiqui, G. et al. (2017) Multi-omics Based Identification of Specific Biochemical Changes Associated With PfKelch13-Mutant Artemisinin-Resistant Plasmodium falciparum. J Infect Dis 215 (9), 1435-1444.

133. Carey, M.A. et al. (2018) Influential Parameters for the Analysis of Intracellular Parasite Metabolomics. mSphere 3 (2).

134. Cordy, R.J. et al. (2019) Distinct amino acid and lipid perturbations characterize acute versus chronic malaria. JCI Insight 4 (9).

135. Gardinassi, L.G. et al. (2018) Integrative metabolomics and transcriptomics signatures of clinical tolerance to Plasmodium vivax reveal activation of innate cell immunity and T cell signaling. Redox Biol 17, 158-170.

136. Ray, S. et al. (2017) Quantitative Proteomics Analysis of Plasmodium vivax Induced Alterations in Human Serum during the Acute and Convalescent Phases of Infection. Sci Rep 7 (1), 4400.

137. Reuterswärd, P. et al. (2018) Levels of human proteins in plasma associated with acute paediatric malaria. Malar J 17 (1), 426.

138. Surowiec, I. et al. (2015) Metabolic Signature Profiling as a Diagnostic and Prognostic Tool in Pediatric Plasmodium falciparum Malaria. Open Forum Infect Dis 2 (2), ofv062.

139. Uppal, K. et al. (2017) Plasma metabolomics reveals membrane lipids, aspartate/asparagine and nucleotide metabolism pathway differences associated with chloroquine resistance in Plasmodium vivax malaria. PLoS One 12 (8), e0182819.

140. Pelle, K.G. et al. (2015) Transcriptional profiling defines dynamics of parasite tissue sequestration during malaria infection. Genome Med 7 (1), 19.

141. Organization, W.H., World Malaria Report 2018, WHO, Geneva, Switzerland, 2018.

142. WHO, Guidelines for the treatment of malaria, Geneva, Switzerland, 2015.

143. Blasco, B. et al. (2017) Antimalarial drug resistance: linking Plasmodium falciparum parasite biology to the clinic. Nat Med 23 (8), 917-928.

144. Prevention, C.f.D.C.a. (2018) Biology. https://www.cdc.gov/malaria/about/biology/, (accessed).

145. Ribaut, C. et al. (2008) Concentration and purification by magnetic separation of the erythrocytic stages of all human Plasmodium species. Malaria Journal 7 (1), 45.

146. Allman, E.L. et al. (2016) Metabolomic Profiling of the Malaria Box Reveals Antimalarial Target Pathways. Antimicrob Agents Chemother 60 (11), 6635-6649.

147. Babbitt, S.E. et al. (2012) Plasmodium falciparum responds to amino acid starvation by entering into a hibernatory state. Proceedings of the National Academy of Sciences 109 (47), E3278.

148. Creek, D.J. et al. (2016) Metabolomics-Based Screening of the Malaria Box Reveals both Novel and Established Mechanisms of Action. Antimicrob Agents Chemother 60 (11), 6650-6663.

149. Olszewski, K.L. et al. (2009) Host-parasite interactions revealed by Plasmodium falciparum metabolomics. Cell Host Microbe 5 (2), 191-9.

150. Park, Y.H. et al. (2015) High-resolution metabolomics to discover potential parasite-specific biomarkers in a Plasmodium falciparum erythrocytic stage culture system. Malaria Journal 14 (1), 122.

151. Parvazi, S. et al. (2016) The Effect of Aqueous Extract of Cinnamon on the Metabolome of Plasmodium falciparum Using (1)HNMR Spectroscopy. Journal of tropical medicine 2016, 3174841-3174841.

152. Teng, R. et al. (2014) 1H-NMR metabolite profiles of different strains of Plasmodium falciparum. Biosci Rep 34 (6), e00150.

153. Daily, J. (2019) Treatment of uncomplicated falciparum malaria in nonpregnant adults and children.

154. Codd, A. et al. (2011) Artemisinin-induced parasite dormancy: a plausible mechanism for treatment failure. Malar J 10, 56.

155. Witkowski, B. et al. (2010) Increased tolerance to artemisinin in Plasmodium falciparum is mediated by a quiescence mechanism. Antimicrob Agents Chemother 54 (5), 1872-7.

156. Jackson, K.E. et al. (2007) Selective permeabilization of the host cell membrane of Plasmodium falciparum-infected red blood cells with streptolysin O and equinatoxin II. The Biochemical journal 403 (1), 167-175.

157. Gulati, S. et al. (2015) Profiling the Essential Nature of Lipid Metabolism in Asexual Blood and Gametocyte Stages of Plasmodium falciparum. Cell host & microbe 18 (3), 371-381.

158. Vial, H.J. et al. (2003) Phospholipids in parasitic protozoa. Mol Biochem Parasitol 126 (2), 143-54.

159. Krugliak, M. et al. (2002) Intraerythrocytic Plasmodium falciparum utilizes only a fraction of the amino acids derived from the digestion of host cell cytosol for the biosynthesis of its proteins. Mol Biochem Parasitol 119 (2), 249-56.

160. Phillips, M.A. (2018) Polyamines in protozoan pathogens. J Biol Chem 293 (48), 18746-18756.

161. Ramya, T.N. et al. (2006) Polyamine synthesis and salvage pathways in the malaria parasite Plasmodium falciparum. Biochem Biophys Res Commun 348 (2), 579-84.

162. Gray, K.-A. et al. (2016) Correlation between Cyclin Dependent Kinases and Artemisinin-Induced Dormancy in Plasmodium falciparum In Vitro. PLOS ONE 11 (6), e0157906.

163. Peatey, C.L. et al. (2015) Mitochondrial Membrane Potential in a Small Subset of Artemisinin-Induced Dormant Plasmodium falciparum Parasites In Vitro. J Infect Dis 212 (3), 426-34.

164. Tokumasu, F. et al. (2014) Inward cholesterol gradient of the membrane system in P. falciparum-infected erythrocytes involves a dilution effect from parasite-produced lipids. Biol Open 3 (6), 529-41.

165. Quarfordt, S.H. and Hilderman, H.L. (1970) Quantitation of the in vitro free cholesterol exchange of human red cells and lipoproteins. J Lipid Res 11 (6), 528-35.

166. Daily, J.P. et al. (2007) Distinct physiological states of Plasmodium falciparum in malaria-infected patients. Nature 450 (7172), 1091-5.

167. Peters, J.M. et al. (2007) Differential changes in Plasmodium falciparum var transcription during adaptation to culture. The Journal of infectious diseases 195 (5), 748-755.

168. White, J. et al. (2016) In vitro adaptation of Plasmodium falciparum reveal variations in cultivability. Malaria Journal 15 (1), 33.

169. Barrett, M.P. et al. (2019) Protozoan persister-like cells and drug treatment failure. Nat Rev Microbiol 17 (10), 607-620.

170. Cooper, K.D. et al. (1976) Polyamine distribution in cellular compartments of blood and in aging erythrocytes. Clin Chim Acta 73 (1), 71-88.

171. Shen, H.M. et al. (2018) Whole-genome sequencing and analysis of Plasmodium falciparum isolates from China-Myanmar border area. Infect Dis Poverty 7 (1), 118.

172. Coppens, I. and Joiner, K.A. (2003) Host but not parasite cholesterol controls Toxoplasma cell entry by modulating organelle discharge. Molecular biology of the cell 14 (9), 3804-3820.

173. Hirsch, J.G. et al. (1963) MOTION PICTURE STUDY OF THE TOXIC ACTION OF STREPTOLYSINS ON LEUCOCYTES. The Journal of experimental medicine 118 (2), 223-228.

174. Launay, J.-M. and Alouf, J.E. (1979) Biochemical and ultrastructural study of the disruption of blood platelets by streptolysin O. Biochimica et Biophysica Acta (BBA) - Biomembranes 556 (2), 278-291.

175. Lim, C. et al. (2013) Expansion of host cellular niche can drive adaptation of a zoonotic malaria parasite to humans. Nat Commun 4, 1638.

176. Trager, W. and Jensen, J.B. (1976) Human malaria parasites in continuous culture. Science 193 (4254), 673-5.

177. Bei, A.K. et al. (2010) A flow cytometry-based assay for measuring invasion of red blood cells by Plasmodium falciparum. Am J Hematol 85 (4), 234-7.

178. Lambros, C. and Vanderberg, J.P. (1979) Synchronization of Plasmodium falciparum erythrocytic stages in culture. J Parasitol 65 (3), 418-20.

179. Witkowski B, M.D., Amaratunga C, Fairhurst RM, Ring-stage Survival Assays (RSA) to evaluate the in-vitro and ex-vivo susceptibility of Plasmodium

falciparum to artemisinins, Institute Pasteur du Cambodge – National Institutes of Health Procedure RSAv1, 2013.

180. Grimberg, B.T. et al. (2009) Addressing the malaria drug resistance challenge using flow cytometry to discover new antimalarials. Bioorganic & medicinal chemistry letters 19 (18), 5452-5457.

181. Doolan, D.L. (2002) Malaria methods and protocols. Springer Science & Business Media 72.

182. David Robinson, A.H., Matthieu Gomez, Boris Demeshev, Dieter Menne, Benjamin Nutter, Luke Johnston, Ben Bolker, Francois Briatte, Jeffrey Arnold, Jonah Gabry, Luciano Selzer, Gavin Simpson, Jens Preussner, Jay Hesselberth, Hadley Wickham, Matthew Lincoln, Alessandro Gasparini, Lukasz Komsta, Frederick Novometsky, Wilson Freitas, Michelle Evans, Jason Cory Brunson, Simon Jackson, Ben Whalley, Michael Kuehn, Jorge Cimentada, Erle Holgersen, Karl Dunkle Werner, broom: Convert Statistical Analysis Objects into Tidy Tibbles, 2019.

183. Jari Oksanen, F.G.B., Michael Friendly, Roeland Kindt, Pierre Legendre, Dan McGlinn, Peter R. Minchin, R. B. O'Hara, Gavin L. Simpson, Peter Solymos, M. Henry H. Stevens, Eduard Szoecs, Helene Wagner, vegan: Community Ecology Package, 2019.

184. Wickman, H., tidyverse: Easily Install and Load the 'Tidyverse', 2017.

185. Sugimoto, M. et al. (2012) Bioinformatics Tools for Mass Spectroscopy-Based Metabolomic Data Processing and Analysis. Curr Bioinform 7 (1), 96-108.

186. Berney, M. and Berney-Meyer, L. (2017) Mycobacterium tuberculosis in the Face of Host-Imposed Nutrient Limitation. Microbiol Spectr 5 (3).

187. Mancio-Silva, L. et al. (2017) Nutrient sensing modulates malaria parasite virulence. Nature 547 (7662), 213-216.

188. Mansour, S.C. et al. (2016) Bacterial Abscess Formation Is Controlled by the Stringent Stress Response and Can Be Targeted Therapeutically. EBioMedicine 12, 219-226.

189. Tattoli, I. et al. (2012) Amino acid starvation induced by invasive bacterial pathogens triggers an innate host defense program. Cell Host Microbe 11 (6), 563-75.

190. Calabrese, E.J. (2018) Hormesis: Path and Progression to Significance. Int J Mol Sci 19 (10).

191. Rossnerova, A. et al. (2020) The Molecular Mechanisms of Adaptive Response Related to Environmental Stress. International journal of molecular sciences 21 (19), 7053.

192. Martínez, J.L. and Rojo, F. (2011) Metabolic regulation of antibiotic resistance. FEMS Microbiology Reviews 35 (5), 768-789.

193. Yang, J.H. et al. (2017) Antibiotic efficacy-context matters. Curr Opin Microbiol 39, 73-80.

194. Dumoulin, P.C. et al. (2020) Glutamine metabolism modulates azole susceptibility in Trypanosoma cruzi amastigotes. Elife 9.

195. Meylan, S. et al. (2017) Carbon Sources Tune Antibiotic Susceptibility in Pseudomonas aeruginosa via Tricarboxylic Acid Cycle Control. Cell Chem Biol 24 (2), 195-206.

196. Brown, A.C. and Guler, J.L. (2020) From Circulation to Cultivation: Plasmodium In Vivo versus In Vitro. Trends in Parasitology 36 (11), 914-926.

197. Cantor, J.R. (2019) The Rise of Physiologic Media. Trends in cell biology 29 (11), 854-861.

198. Pethe, K. et al. (2010) A chemical genetic screen in Mycobacterium tuberculosis identifies carbon-source-dependent growth inhibitors devoid of in vivo efficacy. Nat Commun 1 (5), 57.

199. Ismail, H.M. et al. (2016) Artemisinin activity-based probes identify multiple molecular targets within the asexual stage of the malaria parasites Plasmodium falciparum 3D7. Proc Natl Acad Sci U S A 113 (8), 2080-5.

200. Meunier, B. and Robert, A. (2010) Heme as Trigger and Target for Trioxane-Containing Antimalarial Drugs. Accounts of Chemical Research 43 (11), 1444-1451.

201. Pholwat, S. et al. (2017) The Malaria TaqMan Array Card Includes 87 Assays for Plasmodium falciparum Drug Resistance, Identification of Species, and Genotyping in a Single Reaction. Antimicrob Agents Chemother 61 (5).

202. Babbitt, S.E. et al. (2012) Plasmodium falciparum responds to amino acid starvation by entering into a hibernatory state. Proceedings of the National Academy of Sciences 109 (47), E3278.

203. Fennell, C. et al. (2009) PfeIK1, a eukaryotic initiation factor 2α kinase of the human malaria parasite Plasmodium falciparum, regulates stress-response to amino-acid starvation. Malaria Journal 8 (1), 99.

204. Choi, H.J. et al. (2019) A novel PI3K/mTOR dual inhibitor, CMG002, overcomes the chemoresistance in ovarian cancer. Gynecologic Oncology 153 (1), 135-148.

205. Deegan, S. et al. (2013) Stress-induced self-cannibalism: on the regulation of autophagy by endoplasmic reticulum stress. Cell Mol Life Sci 70 (14), 2425-41.

206. Dwivedi, A. et al. (2017) Functional analysis of Plasmodium falciparum subpopulations associated with artemisinin resistance in Cambodia. Malar J 16 (1), 493.

207. Walczak, M. et al. (2018) ATG8 Is Essential Specifically for an Autophagy-Independent Function in Apicoplast Biogenesis in Blood-Stage Malaria Parasites. mBio 9 (1), e02021-17.

208. Cantor, J.R. et al. (2017) Physiologic Medium Rewires Cellular Metabolism and Reveals Uric Acid as an Endogenous Inhibitor of UMP Synthase. Cell 169 (2), 258-272.e17.

209. Demas, A.R. et al. (2018) Mutations in Plasmodium falciparum actin-binding protein coronin confer reduced artemisinin susceptibility. Proc Natl Acad Sci U S A 115 (50), 12799-12804.

210. Mok, S. et al. (2021) Artemisinin-resistant K13 mutations rewire Plasmodium falciparum's intra-erythrocytic metabolic program to enhance survival. Nature Communications 12 (1), 530.

211. Rocamora, F. et al. (2018) Oxidative stress and protein damage responses mediate artemisinin resistance in malaria parasites. PLOS Pathogens 14 (3), e1006930.

212. WHO, World Malaria Report, World Health Organization, Geneva, Switzerland, 2021.

213. Johnson, C.R. et al. (2019) Thiamin deficiency in low- and middle-income countries: Disorders, prevalences, previous interventions and current recommendations. Nutr Health 25 (2), 127-151.

214. Whitfield, K.C. et al. (2017) High prevalence of thiamine (vitamin B1) deficiency in early childhood among a nationally representative sample of Cambodian women of childbearing age and their children. PLoS Negl Trop Dis 11 (9), e0005814.

215. Mayxay, M. et al. (2007) Thiamin deficiency and uncomplicated falciparum malaria in Laos. Trop Med Int Health 12 (3), 363-9.

216. Humeau, J. et al. (2020) Phosphorylation of eukaryotic initiation factor-2α (eIF2α) in autophagy. Cell death & disease 11 (6), 433-433.

217. Fridman, O. et al. (2014) Optimization of lag time underlies antibiotic tolerance in evolved bacterial populations. Nature 513 (7518), 418-21.